



MISSOURI  
**S&T**

# CENTER FOR TRANSPORTATION INFRASTRUCTURE AND SAFETY

## **Design of Ultra High performance Concrete as an Overlay in Pavements and Bridge Decks**

by

Kamal H. Khayat, P.Eng., Ph.D.  
Mahdi Valipour, Ph.D. Candidate

**August 2014**



**NUTC  
R321**

**A National University Transportation Center  
at Missouri University of Science and Technology**

## ***Disclaimer***

The contents of this report reflect the views of the author(s), who are responsible for the facts and the accuracy of information presented herein. This document is disseminated under the sponsorship of the Department of Transportation, University Transportation Centers Program and the Center for Transportation Infrastructure and Safety NUTC program at the Missouri University of Science and Technology, in the interest of information exchange. The U.S. Government and Center for Transportation Infrastructure and Safety assumes no liability for the contents or use thereof.

### Technical Report Documentation Page

1. Report No. NUTC R321	2. Government Accession No.	3. Recipient's Catalog No.
4. Title and Subtitle  Design of Ultra High performance Concrete as an Overlay in Pavements and Bridge Decks	5. Report Date August 2014	6. Performing Organization Code
	8. Performing Organization Report No. Project #00040520	
7. Author/s Kamal H. Khayat and Mahdi Valipour	10. Work Unit No. (TRAIS)	
9. Performing Organization Name and Address Center for Transportation Infrastructure and Safety/NUTC program Missouri University of Science and Technology 220 Engineering Research Lab Rolla, MO 65409	11. Contract or Grant No. DTRT06-G-0014	
	13. Type of Report and Period Covered Final	
12. Sponsoring Organization Name and Address U.S. Department of Transportation Research and Innovative Technology Administration 1200 New Jersey Avenue, SE Washington, DC 20590	14. Sponsoring Agency Code	
	15. Supplementary Notes	
16. Abstract <p>The main objective of this research was to develop ultra-high performance concrete (UHPC) as a reliable, economic, low carbon foot print and durable concrete overlay material that can offer shorter traffic closures due to faster construction. The UHPC was optimized using supplementary cementitious materials (SCMs), proper combinations of aggregates, and adequate selection of fiber types and contents. Three types of SCMs, including silica fume, Class C and F fly ash, and ground granulated blast-furnace slag (GGBS) were used to optimize cement paste with high packing density. The optimized pastes were then used to produce UHPC materials with various contents of fine aggregates and fibers to prove the feasibility of using the UHPC for bonded overlay. The optimized materials were evaluated for workability, rheology, mechanical properties, and shrinkage, as well as their performance was compared to the reference UHPC. In addition, the robustness of the optimized UHPC mixtures to variations of the mixing and curing temperatures was also examined. Bond behavior and the effect of overlay thickness of the developed UHPC materials were also investigated in this study.</p> <p>The experimental study reported herein proved that the optimized UHPC mixtures can develop comparable performance to the commercially available UHPC proportioned with 100% silica sand and 25% silica fume replacement, which was used as the reference UHPC. Given the mix design of the reference UHPC, the UHPC mixtures developed in this study could be more environmental friendly and cost-effective overlay materials compared to the reference UHPC. It is important to note that the optimized UHPC materials can develop adequate mechanical properties without any accelerated curing or special treatment, which contributes to a reduction of overall construction cost of the overlay. The developed UHPC mixtures had equal to or lower drying shrinkage than the reference UHPC.</p> <p>The bond strength between the substrate concrete and the UHPC overlay was shown to be greater than that of the substrate concrete, and the use of the UHPC overlay led to significant increase in flexural strength and toughness over the monolithic beam cast with conventional concrete, regardless of the overlay thickness. These results indicate the feasibility of using the UHPC as a bonded overlay.</p>		
17. Key Words Fiber-Reinforced Mortar, Concrete, Ultra-High Performance Concrete, Rapid Construction	18. Distribution Statement No restrictions. This document is available to the public through the National Technical Information Service, Springfield, Virginia 22161.	
19. Security Classification (of this report) unclassified	20. Security Classification (of this page) unclassified	21. No. Of Pages 127
		22. Price



Missouri University of Science and Technology

*Civil, Architectural and Environmental Engineering Department*

Final Report:

**Design of Ultra High performance Concrete as an Overlay in  
Pavements and Bridge Decks**

August 2014

Prepared by:

Kamal H. Khayat, P.Eng., Ph.D.

Mahdi Valipour, Ph.D. Candidate

## **ACKNOWLEDGEMENTS**

This project was supported by the Center for Transportation Infrastructure and Safety, a National Universities Transportation Center at Missouri University of Science and Technology, and the Innovation Center Iceland (ICI). Authors would like to give special thanks to Dr. Soo Duck Hwang, Mrs. Weina Meng, Mr. Jason Cox, Mr. John Bullock, and all the staff members of the Center for Infrastructure Engineering Studies (CIES) for the efforts and team work during the project. The authors would also like to thank Dr. Olafur H. Wallevik from ICI for his guidance and collaboration for this project.

## **Table of Contents**

<b>Chapter 1 - Introduction</b>	1
1-1 Need for research	1
1-2 Objectives	2
1-3 Scope of the work	2
<b>Chapter 2 - Concrete Overlay</b>	4
2-1 Benefits of concrete overlay	4
2-2 Bonded concrete overlay	5
2-3 Unbonded concrete overlay	6
2-4 Test methods for bond strength	11
2-5 Conclusions	13
<b>Chapter 3 - Ultra-High Performance Concrete (UHPC)</b>	14
3-1 Characteristics of UHPC	14
3-2 Use of UHPC as a bonded overlay	18
3-3 Modeling aspects of UHPC overlay	19
3-4 Effect of surface preparation on the bond strength of UHPC overlay	23
3-5 Conclusions	26
<b>Chapter 4 - Optimization of Cementitious Materials for UHPC</b>	28
4.1 Mixing procedure	28
4.2 Test methods used for the optimization	29
4.3 Optimization based on flow properties	33
4.4 Optimization based on compressive strength	37
4.5 Optimization based on rheological properties	39
4.6 Comparison of overall performance	42
4.7 Conclusions	48
<b>Chapter 5 - Optimization of Fine Aggregate</b>	49
5.1 Preparation of mortar	49
5.2 Test methods	50
5.3 Optimization of aggregate combination and content	51

<b>Chapter 6 - Effect of Fiber Types and Contents on UHPC Performance</b>	58
6.1 Scope of the work	58
6.2 Mixing procedure and sampling	59
6.3 Test methods	60
6.4 Fresh properties and compressive strength	62
6.5 Flexural behavior	64
6.6 Conclusions	68
<b>Chapter 7 - Performance of Optimized UHPC</b>	69
7.1 Mixture proportioning and test methods	69
7.2 Mixing procedure	69
7.3 Fresh properties	71
7.4 Mechanical properties	72
7.5 Drying and autogenous shrinkage	79
7.6 Electrical resistivity	80
7.7 Conclusions	81
<b>Chapter 8 - Effect of Temperature on UHPC Performance</b>	82
8.1 Introduction	82
8.2 Fresh concrete properties	82
8.3 Compressive strength	84
8.4 Splitting Tensile strength	85
8.5 Flexural behavior	86
8.6 Conclusions	91
<b>Chapter 9 - Bond Behavior of UHPC</b>	92
9.1 Introduction	92
9.2 Bonding test methods	92
9.3 Flexural bonding	97
9.4 Conclusions	101
<b>Chapter 10 - Conclusions</b>	102
<b>References</b>	105
<b>Appendix</b>	110

## **Executive Summary**

The United States has a significant investment in civil infrastructure, which is deteriorating under heavy use, age, and environmental attack. A considerable number of the infrastructure is already well beyond the planned service life. Concrete overlays have been used for pavement and bridge deck rehabilitation for many years given the benefit of strengthening the structure against further deterioration due to fatigue cracking. In addition, the overlay repair can improve smoothness and restore ride quality, and add skid resistance.

The main objective of this research was to develop ultra-high performance concrete (UHPC) as a reliable, economic, low carbon foot print and durable concrete overlay material that can offer shorter traffic closures due to faster construction. The UHPC was optimized using supplementary cementitious materials (SCMs), proper combinations of aggregates, and adequate selection of fiber types and contents. Three types of SCMs, including silica fume, Class C and F fly ash, and ground granulated blast-furnace slag (GGBS) were used to optimize cement paste with high packing density. The optimized pastes were then used to produce UHPC materials with various contents of fine aggregates and fibers to prove the feasibility of using the UHPC for bonded overlay. The optimized materials were evaluated for workability, rheology, mechanical properties, and shrinkage, as well as their performance was compared to the reference UHPC. In addition, the robustness of the optimized UHPC mixtures to variations of the mixing and curing temperatures was also examined. Bond behavior and the effect of overlay thickness of the developed UHPC materials were also investigated in this study.

The experimental study reported herein proved that the optimized UHPC mixtures can develop comparable performance to the commercially available UHPC proportioned with 100% silica sand and 25% silica fume replacement, which was used as the reference UHPC. Given the mix

design of the reference UHPC, the UHPC mixtures developed in this study could be more environmental friendly and cost-effective overlay materials compared to the reference UHPC. It is important to note that the optimized UHPC materials can develop adequate mechanical properties without any accelerated curing or special treatment, which contributes to a reduction of overall construction cost of the overlay. The developed UHPC mixtures had equal to or lower drying shrinkage than the reference UHPC.

The bond strength between the substrate concrete and the UHPC overlay was shown to be greater than that of the substrate concrete, and the use of the UHPC overlay led to significant increase in flexural strength and toughness over the monolithic beam cast with conventional concrete, regardless of the overlay thickness. These results indicate the feasibility of using the UHPC as a bonded overlay.

# Chapter 1 - Introduction

## 1.1 Need for research

Pavements usually consist of a base and sub-base layers which last 20-40 years or more, covered with a wearing coarse material having a much shorter service life. The maintenance work for these surface layers induces high external cost [1]. Intensive effort is devoted to introduce new generations of materials to enhance the performance of such surface layers to prolong the service life of concrete pavement. Given their superior mechanical properties and durability, overlay cast using ultra-high performance concrete (UHPC) can provide significant improvement in durability and service life of the overlay pavement. In addition, the absence of mechanical consolidation due to the high fluid nature of the UHPC materials can reduce construction time for new overlay and/or rehabilitation of the pavement.

Degradation of concrete bridge decks can be in the form of spalling, delamination, scaling due to poor material design, freeze-thaw damage, and/or corrosion of reinforcing steel due to infiltration of chloride ions and moisture or inadequate clear cover [2,3]. Overlays are often applied to bridge decks to protect the superstructure from these mechanisms [5,6]. However, traditional overlays have several limitations; for instance they have relatively short service lives (typically between 5-25 years), which results in continuous maintenance, repair, and replacement of the system. Furthermore, several typical overlays require experienced contractors and specialized equipment for proper implementation, which significantly increase dead load. They also often have compatibility issues associated with differences in time-dependent properties between materials [2,3].

It is important to note that due to the time, cost, and environmental considerations, the thickness of overlay materials for the pavement is required to be minimized. In general, the shallow overlays are more prone to have high risk of shrinkage cracking. Therefore, the incorporation of

proper type of steel and/or synthetic fibers is needed to minimize the risk of cracking as well as delamination over time. In addition, the use of fibers can reduce the depth of pavement overlay, thus reducing the overall costs and speeding up the construction process [2]. This research aims at developing an ultra-high strength fiber-reinforced concrete overlay on concrete pavements and/or bridge decks. The feasibility of producing an ultra-high strength and abrasion resistance concrete overlay with a thickness of 8 mm or less is evaluated in this research.

## 1.2 Objectives

The main objective of this research is to develop UHPC materials to enhance pavement service life. This research aims at the development of UHPC materials for use as thin layer of pavement overlay. The UHPC composition is optimized using supplementary cementitious materials (SCMs), proper combinations of aggregates, and adequate selection of fiber types and contents. The specific objectives of the proposed research are summarized as follows:

- Develop sustainable cement-based materials for pavement applications with an optimized combination of SCMs and fibers to prolong service life of rigid and flexible pavement.
- Evaluate the performance of the proposed materials in the laboratory.

## 1.3 Scope of the work

Considering the positive effect of pozzolanic materials on durability and mechanical properties of cement-based materials, the research involved the design of UHPC using various types and contents of SCMs and the investigation of their effect on the performance of the UHPC. The research evaluated the use of fibers to enhance cracking resistance of UHPC that can be high due to shrinkage, environmental effects, and repetitive traffic loading. Steel and/or synthetic fibers

were used for that purpose. The use of fibers can also lead to a reduction in pavement depths, thus reducing overall cost of the overlay.

Several concrete mixtures were evaluated for workability, rheology, and compressive strength to select and optimize mixtures that satisfied the targeted performance. In the second part of the research program, key engineering properties of the optimized UHPC mixtures were investigated in detail. The robustness of the UHPC materials were also evaluated by employing different mixing and curing temperatures of  $10 \pm 2^{\circ}\text{C}$  and  $30 \pm 2^{\circ}\text{C}$  to investigate their effect on the workability and mechanical properties. The performance of the interface layer under the flexural and shear loads was also characterized to investigate the bond capacity between the overlay with various thickness and sub-surface pavement layers.

# Chapter 2 - Concrete Overlay

## 2.1 Benefits of concrete overlay

A large percentage of bridges in the United States will reach their design service lives in the coming decades and more than 11% are currently listed as structurally deficient and over 12% is rated as functionally obsolete [2,6]. Concrete bridge decks are a major contributor to the degradation of an entire bridge system, as they are often directly exposed to de-icing salts and serve as protection for the underlying superstructure [2,4]. This degradation is critical because the deck serves not only as the riding surface, but as a protective barrier exposed to maintenance strategies such as plowing and de-icing agents, environmental conditions, and vehicle traffic, all of which contribute to the deck's degradation [2-4,7].

The main purpose of constructing concrete overlays is to optimize and/or extend the use of the remaining life of the existing pavement by placing an additional layer of concrete above it. The benefits of concrete overlay include expedited construction, reduced cost, increased structural integrity, improved riding quality, and protection of the structure against deleterious environmental effects.

Concrete overlays on pavements or bridge decks can strengthen the structure against further deterioration due to fatigue cracking and can also be an effective means to enhance pavement sustainability by improving surface reflectance, increasing structural longevity, and enhancing surface profile stability. The overlays can serve as complete preventive maintenance or rehabilitation solutions or can be used in conjunction with spot repairs of isolated distresses. In addition, concrete overlays can provide cost-effective solutions for pavement and bridge deck repairs. In concrete overlays, the existing pavement does not need to be removed. It needs few or no pre-overlay repairs. Concrete overlays can be placed using conventional concrete pavement

practices. One of the best benefits of concrete overlay is that the pavement or bridge can be opened to traffic within a day of placement as well as accelerated construction practices can be used throughout the normal construction season [2].

Concrete overlays are categorized into two types: bonded type concrete overlay and unbonded type concrete overlay. In bonded type concrete overlays, there are ultra-thin and thin whitetoppings and bonded concrete overlay. These concrete overlays require bonding between the concrete overlay and the existing pavement. In unbonded type concrete overlays, there are conventional whitetopping, and unbonded depending on their thickness [2].

## 2.2 Bonded concrete overlay

A bonded concrete overlay is a relatively thin concrete that is used to resurface an existing concrete pavement. This type of overlay is typically 50 to 100 mm. thick and its performance depends on the bond strength of the overlay to the existing pavement. The purpose of bonded concrete overlay is to rehabilitate deteriorating concrete pavement to increase load capacity and ride quality. Bonded concrete overlay is recommended when the existing pavement is considered to be in fair or better condition with minor surface distresses and less than a few punch-outs per lane mile [8].

The effectiveness of bond is necessary in the case of bonded concrete overlay. Proper bond will provide monolithic behavior, ensuring that the stiffness of the rehabilitated pavement will carry the traffic load as one structure. Since bonded concrete overlays rely on the existing pavement to assist in carrying the traffic load; the condition of the existing pavement affects the performance of the rehabilitated pavement. Proper repairs or upgrades should be made to provide adequate support as required by design. In addition, if joints are made, well designed joint spacing helps to

reduce curling and bending stresses due to traffic and environmental loads. It is crucial that the transverse joints in the bonded concrete overlays match those in the existing pavement to promote monolithic behavior.

In bonded concrete overlay, different modes of failure can occur, and the loss of bond is one of the critical issues. The bond between the overlay and the existing pavement can be lost due to lack of quality control in surface preparation or placement during construction. Another failure mode is delamination due to differences in coefficient of thermal expansion (CTE): if bonded concrete overlay have a CTE that is greater than the CTE of the existing pavement, then the overlay will expand or contract more than the existing pavement. These results in shear stresses at the bond, and these induced stresses can cause the cracking and delamination of the overlay. These stresses in general, are higher at the edges of the overlay section and along cracks compared to the bonded areas in the middle of the section. This is due to curling and warping at the top of the overlay as temperatures and moisture conditions change more rapidly at the top surface than the rest of the slab depth [8].

### 2.3 Unbonded concrete overlay

In general, unbonded concrete overlay is categorized as relatively thick concrete overlays that are used to resurface the existing concrete pavement. This type of overlay is typically 130 to 280 mm. thick and is designed to perform without bonding to the existing pavement. Unbonded concrete overlay is used when the existing pavement is severely deteriorated with major surface distresses. A separation layer is used to maintain separation between concrete overlay and existing pavement [8].

Several factors determine the performance of unbonded concrete overlays. The effectiveness of the separation layer is critical. An effective separation layer should act as a shear plane that

prevents migrating cracks from the existing pavement into the overlay. In addition, the separation layer prevents bonding between the new and the old layer allowing them to move independently. Also, a well-constructed drainage system can prevent the building up of pore pressure from the traffic loads. The system serves to prolong the life of the overlay by reducing pumping, asphalt stripping of the separation layer, faulting, and cracking.

Different failure modes can take place in the unbonded concrete overlay. Failure at-grade and overhead structures is one of them. The elevation of the pavement after an unbonded concrete overlay placement will significantly increase. Therefore, at-grade and overhead structures should be raised, or existing pavement should be removed and replaced near these structures. Other failure mode is due to inadequate separation layer. The separation layer prevents reflective cracks. If the new overlay is not structurally separated from the deteriorated existing pavement, the movement of the two structures will affect each other, which will induce heavy reflective stress to the overlay. In addition, poor drainage could be considered as another failure mode. The higher elevation of the pavement necessitates a change in the drainage grade lines. Additional right-of-way may be required to provide the proper slopes for the ditches [8].

Different overlay materials are compared in Table 2.1. Each overlay material has pros and cons, and therefore, care should be taken to select proper type of overlay materials, depending on the type of repair/rehabilitation. In the case of bonded overlay for the pavements and bridge decks, high-performance concrete (HPC) with low overlay thickness could be an effective method to ensure long average life span compared to the other types of overlay materials given the low permeability, high mechanical properties, and good durability. In this regards, the use of properly designed UHPC materials that have significantly greater mechanical properties and durability

can be even more cost-effective solution since the thickness of the overlay can be reduced further compared to the case of HPC and other overlay materials.

Table 2.1- Comparisons of different overlays [2]

Overlay type	Latex-modified concrete (LMC)	Silica fume modified concrete (SFMC)	Low slump dense concrete (LSDC)	Fiber-reinforced concrete
Cost (\$)/S.F.	18-39	More expensive than LMC	13-19	1.4-2.6
Alternative names or types	Latex-modified mortar <sup>2</sup> and high strength LMC <sup>4</sup>	Microsilica modified concrete (MMC), Silica fume concrete (SFC).		
Avg. thickness	1.25", 1.25-3", 1.5", 2.25"	1.25", 2", 2.25"	2-3", 2"	1", 2.75"
Service-life	14-29 yrs	5-10 yrs	16-32 yrs	
Mix components	Portland cement, latex (typically styrene-butadiene), water, coarse and fine aggregates, and antifoamer. Steel or synthetic fibers are often used.	Silica fume, Portland cement, water, coarse and fine aggregates, high-range water reducer, and air-entraining admixture. Steel or synthetic fibers are often used.		Steel, glass, synthetic, plastic fibers, or blends are used with Portland cement, water, and coarse and fine aggregates. High-range water reducer and air-entraining admixture are often needed. Fly ash or microsilica can be added. Steel or synthetic fibers have been used.
W/B	0.35, 0.37, 0.4	0.35-0.4		0.4
MOE	3.8 ksi	4.1 ksi		4.9 ksi
Compressive strength	High early age and 28 day compressive strength	High early age and 28 day compressive strength	5,000 psi at 7 days is required	High early age compressive strength, but low 28 and 90 days
Tensile strength	710 psi at 28 days for splitting tensile strength	680 psi at 28 days for splitting tensile strength		825 psi at 28 days for splitting tensile strength
Resistance to Cl ion penetration	ASTM Rating "Low"	ASTM Rating "Very low"		ASTM Rating "Moderate"
Chloride permeability specification	1000 Coulombs at 90 days	1000 coulombs at 90 days		

Table 2.1(cont'd) - Comparisons of different overlays

Overlay type	Latex-modified concrete (LMC)	Silica fume modified concrete (SFMC)	Low slump dense concrete (LSDC)	Fiber-reinforced concrete
Construction notes	Substrate should be wetted before application of bonding agent, requires special mixing equipment and contractor experience, and is sensitive to weather conditions. Burlap and/or plastic are used during curing, very limited widow for finishing (15-30 min), but typical concrete finishing machines can be used	Fog sprays are used to control water evaporation. Wet burlap sacks and polyethylene sheets should be placed quickly to avoid plastic shrinkage. Overlay should be continuously wet and the area should be well drained. Bull float trowel are often used after screeding. Can be tined, broomed, burlap, or turfed finish early	Requires experienced contractors. Bonding agents should be applied to a dry substrate. Wind fences are commonly used. Mechanical tamping is used in some cases to obtain proper densification, but care must be taken as it is not difficult to overwork the surface. Overlay must be screed and finished immediately	
State use	WV, DE, IL, IN, KS, KY, MA, MI, MO, NC, OK, PA, RI, SD, TN, WA, Ontario	WV, NY, Oregon, OH, RI	KY, MN, NY, ND, Iowa, KS, MI, MO, ND, SD, Puerto Rico	
Overall pros	High bond strength, good durability, high abrasion and skid resistance, low permeability, low cracking. Short cure time, quick installation, and long estimated service-life	Low permeability, high early and ultimate strength, good bond strength, high abrasion and skid resistance, high electrical resistance (suppresses the corrosion reaction in concrete)	Low permeability, good durability and long estimated service-life, increased structural capacity	Post cracking tensile capacity. High early strength. High ductility due to fibers. Many possibilities of specialization within mix design
Overall cons	High cost, placement difficulties and need for experienced contractors. If improperly constructed, cracking and/or debonding are often major issues. Wear has been noted in wheel paths. Some have experienced long curing times. A few mix designs (primarily older designs) have issues odor, toxicity, and flammability	Premature cracking, spalling and delamination due to surface shrinkage and strength failure at interfaces have been experienced	Difficulties of placement and consolidation, long cure times, higher dead loads. Susceptible to cracking. Vulnerable to weather conditions	Additional dead load, not as high compressive strength long-term as some high strength alternatives. Chloride resistance is not superior to other overlay types

Table 2.1(Cont'd) - Comparisons of different overlays

Overlay type	Hot-mix asphalt (HMA) single or multi-layer	Polymer-concrete (PC)	High-performance concrete overlay (HPC)	Portland cement concrete overlay (PCC) standard concrete and reinforced concrete overlay.
Cost (\$) /S.F.	3.1-7.6	10-17	17-25	22-36
Alternative names or types	Layered overlays are also called sandwich seal overlays.			Structural bridge deck overlays (SBDO).
Avg. thickness	2-3.25"	0.5-1.4"	1.6-3.5"	3-3.8"
Avg. lifespan	10-15 yrs	9-18 yrs	16-29 yrs	15-24 yrs
Mix design - Mix components	Can be made with one asphalt layer or as a multiple, sandwich layer. Asphalt and bridge deck sealant (rubber, fiberglass, bitumen, polyester membrane). Layered Overlay includes a tack coat	Aggregate and binder. Binder can be epoxy, polyester styrene, or methacrylate. No Portland cement or water is used		Type I Portland cement, water, and coarse and fine aggregate. High early strength Portland cement is also used
Comparison		Often used as a preventative measure on newer deck. Lower dead load		Used in deck rehabilitation more than other overlays
Curing and construction duration	Total construction time is around 3 days	Total construction can take less than 24 hrs	Total construction time can take over 7 days	1-2 day moist curing
Construction notes	Substrate repairs must be made before overlay placement. Typical asphalt paving equipment and procedures are used. Sealant is placed between bridge deck and first asphalt layer.	Substrate roughening is vital to this overlay's success. Must follow temperature and humidity tolerances. Usually two-component systems: one component contains resin and the second contains the curing agent or initiator. Uniformly graded aggregates are used with slurry and premixed overlays. Gap graded aggregates are used with multiple-layer overlays and are broadcast on the top of slurry and some premix overlays.	Typically contains low w/c ratio. Admixtures may be added for improved workability	Substrate surface preparation is typically achieved through hydro demolition
State use	CO, CT, IL, KY, NE, NY, RI, SD, TN, UT, VT, Alberta, Ontario, Quebec	AK, CA, CO, GA, ID, IL, KS, MA, ME, MO, NM, NV, NY, OK, OR, TN, UT, BT, WY, VA	AK, AZ, ID, IL, KS, MI, MO, NE, NY, OK, OR, WV, WY, Alberta	No agencies reported using PCC overlays for new construction, though half of the agencies surveyed used PCC for over 25years
Overall pros	Low cost, ease and speed of installation, improves ride-ability, effective	High early compressive strength, high bond strength, good durability and skid resistance, low permeability, low dead load. Does not require modification of approaches or existing expansion joints.	Low permeability, good durability, high strength. High cost-effective performance	Long life, familiar and quick installation, good record. Good alternative to repair and replacement.
Overall cons	The layered asphalt overlay can trap moisture in the deck, which can damage bond and/or reinforcement. Short service-life and timely maintenance is required. Some have found difficulty of removal. Effectiveness of membrane is unknown. Poor performance has been found on curved. Does not contribute structurally to the superstructure.	Installation difficulties. Some have found low durability. Higher cost. Cannot be used as a replacement for bridge deck concrete.	Installation difficulties. Cracking has been found during curing. Long cure times. Higher cost.	Long construction time and high cost. Low bond strength. Not conducive to decks containing slag.

## 2.4 Test methods for bond strength

The bond evaluation between different materials is important in repair and rehabilitation work. Different test methods can be used to assess bond strength between two materials. The bond tests are in this section. Different types of bond tests in tension are presented in Figure 2.1. For direct tension test, the tensile force applied to the specimen should be aligned to the axis of the loading direction [9,10]. Indirect tension test includes splitting and flexural tests. The splitting test is found to be more efficient than the flexural test because the splitting test has relatively greater area of the bonded section subjected to the maximum stress compared to that of the flexural bond test [9,12]. The pull-off test involves coring the cleaned surface of concrete with a proper core bit until it passes into the interface layer, then gluing a test disc using epoxy, and pulling the disc through a hydraulic pull machine sitting on the surface to evaluate the pullout bond strength [12].

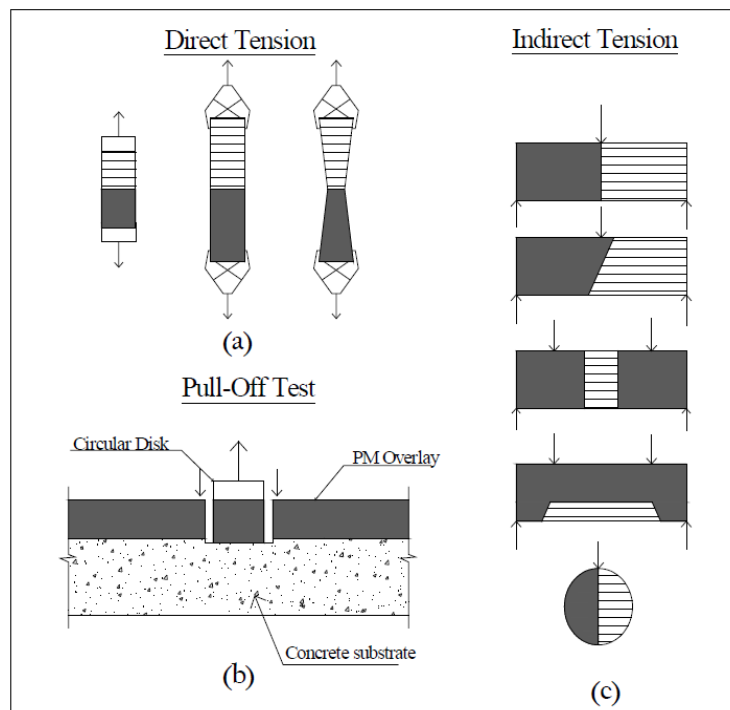


Figure 2.1 - Different types of tensile bond test methods that can be used to evaluate concrete overlays [12]

There are different types of shear tests, as presented in Figure 2.2. In some cases, direct shear test is associated with small bending stress, which can affect the results. The Arizona slant shear test is associated with small bending stress, which can affect the results. The Arizona slant shear test was first proposed by [13] and has a bonding plane at an angle of 30 degrees from vertical plane. The composite cylinder is loaded as in a standard compression test. Wall and Shrive [14] modified the Arizona slant shear test by using a prism with a length three times of the cross sectional dimension. Their results demonstrated that a slight misalignment of the two halves of the prism specimen has negligible effects on the capacity of the composite specimens. Several shear tests are compared in Table 2.2. In most cases, the bonded surface for a direct shear test is subjected to shear stress and a small bending stress. When a steel plate is used to transmit the shear force along the bond line, some stress concentration at the edge of the bonding planes can be induced. In the slant shear test; the shear stress is combined with a compression stress in the axis perpendicular to the bonding plane [12].

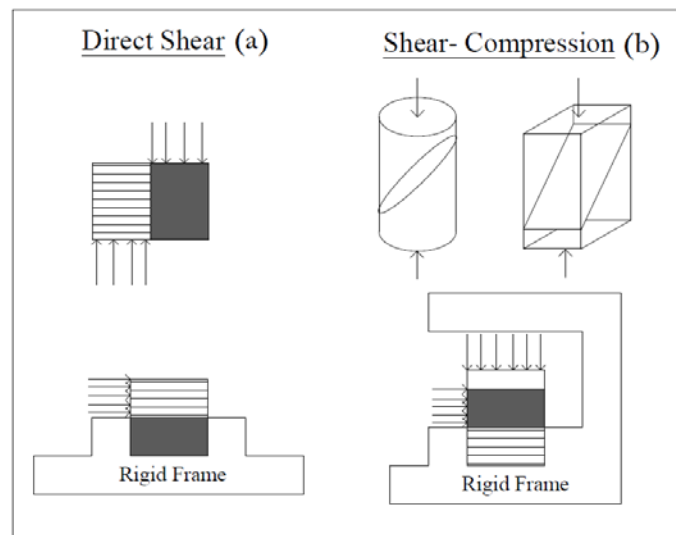


Figure 2.2 - Different types of shear bond test [12]

Table 2.2 - Different bond test methods with their advantages and disadvantages [12]

Bond Test		Advantages	Disadvantages
Direct tension		Most apparent method to evaluate the bond strength in tension.	A very small amount of misalignment may cause big scatter in test result. Time consuming (glue hardening, heads cleaning). Sometimes incompatible with the concrete curing conditions
Direct shear		Most apparent method to evaluate the bond strength in shear.	Some stress concentration induced at the edge of bonding plane and it contributes the scatter in test results.
Indirect tension	Flexure	Easier to perform	Some stress concentration induced at the edge of bonding plane and it contributes the scatter in test results.
	Splitting	More space efficient and simple to perform	Sometime not very convenient to study the bond of old to new concrete.
Shear and compression		Slight misalignment of the two halves of the material does not significantly affects the result	Since it combines the shear and compressive strength together the bond strength is several times higher than other bond test.
Pull-off		Represent more accurate in-service condition precisely assess in situ bond strength	Large variation obtained with different types of apparatus.

## 2.5 Conclusions

Based on the literature research presented in this chapter, the bonded concrete overlay is found to be proper solution to repair and rehabilitate the concrete pavement and bridge decks due to the ease of construction, relatively low cost, and thinner layer of the overlay. In the case of the bonded overly for the pavements and bridge decks, high-performance concrete (HPC) with low overlay thickness could be an effective method for long life span given the low permeability, high mechanical properties, and good durability. In that regards, properly designed UHPC materials having significantly greater mechanical properties and durability could be considered as more cost-effective overlay materials since the thickness of the overlay can be reduced further compared to the case of HPC and other overlay materials or a given thickness of UHPC overlay can secure longer service life of the pavement compared to the other materials.

# Chapter 3 - Ultra-High Performance Concrete

## 3.1 Characteristics of UHPC

Ultra-high performance concrete (UHPC) is a class of concretes that exhibits extremely high durability and mechanical properties. The UHPC belongs to the family of engineered cementitious composites [15] and is defined as a cement-based concrete with compressive strength equal to or greater than 150 MPa [16,17]. In addition, this novel material is characterized as a concrete which has an extremely low water-to-cement ratio (w/c), high binder content, and optimum packing density to eliminate capillary pores and provide an extremely dense matrix, and direct tensile mortar strength higher than 7 MPa [16,17]. In most cases, UHPC contains steel micro fibers which enhance the materials' ductility and mechanical properties [2].

Aïtcin [18] described how UHPC can achieve such a high strength as follows:

“We know how to make 150 MPa concrete on an industrial basis. Because at such a level of strength it is the coarse aggregate which becomes the weakest link in concrete, it is only necessary to take out coarse aggregate, to be able to increase concrete compressive strength and make reactive powder concrete having a compressive strength of 200 MPa; it is only necessary to confine this reactive powder concrete in thin-walled stainless steel tubes to see the compressive strength increased to 375 MPa; and when the sand is replaced by a metallic powder, the compressive strength of concrete increases to 800 MPa”

Due to the large difference in elastic moduli between aggregate and cement paste, conventional concrete and even HPC have a mismatch in the properties of their constituent materials. This is significantly reduced in the case of UHPC by selecting constituent materials with similar elastic moduli [19]. Another problem in conventional and HPC is a weak transition zone in the interface between the aggregate and cement paste compared to UHPC.

Figure illustrates a representation of the force transfer through normal concrete compared to UHPC materials. In the case of conventional concrete, the force or load is transferred through only aggregates. In UHPC, all the material constituents, including cement paste and aggregates, take part in the force transfer, which can result in a significant improvement in the mechanical properties of the novel construction materials.

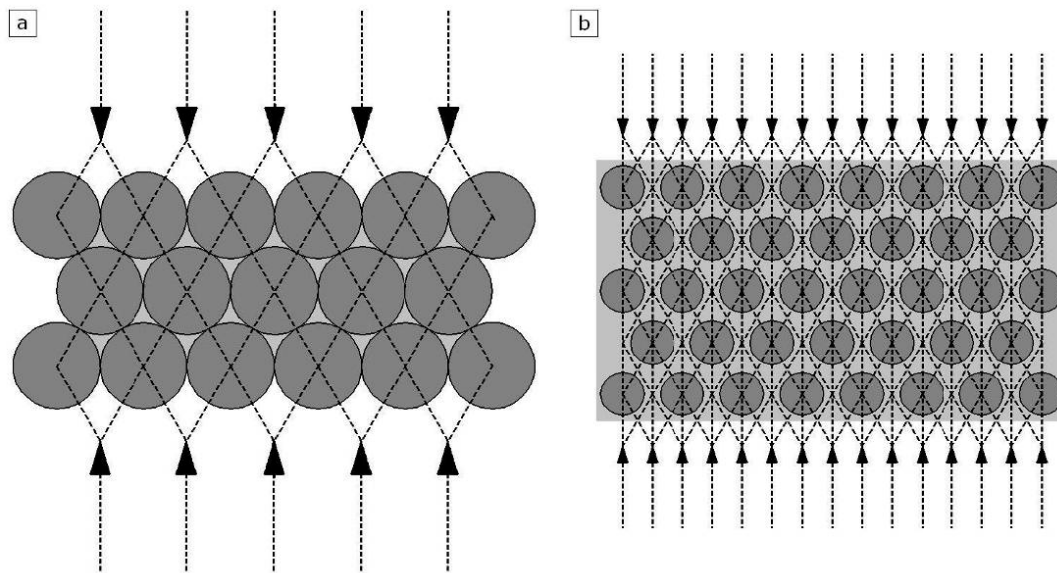


Figure 3.1 - Depiction of force transfer through a) normal concrete and b) UHPC [20,21]

Some of principles that are used in UHPC to achieve high mechanical properties and durability include the enhancement of homogeneity by elimination of coarse aggregate and the packing density by optimization of the granular skeleton of the mixture through a wide distribution of powder size classes. In addition, the addition of SCMs, such as silica fume and the use of low water-to-binder ratio (w/b) can result in significant improvement in the mechanical properties and durability of the cement matrix of the UHPC materials. The enhancement of the microstructure by employing post-set heat-treatment and the improvement of the ductility, tensile

strength, and crack resistance by the incorporation of small fibers, such as steel fibers are the main keys for the proper design of the novel construction materials [22,23].

UHPCs have extremely high packing density which can be achieved by optimizing the proportioning of different components [22]. The particles should be selected to fill up the voids between large particles with smaller particles, leading to a smaller volume of gaps within the aggregate skeleton. The concept of packing density, i.e. the ratio of the volume of solids to a given volume, is introduced to evaluate the arrangement of granular mixtures. Figure 3.2 illustrates how the concept of packing density can be applied with three granular systems, i.e. single-, binary-, and ternary- systems [24]. The single-sized aggregate can be packed together to occupy only a limited space, i.e. it can achieve only a relatively low packing density. However, the multi-sized aggregates can be packed together much more effectively to achieve higher packing density, i.e. binary and ternary mixtures. For a given volume of cement paste, the increase in packing density of the aggregates can increase the workability of concrete at the same w/b, or increase the strength of concrete by reducing the w/b at a given workability. Key engineering properties of conventional concrete, HPC, and UHPC are compared in Table 3.1.

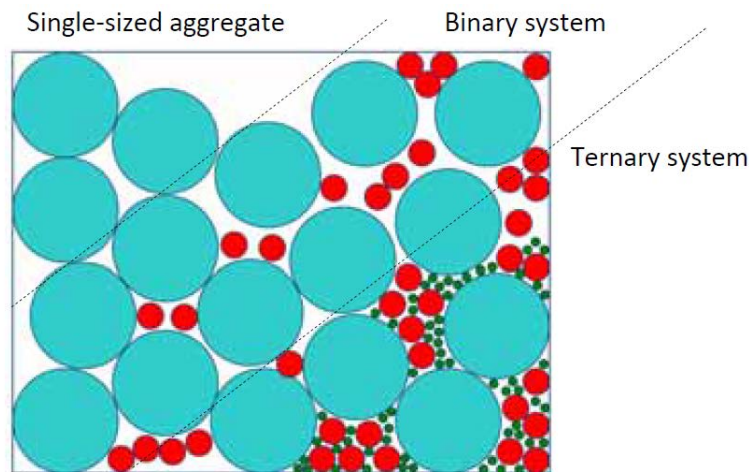


Figure 3.2 - Typical packing arrangements of binary and ternary mixtures [24]

Table 3.1 - Comparison of UHPC material properties to other concrete classifications [25]

<b>Material characteristics</b>	Conventional concrete	HPC	UHPC
Maximum aggregate size, (in.)	0.75-1.00	0.38-0.50	0.016-0.024
w/cm	0.40-0.70	0.24-0.35	0.14-0.27
<b>Mechanical properties</b>			
Compression strength, (ksi)	3.0-6.0	6.0-14.0	25.0-33.0
Split cylinder tensile strength, (ksi)	0.36-0.45	-	1.0-3.5
Poisson's ratio	0.11-0.21	-	0.19-0.24
Creep coefficient, Cu	2.35	1.6-1.9	0.2-0.8
Porosity (%)	20-25	10-15	2-6
Fracture energy, (k-in/in <sup>2</sup> )	0.00057-0.00086	-	0.057-0.228
Young's modulus, (ksi)	2000-6000	4500-8000	8000-9000
Modulus of rupture 1st crack, (ksi)	0.4-0.6	0.8-1.2	2.4-3.2
Flexure strength - ultimate, (ksi)	-	-	3.0-9.0
Shrinkage	-	Post cure 40-80×10 <sup>-5</sup>	Post cure <1×10 <sup>-5</sup> , No autogenous shrinkage after cure
Coefficient of thermal expansion (°F)	4.1-7.3×10 <sup>-6</sup>	-	7.5-8.6 ×10 <sup>-6</sup>
Ductility	-	-	250 Times > NSC
<b>Durability</b>			
Freeze/thaw resistance	10%	90%	100%
Chloride penetration (Coulomb)	> 2000	500-2000	< 100
Air permeability (k) at 24 hrs and 40°C, (in <sup>2</sup> )	4.65×10 <sup>-14</sup>	0	0
Water absorption at 225 hours (lb/in <sup>2</sup> )	4×10 <sup>-3</sup>	5×10 <sup>-4</sup>	7.1×10 <sup>-5</sup>
Chloride ion diffusion coefficient (by steady state diffusion), (in <sup>2</sup> /s)	1.55×10 <sup>-9</sup>	7.75×10 <sup>-10</sup>	3.1×10 <sup>-11</sup>
Penetration of carbon / sulfates	-	-	None
Mass of scaled off (lb/ft <sup>2</sup> )	> 0.205	0.016	< 0.002

It is important to review different components and the microstructural properties of typical UHPC mixtures. Sand, cement, silica fume, crushed quartz, fibers, high-range water reducer (HRWR) or superplasticizer (SP), as well as water, are the main components of a UHPC, as presented in Table 3.2.

Table 3.2 - Range of UHPC mixture components [26-36]

Components	Typical range (kg/m <sup>3</sup> )	Mass ratio/cement	Volume fraction (%)
Sand	490 – 1390	1.43	38.8
Cement	610 – 1080	1.00	22.7
Silica fume	50 – 334	0.32	10.6
Crushed quartz	0 – 410	0.30	8.1
Fibers	40 – 250	0.21	2.0
Superplasticizer	9 – 71	0.02	1.4
Water	126 – 261	0.23	16.5

\*Superplasticizer is expressed as the weight of the solid fraction; the liquid fraction is included in the water weight.

### 3.2 Use of UHPC as a bonded overlay

UHPC has extremely high impermeability, negligible dry shrinkage if properly cured, and excellent post-cracking tensile capacity. UHPC also exhibits high compressive strength, between 125-230 MPa, at 28 days depending on the cure regime, which is required for the rehabilitation of bridge decks when added load capacity and load transfer is desired [37,38]. Furthermore, UHPC develops high early strength, which could reduce traffic closure time and increase the rate of precast bed turnover. In order to fully benefit from the superior properties of UHPC, the bond integrity of the novel material to the conventional concrete deck systems has to be evaluated. The thickness of the UHPC overlay should be optimized to reduce the dead load while maintaining the integrity of the bond interface.

In spite of the aforementioned benefits of UHPC over conventional overlay materials, its high initial cost can limit its broader use. Bonneau et al. [39] reported the ultra-high performance fiber reinforced concrete's price as \$1400/m<sup>3</sup> in 1996 in Europe which decreased to \$750/m<sup>3</sup> in 2000 with more common use [40]. The cost estimation of the UHPC was \$2620/m<sup>3</sup> in North America in 2007 [41]. More recently, a 30-mm thick UHPFRC was used as an overlay to repair a short span of a heavy traffic road bridge [42,43]. Two alternatives were suggested in this overlay project, which were the rehabilitation using UHPFRC without water proofing membrane and

typical repair mortar with water proofing membrane. Cost analysis for the two alternatives indicated that the UHPFRC overlay would have 12% higher material cost than the mortar overlay. It should be noted, however, that the typical mortar overlay necessitates longer traffic closure time due to the drying process before applying the water proofing membrane compared to the UHPFRC overlay which reduces the traffic disruption and can provide superior mechanical properties and durability [43].

The flexural behavior of UHPC overlay was investigated by Yuguang et al. [44] using a multilayer model. This research was done by varying the numbers of rebars and fiber volumes; the fiber volume was set to 0%, 0.8%, and 1.6%. The results indicated that a 30.5-mm thick UHPC overlay made without any rebars could endure the maximum traffic load. Lee and Wang [45] evaluated compressive strength, bond strength, and steel pull out capacity. The results indicated that the use of a 10-mm thick reactive powder concrete (RPC) or UHPC bonding layer increases compressive and flexural strength between 150% and 200% over conventional concrete overlay. In addition, abrasion resistance of RPC overlay was approximately eight times greater than that of conventional concrete overlay.

### 3.3 Modeling aspects of UHPC overlay

This section focuses on the modeling aspects of a thin-bonded UHPC overlay on a concrete bridge deck or pavement taking into considerations various parameters, such as deck and overlay thickness, material strengths, bridge geometry, and live load. In general, finite element models are used to evaluate the effect of the various parameters on the performance of overlay systems. This section reviews relevant literatures regarding the finite element modeling of overlay systems, including how the system can be modeled and what parameters were considered in the analysis.

Shann [2] performed 3D finite element modeling for UHPC thin overlay for bridge decks. The overlay thickness ( $t_o$ ), deck thickness ( $t_d$ ), ratio of the overlay-deck material stiffness ( $E_o/E_d$ ), and fixed and simple girder support (GS) conditions were considered for the variables in this analysis. Geometric and material properties were also included in the modeling. The purpose of this model set was to make direct comparisons of the effect of  $t_o$ ,  $t_d$ ,  $E_o/E_d$ , and boundary conditions on the debonding stresses, as presented in Figure 3.3 through 3.8. The effect of  $t_o$  and  $E_o/E_d$  on debonding and interface shear stress with fixed and simple girder supports ( $t_d$  constant) indicated that the increase in overlay thickness from 7.5 to 51 mm. can lead to increase debonding stress from 0.13 to 0.41 MPa. In addition, an increase in  $E_o/E_d$  results in an increase in debonding and interface shear stresses. The tensile stress of the overlay is shown to decrease with the increase in overlay thickness for both support conditions. In addition, the tensile stress is shown to increase with the increase in  $E_o/E_d$ . Several studies are available for the modeling aspects of the concrete overlay. However, limited information is available regarding the UHPC overlay modeling.

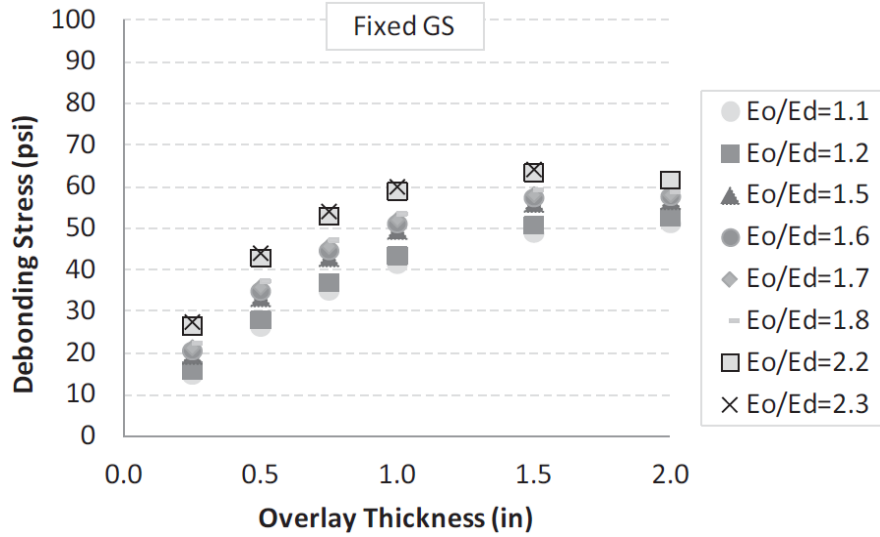


Figure 3.3 - Effect of overlay thickness ( $t_o$ ) and stiffness ratio ( $E_o/E_d$ ) on debonding stress of concrete overlay on bridge deck with fixed girder supports ( $t_d$  constant) [2]

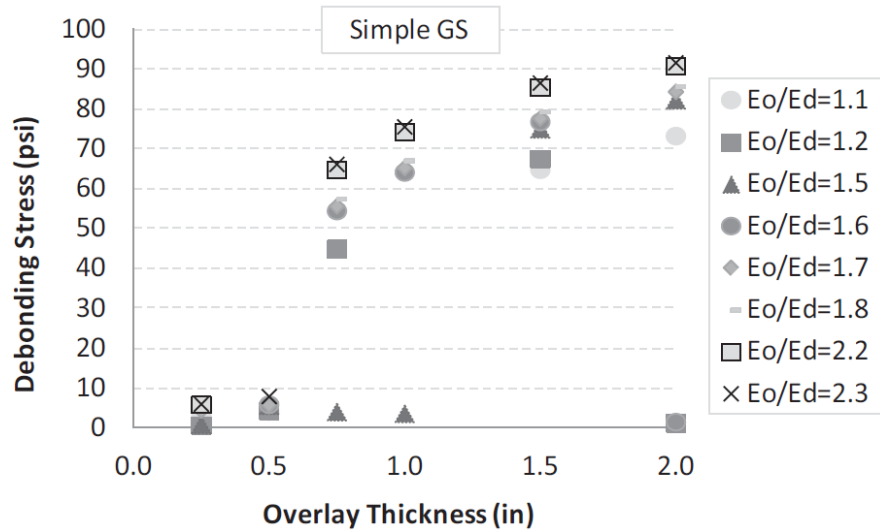


Figure 3.4 - Effect of overlay thickness ( $t_o$ ) and stiffness ratio ( $E_o/E_d$ ) on debonding stress of concrete overlay on bridge deck with simple girder supports ( $t_d$  constant) [2]

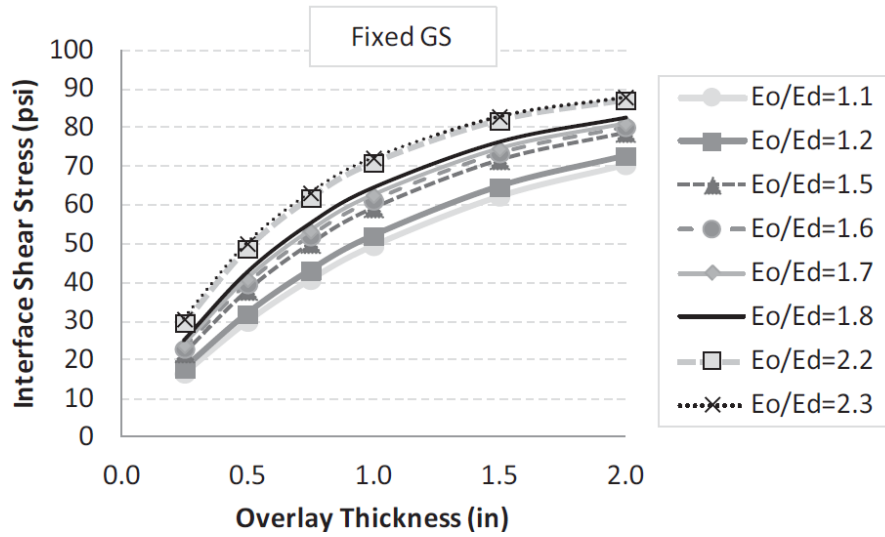


Figure 3.5 - Effect of overlay thickness ( $t_o$ ) and stiffness ratio ( $E_o/E_d$ ) on interface shear stress with fixed girder supports ( $t_d$  constant) [2]

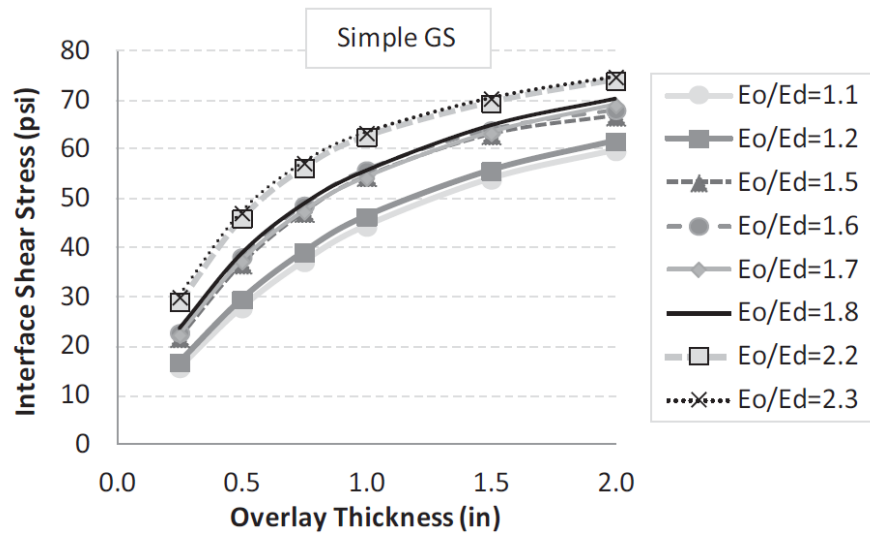


Figure 3.6 - Effect of overlay thickness ( $t_o$ ) and stiffness ratio ( $E_o/E_d$ ) on interface shear stress with simple girder supports ( $t_d$  constant) [2]

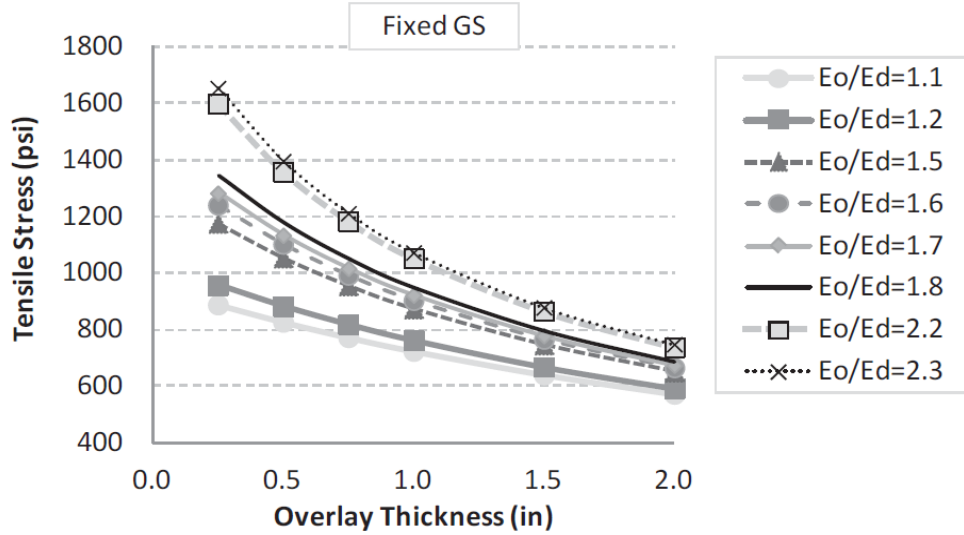


Figure 3.7 - Effect of overlay thickness ( $t_o$ ) and stiffness ratio ( $E_o/E_d$ ) on tensile stress with fixed girder supports ( $t_d$  constant) [2]

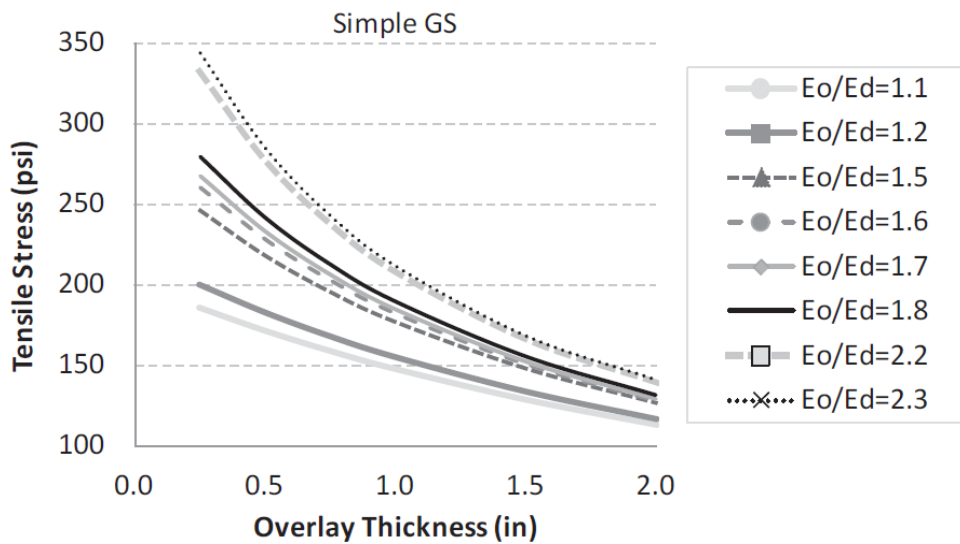


Figure 3.8 - Effect of overlay thickness ( $t_o$ ) and stiffness ratio ( $E_o/E_d$ ) on tensile stress with simple girder supports ( $t_d$  constant) [2]

### 3.4 Effect of surface preparation on the bond strength of UHPC overlay

Julio et al. [46] evaluated bond strength of two concrete layers that are subjected to various surface preparations, which include wire brushing, sand blasting, chipping with a light jackhammer, and unprepared normal surface. Bond strength was determined using both tension

and shear tests. The use of sand blast preparation led to the highest bond strength among the surface preparation methods applied. In addition, the increase in the age difference between the overlay and existing concrete was found to decrease the bond strength. Their results also demonstrated that monolithic rupture can take place, which causes failure of the substrate if the compressive strength of the overlay was greater than the substrate concrete.

Sarkar [12] also evaluated the bond strength between UHPC overlay and conventional concrete substrate made with different types of surface textures, including smooth, low roughness, and high roughness. Slant shear bond strength was found to be highly dependent on the roughness of the surface. The specimens with no surface roughness failed at the interface, whereas those having horizontal grooves and shear keys failed within the repair mortar layer. The results indicate that proper surface preparation yields greater bond strength in the shear/compression than individual substrate material capacity. The splitting tensile capacity of a composite UHPC/concrete test was shown to be not very sensitive to the surface roughness. Most of the specimens experienced failure at the interface with corner breaks or chunk breaks within the concrete half. The horizontally grooved specimens provided the lowest bond strength since the groove did not completely fill with the UHPC overlay material. This resulted in the formation of air voids within the member and lower surface contact area between the two materials. Flexural testing of the composite UHPC/concrete beams yielded no interface failure. Analytical results demonstrated that the maximum stress at the interface ranges from 150 to 200 psi, which is lower than the bond strength observed in the tensile and shear bond tests.

The objective of the study performed by [47] is to evaluate experimentally mechanical properties and permeability characteristics of the interface between normal concrete (NC) substrate which represents old concrete structures and an overlay of UHPFC as a repair material. The different preparation they investigated were (i) as cast; i.e. without surface preparation (AC) as reference;

(ii) sand blasted (SB) purposely exposing the aggregates, (iii) wire brushed (WB) without exposing the aggregates, (iv) drilled holes (DH), each hole having 10 mm diameter and 5 mm depth, and (iv) grooved (GR), with 10 mm width and 5 mm depth. The mechanical interfacial bond characteristics were assessed using the slant shear and splitting tensile tests to quantify the influence of the differently roughened substrate surfaces. Table 3.3 summarizes test results and the associated failure modes. The results showed that the bonding for the surfaced roughened composite specimens is generally strong since most of the composite specimens failed in the NC substrate. The average splitting tensile strength of the composite specimens was similar to or greater than that of the NC substrate specimen. Thus, the UHPFC yielded high bond strength with the NC substrate from the early ages. According to the results, the SB composite specimens achieved the highest splitting tensile strength, with an average tensile strength value of 3.79 MPa recorded at 28 days.

Table 3.3 - Splitting tensile strength and failure type of composite system [47]

Surface treatment	Sample	Max. force P (kN)	T (MPa)	Average T (MPa)	Failure Mode
As cast	1	58.71	1.87	1.85	B
	2	52.7	1.68		A
	3	62.85	2.00		B
Sandblast	1	121.25	3.86	3.79	C
	2	128.36	4.09		C
	3	107.58	3.43		C
Wire brush	1	99.54	3.17	2.96	C
	2	86.64	2.76		C
	3	92.43	2.94		C
Grooved	1	108.13	3.44	3.24	C
	2	100.62	3.20		C
	3	96.11	3.06		C
Drill holes	1	80.03	2.55	2.6	C
	2	89.28	2.84		C
	3	75.39	2.4		C

Type A: pure interfacial failure where no cracking and fracturing can be observed at substrate and the UHPFC.

Type B: interfacial failure combined with minor NC substrate cracking or damage.

Type C: interfacial failure combined with substrate fracture, Type D: substratum failure.

The slant shear test results are summarized in Table 3.4. In general, the interfacial bond strength for all the surface roughened specimens was shown to be adequate as the interfacial failure mostly occurred after the damage of the substrate. In some specimens, the bond strength was distinctively stronger than that of the NC substrate because failure occurred mainly in the substrate without interfacial separation or debonding between the NC substrate and the UHPFC. Overall, the sand blasted (SB) surface specimens exhibited the highest shear bond strength at 28 days of 17.8 MPa compared to the other specimens.

Table 3.4 - Slant shear strength and failure type of composite system [47]

Surface treatment	Sample	Max. Force P (kN)	Shear stress, S (MPa)	Average S (MPa)	Failure Mode
As cast	1	147.63	7.38	8.68	A
	2	208.9	10.45		B
	3	164.39	8.22		B
Sandblast	1	341.67	17.08	17.81	D
	2	362.94	18.15		D
	3	363.82	18.19		D
Wire brush	1	282.66	14.13	12.75	C
	2	213.31	10.67		B
	3	269.2	13.46		C
Grooved	1	294.81	14.74	13.92	D
	2	246.78	12.34		C
	3	293.80	14.69		C
Drill holes	1	222.16	11.11	12.27	C
	2	249.51	12.48		C
	3	264.37	13.22		C

Type A: pure interfacial failure where no cracking and fracturing can be observed at both the NC substrate and the UHPFC overlay.

Type B: interfacial failure combined with minor NC substrate cracking or damage.

Type C: interfacial failure combined with substrate fracture.

Type D: substratum failure.

### 3.5 Conclusions

Given the excellent mechanical properties, low permeability, and high durability, the UHPC can be used as high-performance overlay materials designated for repair and rehabilitation of concrete pavement and bridge deck. It is however, important to understand the effect of

constituent materials on the performance. Mixture optimization of UHPC includes the selection of cementitious materials, proper combinations of aggregates, and the use of adequate type and volume of fibers, which are required to maximize the packing density of the overlay materials.

Modeling study about the UHPC overlay indicated that a decrease in the overlay thickness can reduce interface shear stress but lead to an increase in the tensile stress of the overlay. Therefore, experimental study is needed to verify and optimize the overlay thickness of the UHPC. In addition, proper surface preparation should be employed to the bonded interface.

# Chapter 4 - Optimization of Cementitious Materials for UHPC

This chapter describes the experimental work undertaken to optimize the composition of the cementitious materials used for UHPC. The type and content of SCMs, such as fly ash, GGBS and silica fume, were varied to increase packing density of the powder materials. Binary and ternary combinations of cementitious materials were evaluated for workability, rheology, and compressive strength.

In total, 108 mixtures were investigated to evaluate the workability of the pastes. Minimum water content (MWC) and relative water demand (RWD) were determined for the cement pastes made with various w/cm to evaluate packing density and robustness of the pastes. The selected mixtures that exhibited adequate workability were further used to determine the rheological properties.

## 4.1 Mixing procedure

For a given mixture, mixing time was varied to obtain reliable and consistent results of mini slump testing, as presented in Table 4.1. Four different batches of cement pastes were prepared with different mixing times. The mixing time was increased for step 3 from 3 to 12 minutes. The result showed that 9 minutes of mixing for the last step was adequate to provide homogenous cement paste as the slump diameter became steady (270 mm) beyond the 9 minutes mixing. The optimized mixing time was employed to all the investigated pastes. Mixing procedure used for the workability evaluation of cement pastes is presented in Figure 4.1.

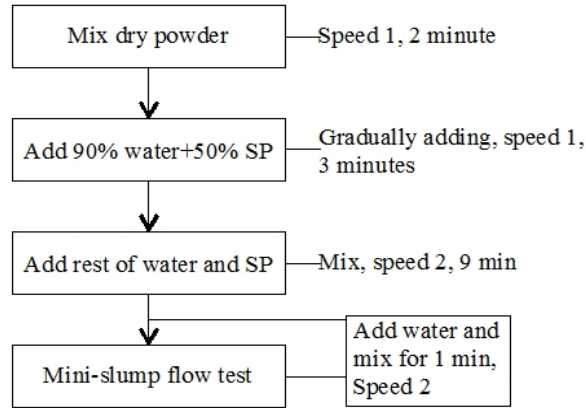


Figure 4.1 - Mixing procedure for workability tests of cement paste

Table 4.1 - Optimization of mixing time

Mixing procedure	HRWR/ powder	w/c m	Test time (min)	Slump flow (mm)
Step 1: Dry materials for 3 min			3	230
Step 2: Add 90%+50%HRWR speed 1 for 3 min	4%	0.18	6	250
Step 3: Add 10% water + 50% HRWR speed 2 for			9	270
various test time			12	270

#### 4.2 Test methods used for the optimization

In this research, mini slump test was used to determine minimum water content (MWC) to initiate flow and relative water demand (RWD) to increase a given flowability, which are closely related to the packing density and robustness, respectively. As indicated in Figure 4.2, the test consists of determining the variations of fluidity of a given mortar with changes in water-to-powder ratio ( $W/P$ ), by volume ( $W_v/P_v$ ). The intercept of the curve with the ordinates axe ( $W_v/P_v$ ) and the slope of the curve represent the MWC to initiate flow and RWD to increase a given fluidity, respectively. For each mixture, a minimum of five  $W_v/P_v$  values was used to evaluate two flow parameters. After the completion of mixing, the paste was poured into a cone to full capacity in accordance with ASTM C230/C230M. The cone was then removed, allowing the paste to spread on the plate while the plate remained steady. After 30 seconds, the spread value was measured. In addition, 50-mm cube specimens were sampled for testing the

compressive strength. These specimens were demolded after 24 hours and then, were cured in lime-saturated water at  $23 \pm 3$  °C until the age of testing. The cement paste mixtures used for the workability and packing density evaluation were made using 20-quart capacity mixer (Figure 4.3).

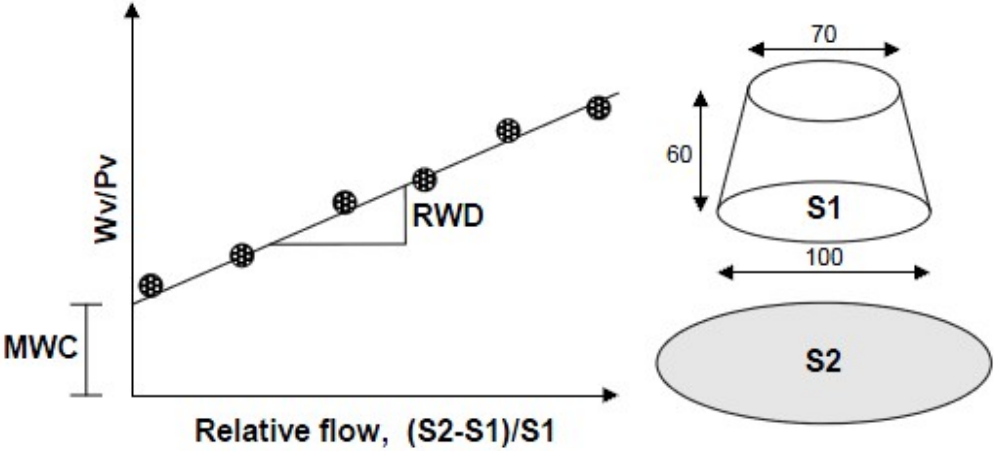


Figure 4.2 - Definition of MWC and RWD parameters from mini slump test



Figure 4.3 - Hobart Mixer

Unit weight was determined in accordance with ASTM C138. The flow cone with 19-mm opening diameter was used to determine the flow time that is related to flowability and viscosity.

This test method determines the time of efflux of a specified volume of the mortar through a standardized flow cone in accordance with ASTM C939.

Modular compacter rheometer (MCR) was used to evaluate the rheological properties of cement paste. The initial rheology testing was carried out at the age of 20 min after the initial water addition. The retention of rheological properties was monitored up to 90 min (30, 60, and 90 min). The first step in the rheology testing involved the determination of static yield stress using the shear growth approach. The paste was allowed to be sheared at a low rate of 0.01 per sec for 60 sec (Figure 4.4). For the evaluation of dynamic yield stress and plastic viscosity, the paste in the rheometer then underwent a pre-shearing period for one minute at a high shear rate of  $100 \text{ s}^{-1}$  before each testing to minimize any effect of structural build-up on the dynamic test results. Then, the shear rate was reduced by  $10 \text{ s}^{-1}$  at 5 sec intervals until the shear rate became zero. The paste was not agitated between each testing campaign to monitor the rate of structural build up with respect to time.

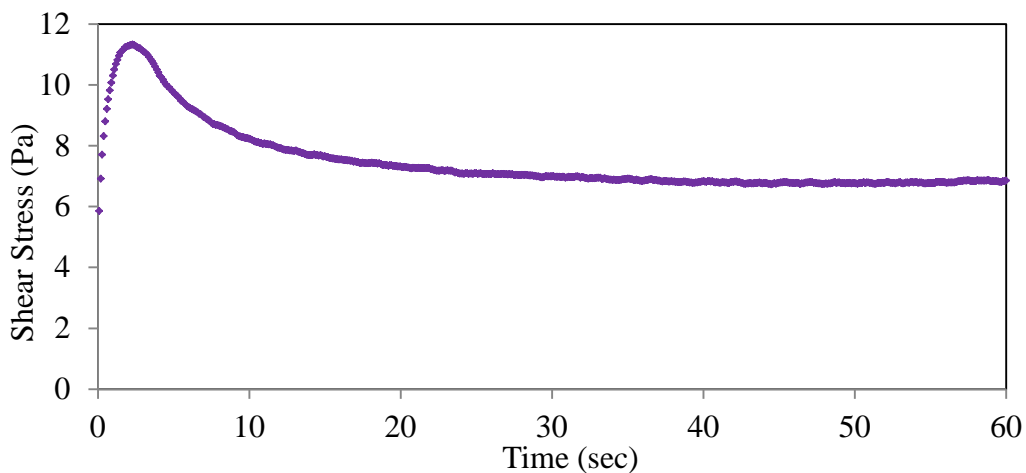


Figure 4.4 - Static yield stress

Figure 4.5 presents typical variations of torque with respect to shearing time. Torque value for

each shear rate was stabilized after certain period of time, and then the torque of equilibrium was used to determine dynamic yield stress and plastic viscosity. It is important to note that the shearing time should be long enough to ensure that the flow of the paste reaches an equilibrium condition, thus indicating the complete breakdown of the material. The set up used for this step procedure is shown in Figure 4.6.

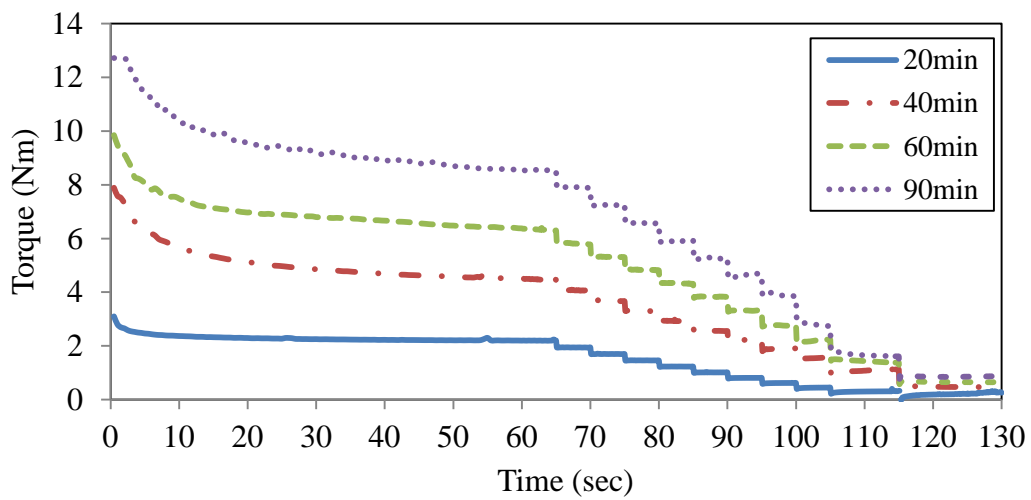


Figure 4.5 - Torque values as a function of time



Figure 4.6 - Rheology test set up

Given the non-linear relationship between shear rate and the shear stress, the modified Bingham model was used for the interpretation of the rheological parameters since the modified model provides a better description of the non-linear behavior. The modified Bingham model is expressed in Equation (1):

$$\tau = \tau_0 + \mu \cdot \dot{\gamma} + c \cdot \dot{\gamma}^2 \quad (1)$$

c - Second order term: modified Bingham model (Pa.s<sup>2</sup>);

$\dot{\gamma}$  - Shear rate (s<sup>-1</sup>);

$\tau_0$  - Yield stress (Pa);

$\tau$  - Shear stress (Pa).

$$\tau_0 = \frac{\left(\frac{1}{R_i^2} - \frac{1}{R_o^2}\right)}{4\pi h \ln\left(\frac{R_o}{R_i}\right)} G, \mu = \frac{\left(\frac{1}{R_i^2} - \frac{1}{R_o^2}\right)}{8\pi^2 h} H \quad \text{and}$$

$$c = \frac{\left(\frac{1}{R_i^2} - \frac{1}{R_o^2}\right)}{8\pi^3 h} \frac{(R_o - R_i)}{(R_o + R_i)} C$$

where:  $R_i$  = Inner cylinder radius of coaxial cylinders rheometer (m);

$R_o$  = Outer cylinder radius of coaxial cylinders rheometer (m);

G = Intercept of curve in T-N graph with T-axis (Nm);

H = First order term of second order curve in T-N graph: modified Bingham model (Nm s);

C = Second order term of second order curve in T-N graph: modified Bingham model (Nm s);

h = Height of the inner cylinder submerged in concrete in coaxial cylinders rheometer (m).

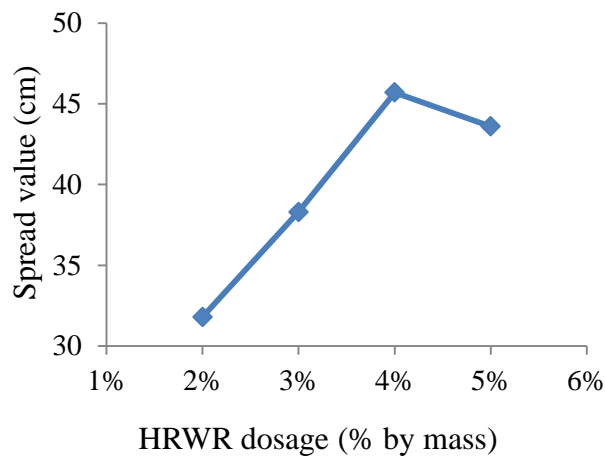
The compressive strengths of the cement pastes were determined using 50 mm cubes in accordance with ASTM C39 at the age of 1, 3 and 28 days. The samples were demolded after 24 hours and saturated in lime-saturated water until the time of testing.

#### 4.3 Optimization based on flow properties

The cement content of UHPC is generally between 800 and 1000 kg/m<sup>3</sup>. A high amount of

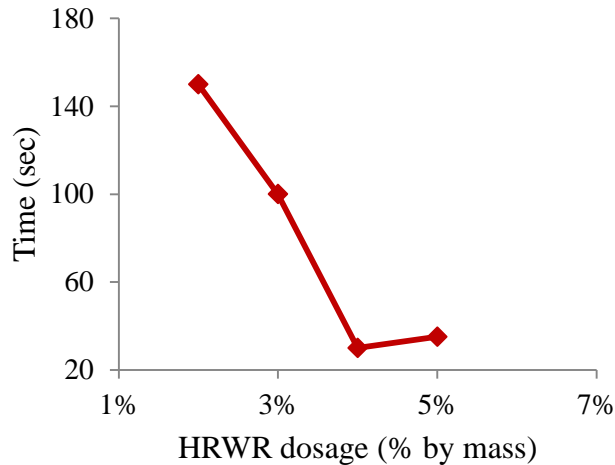
cement not only increases the production costs, but also has a negative effect on the heat of hydration and shrinkage cracking. Replacing cement with a SCM is a feasible solution to these problems. Furthermore, incorporation of SCMs may positively affect the durability of concrete. The aim of studying binary and ternary cementitious systems is to decrease the cement and SF content of the UHPC using with FAC and/or GGBS.

Since HRWR have an important role in producing UHPC, especially with very low w/cm, before beginning the optimization process for SCMs, the type and optimum dosage of HRWR was carefully selected. Polycarboxylate-based superplasticizer was used as a HRWR in this study. Saturation point of HRWR for a given w/cm was determined by measuring the flow cone and mini slump tests with respect to the dosage of the HRWR. The slump spread and flow cone results were stayed a given values beyond 4% of the HRWR, the weight of total cementitious materials, as presented in Figure 4.7. The 4% HRWR concentration was used for all the cement pastes for this optimization.



(a) Spread value vs. HRWR dosage

Figure 4.7 - Results of saturation point for HRWR



(b) Flow time vs. HRWR dosage

Figure 4.7 (cont'd) - Results of saturation point for HRWR

Different types and contents of SCMs were used to optimize cementitious materials that increase the packing density of cement paste. Table 4.2 and Figure 4.8 compare the effect of the binder type and content on the MWC and RWD. It should be noted that Class C and F fly ash, silica fume, and GGBS are coded as “FAC”, “FAF”, “SF”, and “G”, respectively, for mixture codifications. Numbers in front of these abbreviations indicate the percentage of replacement for each SCM.

For the binary system, the increase in FAC is shown to reduce MWC and increase RWD. The replacement rate that led to the highest packing density (the lowest MWC) varied with the type of SCM. For example, in the case of Class C fly ash, the FAC containing 60% of Class C fly ash had the lowest MWC, thus indicating the higher packing density among the FAC group. On the other hand, the G50 made with 50% GGBS replacement exhibited the best performance for corresponding category. Based on the flow characteristics, the 60% FAC, 5% SF, and 50% GGBS that had the highest packing density (lowest MWC) and robustness (highest RWD) in each SCM were selected to use for further optimization of ternary system.

MWC and RWD results of binary and ternary systems are compared in Figure 4.8. In the case of ternary system, the G50SF5 mixture containing 5% SF and 50% GGBS replacement had the highest RWD and lowest MWC. In the case of quaternary systems, the FAC40SF5G10 mixture with 40% FAC, 5% SF, and 10% GGBS achieved high robustness and low water demand. Among all the investigate pastes, the FAC60 yielded the lowest MWC and the highest RWD. Mixtures exhibited excessively high MWC or low RWD were excluded for further optimization of rheological properties and compressive strength. The mixtures selected for the further optimization are detailed in the following section.

Table 4.2 - Test result of workability

Code	RWD	MWC	r <sup>2</sup>	Code	RWD	MWC	r <sup>2</sup>
Ref	0.09	0.51	0.99	FAC40SF5	0.13	0.23	1.00
G70	0.10	0.38	0.99	FAC50SF5	0.14	0.21	0.98
G60	0.12	0.34	0.98	FAC50SF8	0.14	0.22	0.98
G50	0.14	0.26	0.98	FAC60SF5	0.10	0.39	0.98
G40	0.10	0.41	1.00	G60SF5	0.13	0.30	0.99
FAC60	0.20	0.12	0.97	G50SF5	0.16	0.20	0.98
FAC50	0.13	0.22	0.99	G40SF5	0.10	0.38	0.99
FAC40	0.11	0.22	0.98	G50SF8	0.11	0.31	0.99
FAC30	0.11	0.25	0.98	G50SF11	0.11	0.31	0.99
SF5	0.11	0.44	0.97	FAC40SF5G30	0.14	0.25	1.00
SF8	0.09	0.48	0.97	FAC40SF5G20	0.12	0.24	0.99
SF11	0.10	0.45	0.98	FAC40SF5G10	0.15	0.15	0.99
SF14	0.09	0.50	0.98				
SF20	0.10	0.48	0.97				
SF25	0.11	0.51	0.98				

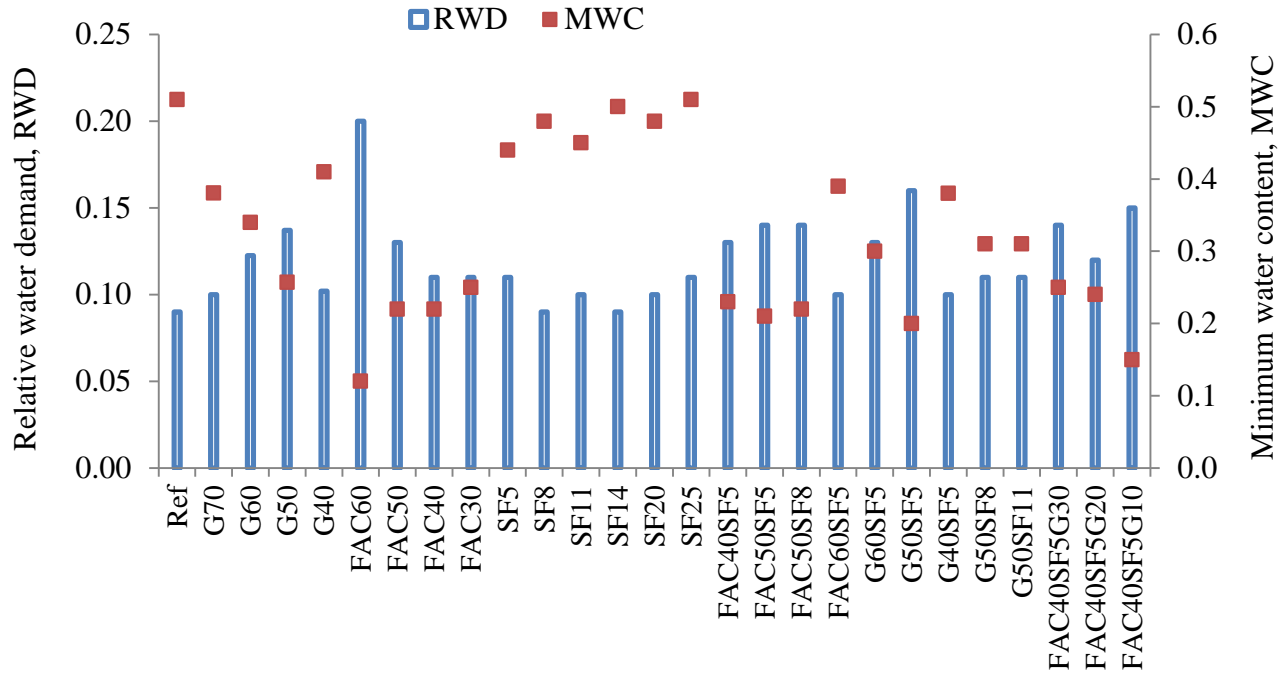


Figure 4.8 - Effect of binder type on minimum water content and relative water demand

#### 4.4 Optimization based on compressive strength

Mixtures that exhibited adequate flow characteristics were tested for compressive strength. Figure 4.9 shows the 1 day compressive strength and mini-slump value for the selected mixtures. As expected, the addition of silica fume led to a significant increase in the 1-day compressive strength. It should be noted that however, the silica fume mixtures exhibited lower slump spread compared to those containing the other SCMs.

The 28-day compressive strengths are compared in Figure 4.10. In general, mixtures containing GGBS exhibited higher 28-day compressive strength compared to those with Class C and Class F fly ash. For example, the G50SF5 paste developed 28-day compressive strength greater than 140 MPa, and that of the G50 mixture was close to 140 MPa. On the other hand, the compressive strengths of binary mixtures containing fly ash were between 123 and 128 MPa. The addition of 5% silica fume to the 40% FAC mixture led to considerable increase in the compressive strength.

It is important to note that beyond 5%, the incorporation of silica fume did not contribute to the strength increase. All the compressive strength results are summarized in the Table 4.3.

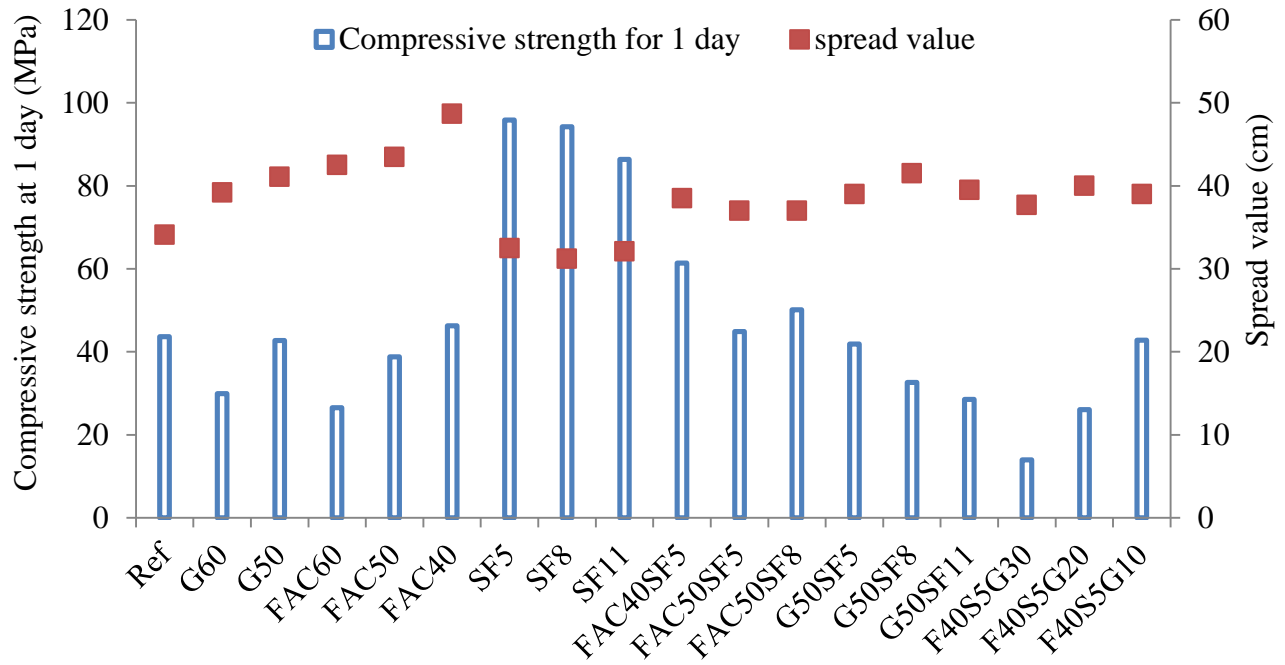


Figure 4.9 - Compressive strength at 1 day and slump spread results

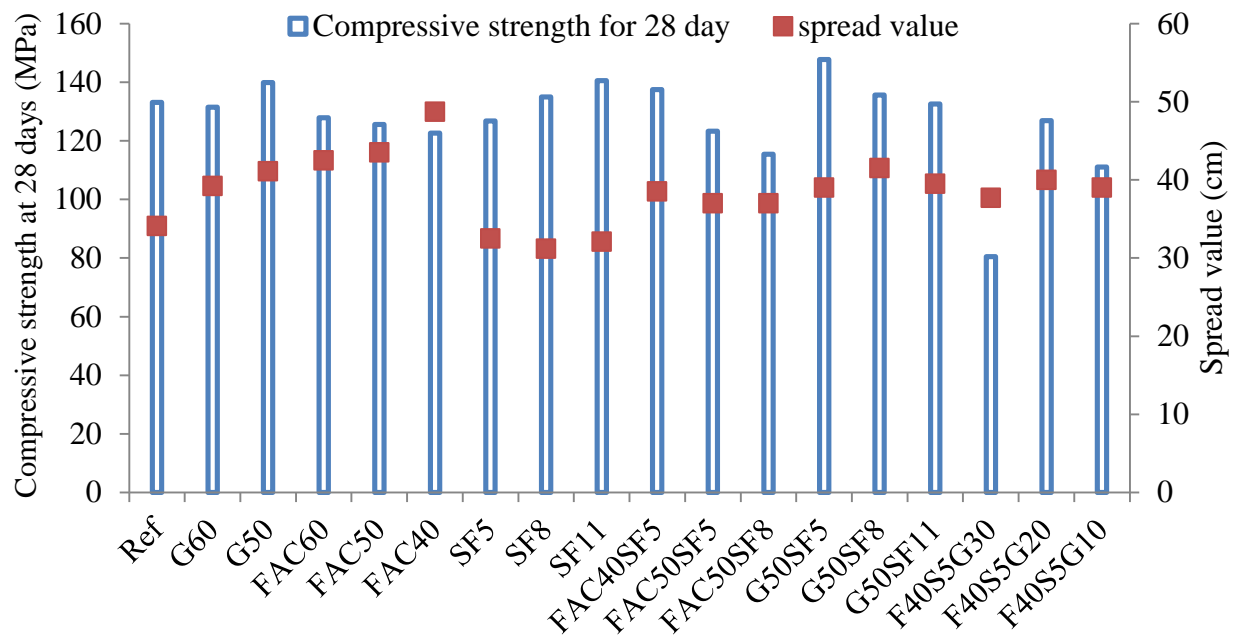


Figure 4.10 - Compressive strength at 28 days vs. spread value

Table 4.3 - Summary of testing result

Code	f <sub>c</sub> , 1day (MPa)	f <sub>c</sub> , 28days (MPa)	flow time (sec)	spread value (mm)	RWD	MWC
Ref	43.7	133.1	47	340	0.09	0.51
G60	29.9	131.4	34	390	0.12	0.34
G50	42.7	139.9	44	410	0.14	0.26
FAC60	26.5	127.9	16	420	0.20	0.12
FAC50	38.8	125.6	17	430	0.13	0.22
FAC40	46.2	122.6	13	480	0.11	0.22
SF5	95.8	126.7	43	320	0.11	0.44
SF8	94.21	134.9	49	310	0.09	0.48
SF11	86.3	140.5	48	320	0.10	0.45
FAC40SF5	61.4	137.4	33	380	0.13	0.23
FAC50SF5	44.9	123.3	31	370	0.14	0.21
FAC50SF8	50.1	115.4	33	370	0.14	0.22
G50SF5	41.9	147.7	35	390	0.16	0.20
G50SF8	32.6	135.6	34	410	0.11	0.31
G50SF11	28.5	132.6	37	390	0.11	0.31
F40S5G30	13.9	80.5	32	370	0.14	0.25
F40S5G20	26.0	126.8	28	400	0.12	0.24
F40S5G10	42.8	111.1	31	390	0.15	0.15

#### 4.5 Optimization based on rheological properties

In this phase, cement paste was considered as a concentrated suspension of cement particles in water. Therefore, the yield stress and plastic viscosity depends on the particle size distribution and concentration of the cement. For the rheology test, the initial w/cm was set at 0.23, by mass (0.73, by volume), and the HRWR was adjusted to secure a targeted mini slump flow of 350 mm. HRWR dosages to secure the targeted slump flow are presented in Figure 4.11. The use of high volumes of GGBS and FAC, the HRWR demand can be reduced by more than 75% compared to the reference (C100) and SF5 mixtures. It can be observed that the FAC60 and G50SF5 mixtures required relatively low HRWR content to obtain 350 mm spread value.

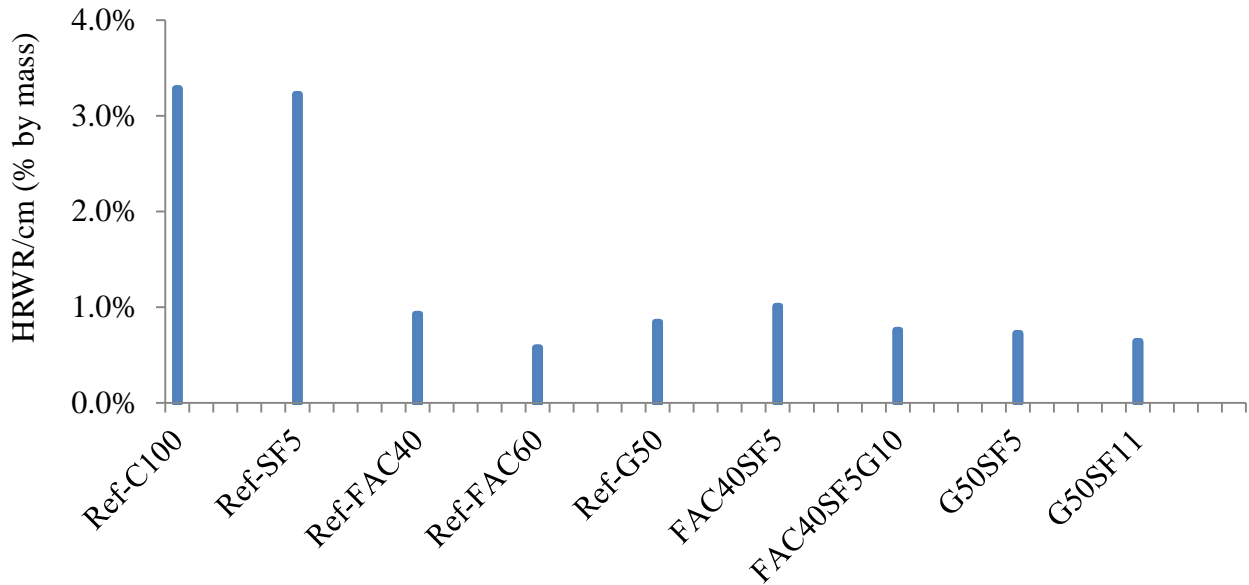


Figure 4.11 - HRWR demand

Figures 4.12 to 4.15 present the viscosity results determined at 20 to 90 min. For a given w/cm, low viscosity indicates greater packing density. The G50 mixture had the lowest viscosity, which could be related to the high packing density of this mixture. However, this is different than the MWC results, which proved that the FAC60 mixture had the highest packing density. This is in part due to the difference in surface texture of the particle of FAC and GGBS. In general, GGBS particles have glassier surface, which reduce the viscosity of the mixture. As presented in Figure 4.12 to 4.15, the G50 mixture containing 50% GGBS had the lowest plastic viscosity at all testing ages among the tested mixtures. The reduction in the viscosity by the use of GGBS can be good solution to develop UHPC with very low w/cm, however, care should be taken to adjust its content to ensure stability of the GGBS mixture due to the glassy surface of the GGBS particle. Further research should be carried out to find the appropriate indirect way of expressing packing density of cementitious materials.

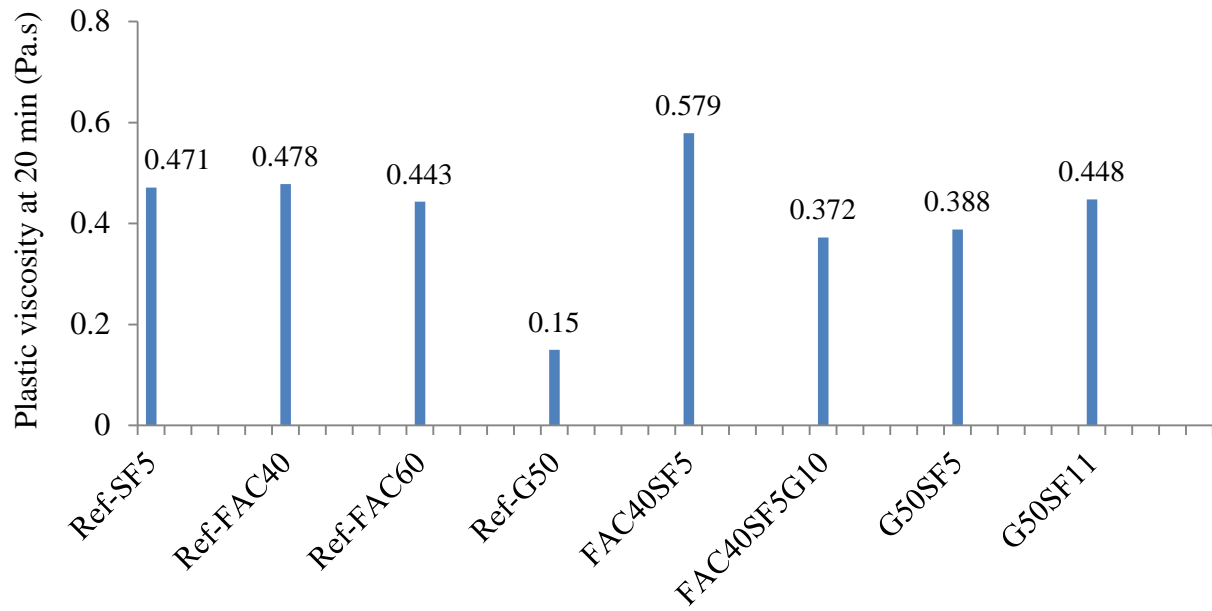


Figure 4.12 - Plastic viscosity at 20 minute

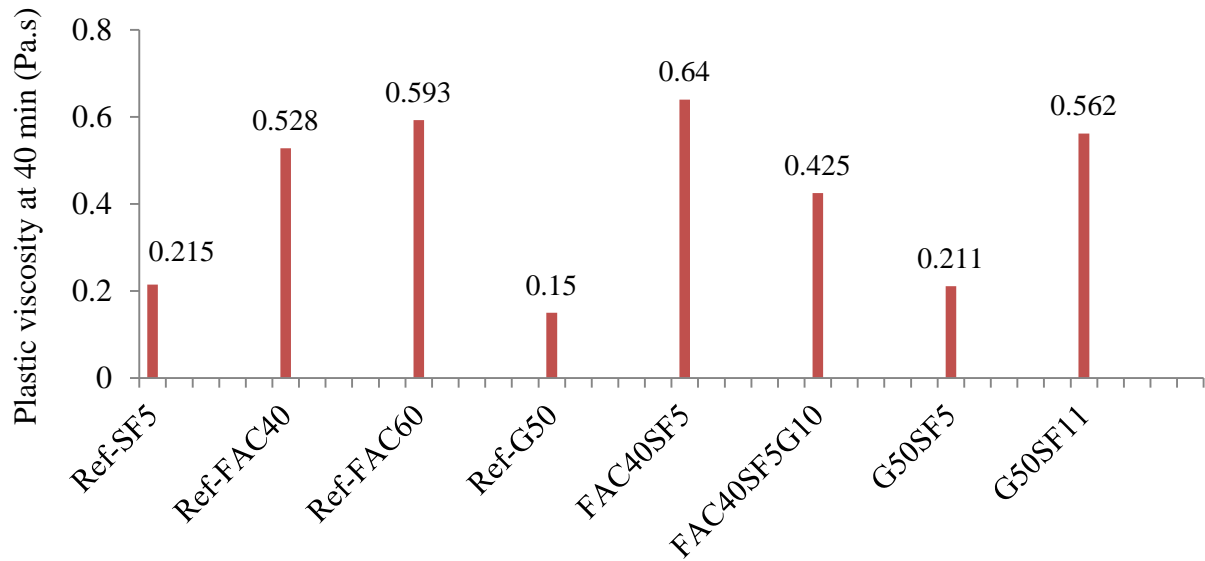


Figure 4.13 - Plastic viscosity at 40 minutes

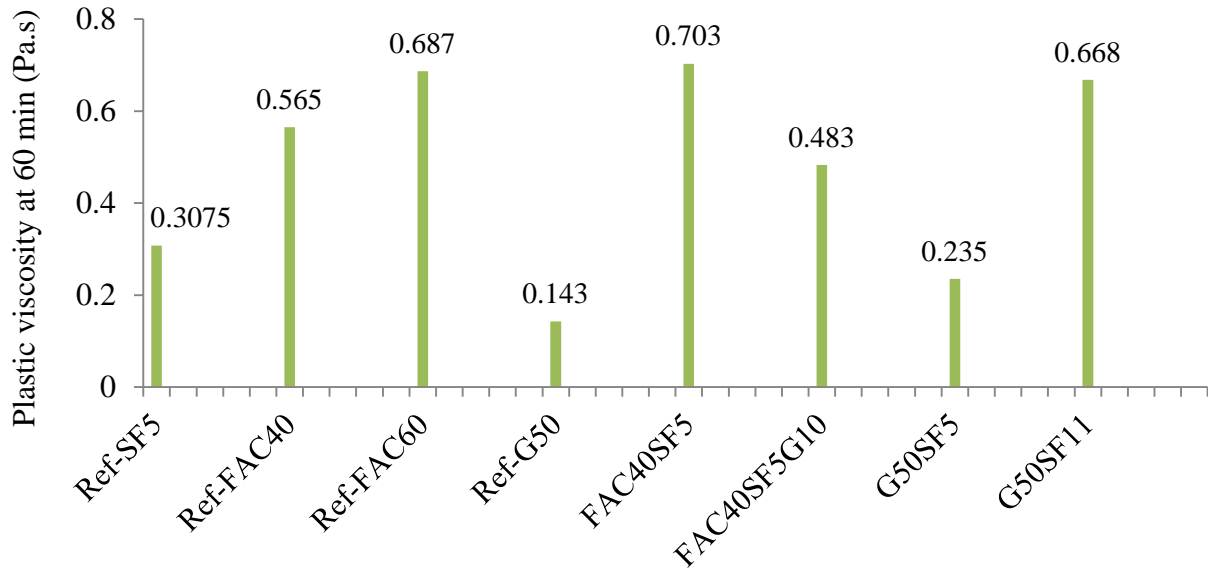


Figure 4.14 - Plastic viscosity at 60 minutes

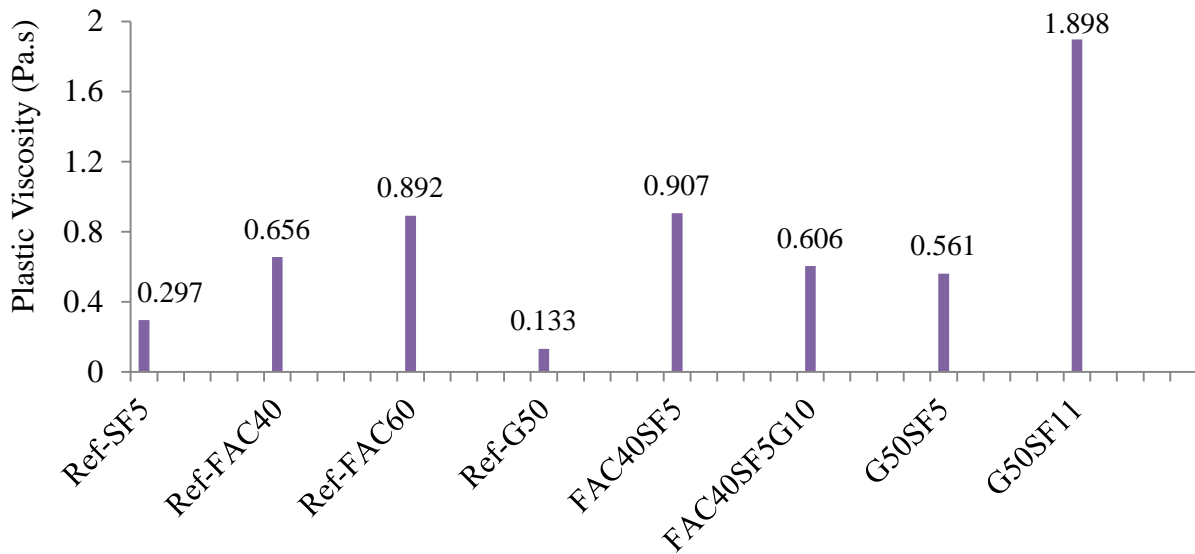


Figure 4.15 - Plastic viscosity at 90 minutes

#### 4.6 Comparison of overall performance

Flowability, compressive strength, and rheological properties were investigated in order to optimize the cementitious materials for UHPC. Since the effects of these parameters are not the

same degree of importance, especially for the intended application, it was proposed to assign appropriate weight to each parameter in order to have the actual and effective optimization results. A star plot was used to compare various properties and synthesize the overall performance of the investigated mixtures. The results of flowability, compressive strength, viscosity, yield stress and slump loss at different times are presented in Tables 4.4 to 4.6.

Table 4.4 - Flowability and compressive strength results

Code	f <sub>c</sub> , 1 day (MPa)	f <sub>c</sub> , 28 days (MPa)	Flow time (sec)	Spread (mm)	RWD	MWC
Reference	43.7	133.1	47	340	0.09	0.51
G60	29.9	131.4	34	390	0.12	0.34
G50	42.7	139.9	44	410	0.14	0.26
FAC60	26.5	127.8	16	420	0.2	0.12
FAC50	38.8	125.6	17	430	0.13	0.22
FAC40	46.25	122.6	13	480	0.11	0.22
SF5	95.8	126.7	43	320	0.11	0.44
SF8	94.2	134.9	49	310	0.09	0.48
SF11	86.3	140.5	48	320	0.1	0.45
FAC40SF5	61.4	137.4	33	380	0.13	0.23
FAC50SF5	44.9	123.3	31	370	0.14	0.21
FAC50SF8	50.1	115.4	33	370	0.14	0.22
G50SF5	41.9	147.7	35	390	0.16	0.2
G50SF8	32.6	135.6	34	410	0.11	0.31
G50SF11	28.5	132.6	37	390	0.11	0.31
F40S5G30	13.9	80.5	32	380	0.14	0.25
F40S5G20	26.1	126.8	28	400	0.12	0.24
F40S5G10	42.8	111.1	31	390	0.15	0.15

Table 4.5 - Viscosity and yield stress results at different times

Code	Viscosity at 20 min (Pa.s)	Viscosity at 40 min (Pa.s)	Viscosity at 60 min (Pa.s)	Viscosity at 90 min (Pa.s)	Yield stress at 20 min (Pa)	Yield stress at 40 min (Pa)	Yield stress at 60 min (Pa)	Yield stress at 90 min (Pa)
Reference	0.36	0.48	0.49	0.47	7.15	9.04	7.91	23.7
G50	0.15	0.15	0.14	0.13	3.37	14.23	19.29	224.0
FAC60	0.44	0.59	0.69	0.89	16.86	61.60	98.39	196.7
FAC40	0.48	0.53	0.56	0.65	12.26	37.41	41.10	131.6
SF5	0.47	0.21	0.31	0.29	26.02	10.20	10.26	30.26
FAC40SF5	0.58	0.64	0.71	0.91	15.90	51.61	69.72	214.7
G50SF5	0.38	0.21	0.23	0.56	69.99	19.33	26.19	438.2
G50SF11	0.44	0.56	0.67	1.89	33.61	60.73	80.26	642.1
F40S5G10	0.37	0.42	0.48	0.61	14.60	17.67	24.76	79.2

Table 4.6 - slump loss at different times

Code	Slump loss at 25 min (%)	Slump loss at 45 min (%)	Slump loss at 65 min (%)	Slump loss at 95 min (%)	HRWR/cm (%)
Reference	1.9	4.2	1.4	1.1	3.2
G50	2.7	12.5	45.8	72.2	0.8
FAC60	11.6	28.9	31.1	28.9	0.5
FAC40	4.3	10.1	10.7	12.4	0.9
SF5	-0.3	1.1	4.1	-1.7	3.2
FAC40SF5	10.6	18.6	21.4	27.8	1.1
G50SF5	2.8	5.6	8.4	23.9	0.7
G50SF11	12.2	23.1	32.8	45.6	0.6
F40S5G10	6.9	1.3	5.5	12.2	0.8

Two sets of weights were applied to compare overall performance in the start diagram. The plastic viscosity was measured using a rotational rheometer as a direct method, and flow time as an indirect method of characterizing flow characteristics of the cement paste. Both results are related to viscosity. It is not appropriate to consider both the flow time and plastic viscosity for the performance comparison chart, since they were not independent (interrelated). This is the same case for the spread value and dynamic yield stress.

Weight factor used in the star plot was determined based on the degree of importance of each property for this type of cement-based materials. In this research, fresh properties such as spread value, flow time, plastic viscosity and yield stress at 60 min, and 28-day compressive strength were considered as the key factors on the performance. For the first stage of performance comparison, the weight factors presented in Table 4.7 were applied on the flowability and compressive strength. The Star plots presented in Figures 4.16 and 4.17 indicated that high volume of Class C fly ash, especially FAC60, exhibited the best overall performance. Further rheology tests were carried out to confirm the findings.

Table 4.7 - Weight factor set I

	$f'_c$ , 1day	$f'_c$ , 28 days	1/flow time	spread value	RWD	1/MWC
Weight factor set I	1	3	3	3	2	2

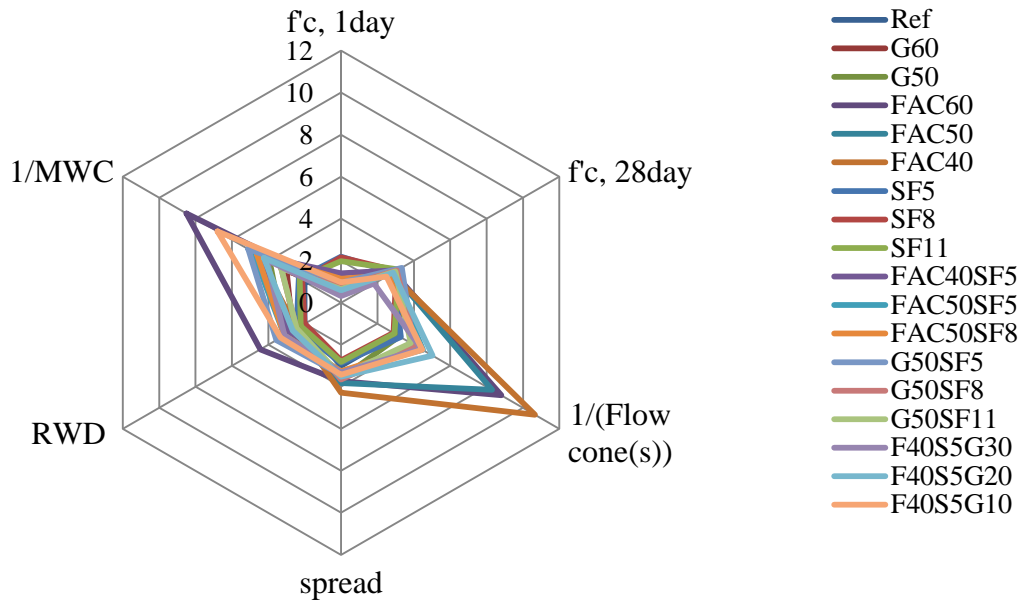


Figure 4.16 - Weighted amounts of flowability and compressive strength parameters- weight factor set I

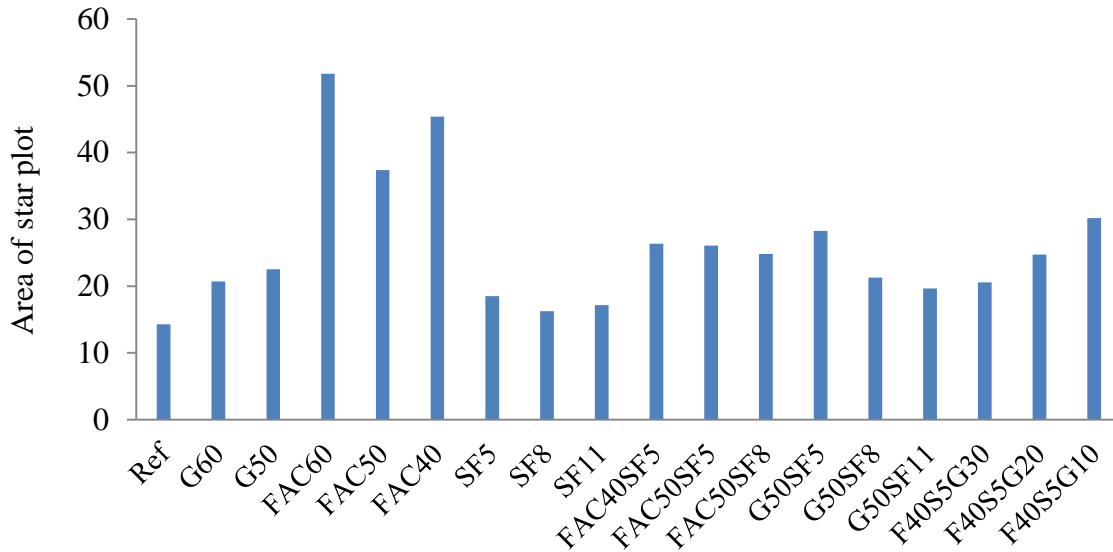


Figure 4.17 - Area for star plot representing overall performance – weight factor set I

The second set of weight factors was listed in Table 4.8. Star plot that compares overall performance with the second set of weights is presented in Figure 4.18, and the performance area of each mixture is compared in Figure 4.19. From the presented results, the FAC60 and G50SF11 mixtures were shown to have greater performance area, which indicating better overall performance of these mixtures. The G50, FAC40, FAC40SF5, G50SF5 and FAC40SF5G10 can be considered as the second best performance.

Table 4.8 - Weight factor set II

	f'c, 1 day	f'c, 28 day	1/Flow time	spread value	RWD	1/MWC	Spread Value (60 min)
Weight factor II	1	3	3	3	2	2	2

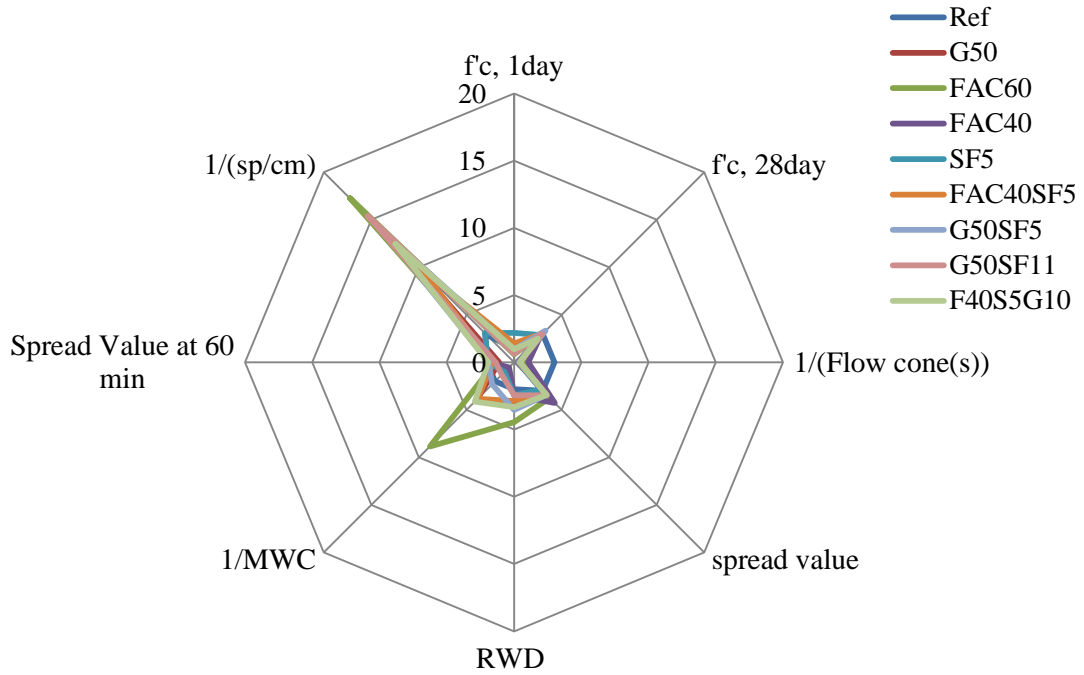


Figure 4.18 - Weighted amounts of flowability and compressive strength - weight factor set II

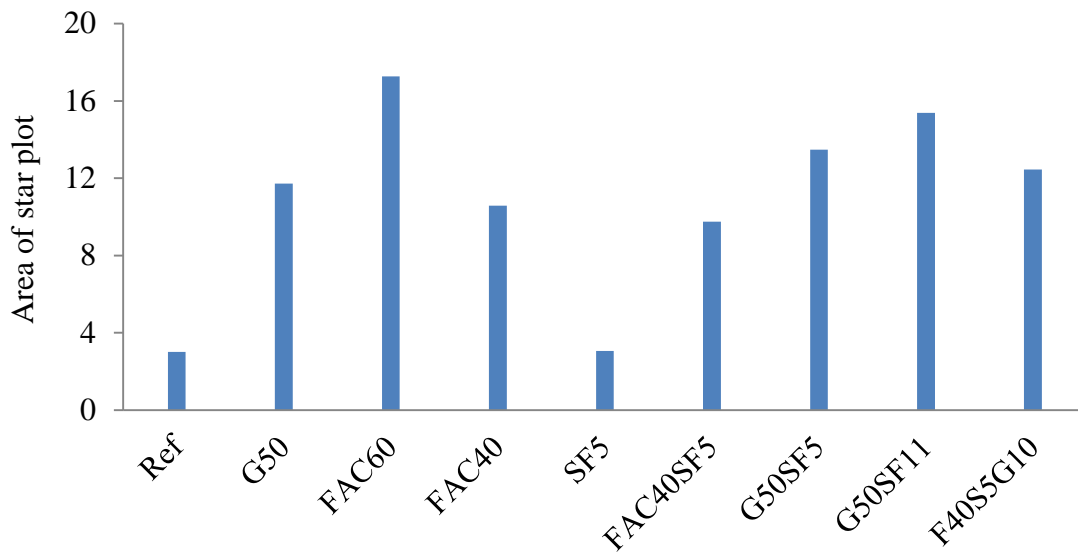


Figure 4.19 - Area for weighted amounts of flowability and compressive strength - weight factor set II

## 4.7 Conclusions

Based on the performance comparison reported in this chapter, the G50, FAC60, FAC40SF5, and G50SF5 mixtures were selected for the optimized paste mixtures for UHPC. The optimized pastes were used for further optimization of aggregates and fibers and were evaluated for key engineering properties.

## Chapter 5 – Optimization of Fine Aggregate

The packing density of aggregate particles has marked effect on performance of concrete. In this study, fine aggregates of different size and gradation were combined to increase the packing density of the materials. The packing density of the aggregates was determined using the gyratory compaction tester. The optimized combination of the fine aggregates were then, used for various mortar mixtures that were prepared with different contents of total aggregates to secure maximum packing density of the UHPC materials. The rheological properties of the mortars were also determined using ConTec viscometer 5.

### 5.1 Preparation of mortar

River sand (0-5 mm) and masonry sand (0-2 mm) were combined at various combinations in order to reach the possible highest packing density. Optimized combination of fine aggregates with highest packing density was used for the five mortar mixtures that are prepared with different aggregate contents of 0.8, 1, 1.2, 1.3, and 1.4, by volume of cementitious materials. The mortars were evaluated for workability, mechanical properties, and rheological behavior. In this step, mixer with a maximum capacity of 20 quarts was used in order to make mortar with different contents of optimized aggregates. The mortars were prepared with the mixing procedure presented in Figure 5.1 and in 5-liter batch quantity.

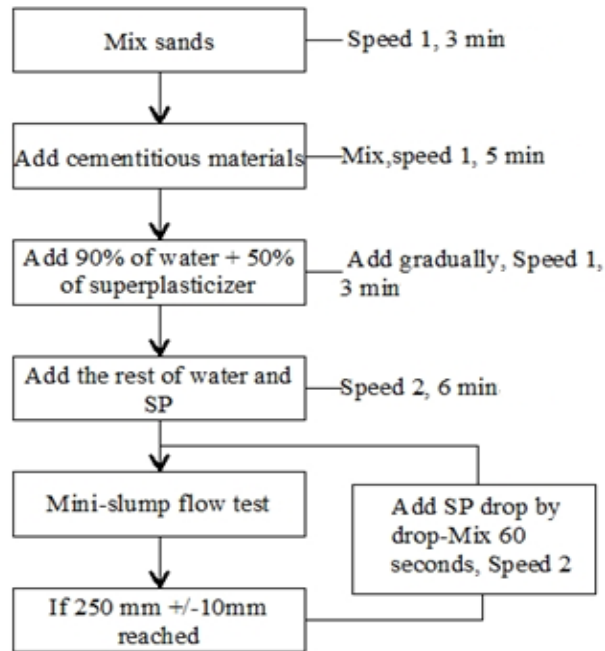


Figure 5.1 - Mixing procedure for making mortar

## 5.2 Test methods

Gyratory compaction tester was used to determine the packing density of different combinations of fine aggregates, as showed in Figure 5.2. In this method, a sample of aggregate is compacted by a continuous gyratory action, consisting of axial pressure and shear. Shear movement under constant pressure allows particles to move closer to one another to reach a higher level of density. The constant vertical pressure, applied to a material in the compaction tester, is obtained by compressing the mass in a test cylinder between top and bottom plates. Gyratory movement of the cylinder during the test creates the required shear force. Measurement setup parameters defined to the compaction tester are summarized in Table 5.1.

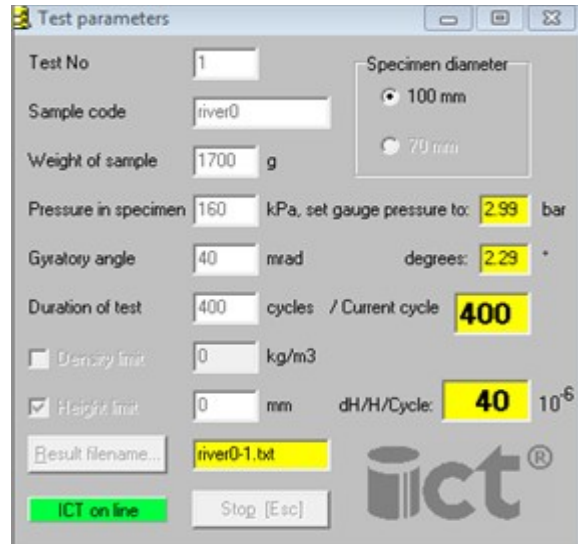


Figure 5.2 - Gyratory compaction tester

Table 5.1 - Measurement setup parameters used for gyratory compaction tester

Parameters	Values
Cylinder diameter	100 mm
Sample height	100 mm
Air pressure	4 bar
Gyrator angle	40 micro rad
Number of cycles	200 cycle
Working speed	60 rpm

### 5.3 Optimization of aggregate combination and content

Dry packing density results of various combinations of aggregates are presented in Table 5.2. A combination of 30% masonry sand (0-2 mm) with 70% river sand (0-5 mm) exhibited the highest density of 1870 kg/m<sup>3</sup> among the various combinations, thus indicating the highest packing density of that aggregate combination.

Table 5.2 - Results obtained from Gyratory compaction tester

River sand (% by mass)	0	10	50	60	70	80	90	100
River sand (g)	0	130	650	780	910	1040	1170	1300
Masonry sand (g)	1300	1170	650	520	390	260	130	0
Density (kg/m <sup>3</sup> )	1727.5	1754	1825	1850	<b>1870</b>	1855	1860	1857

The mortars were tested for rheological properties to assess the effect of the aggregate content on the wet packing density. Variations of the rheological properties of the mortar mixtures with respect to time are presented in Table 5.3. The HRWR dosage was adjusted to secure the same mini slump spread. According to obtained results, three selected mixture were planned to further investigations considering flowability and compressive strength parameters. The results are presented in Table 5.4. Results indicated that the flow time increased with the increase in agg/cm. The compressive strengths at 1, 7, and 28 days were similar, regardless of the aggregate contents. Figure 5.3 compares the HRWR demand of mortars with various aggregate contents with constant slump flow of 250 mm. In general, the increase in aggregate content reduced the HRWR demand.

Table 5.3 - rheological properties of the mortars with different aggregate contents

Agg/cm (% by volume)	Testing Time (min)	Slump (mm)	HRWR (%)	HRWR/cm	Plastic viscosity (Pa.s)	Yield stress (Pa)
1	first	251	36	0.008	6.3	30.5
	20	213				
	40	143				
	60	109				
1.2	first	263	29.4	0.007	5.4	21.4
	20	210				
	40	147				
	60	100				
0.8	first	246	51.9	0.01	12.04	23.8
	20	150				
	40	107				
	60	100				
1.3	first	245	22.3	0.005	7.5	26.2
	20	194				
	40	172				
	60	134				
1.4	first	247	22.84	0.006	7.5	26.5
	20	225				
	40	174				
	60	119				

Table 5.4 - Flow properties and compressive strength of selected mixtures

Agg/cm	Mini-slump (mm)	Flow time (sec)	1-day compressive strength (MPa)	7-day compressive strength (MPa)	28-day compressive strength (MPa)
1	332	64	42.3	88.4	123.2
1.2	322	104	43.2	87.4	111.3
1.4	301	129	43.6	83.2	115.6

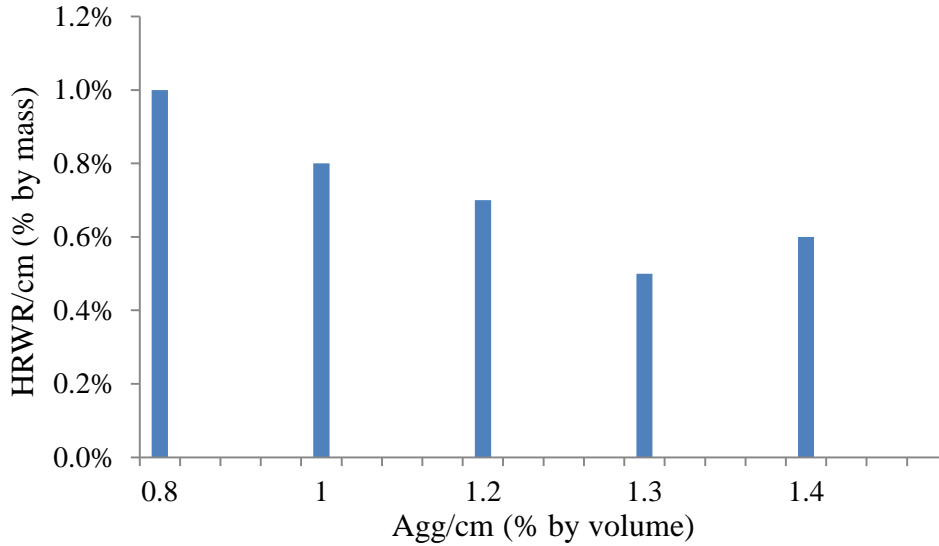


Figure 5.3 - HRWR demand

Similar to the optimization of cementitious materials, star plots were used to compare overall performance of the UHPC mortars made with different aggregate contents. The first set of weight factor for this comparison is summarized in Table 5.5. As presented in Figures 5.4 and 5.5, the first performance comparison was carried out using only rheological properties. The mortar made with agg/cm of 1.2 exhibited the best rheological behavior among the five mixtures. The three mortars containing the aggregate contents of 1, 1.2, and 1.3 were compared for the workability and compressive strength.

Table 5.5 - Weight factor set I

	1/ (HRWR/cm)	1/plastic viscosity at 20 min	1/plastic viscosity at 60 min	1/static yield stress at 20 min	1/static yield stress at 60 min
Weight factor I	3	3	2	3	2

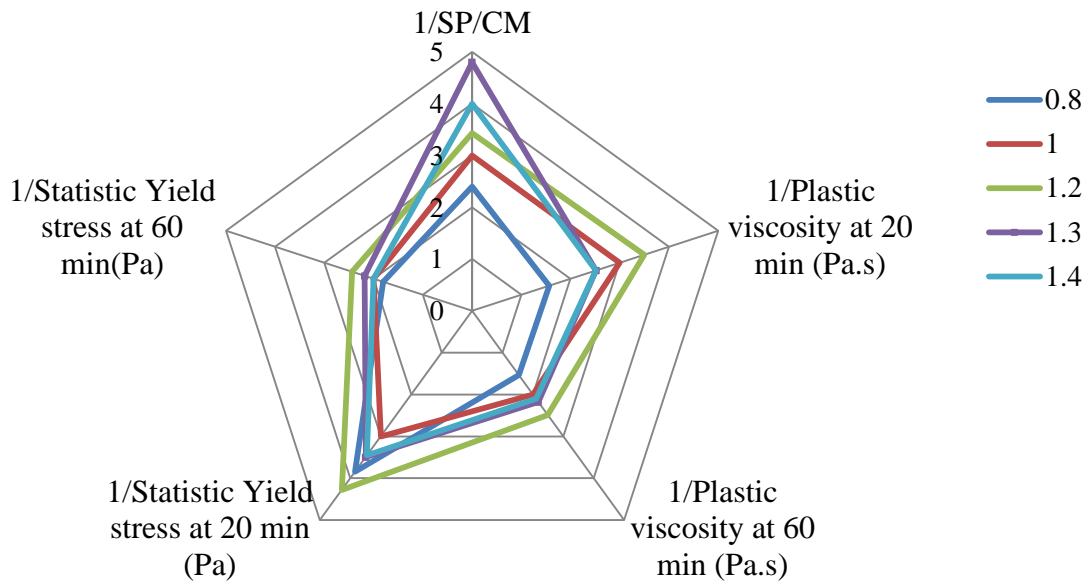


Figure 5.4 - Star diagram to compare rheological performance of the mortars made with different aggregate contents - weight factor set I

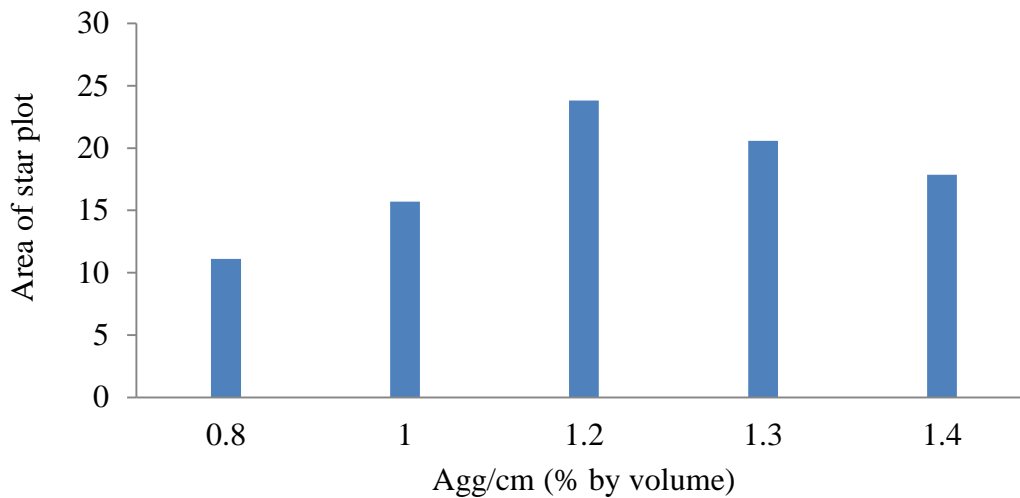


Figure 5.5 - Area generated for star diagram representing rheological performance of mortars - weight factor set I

For the three selected mortars, HRWR demand, plastic viscosity and yield stress at 20 minutes, and compressive strength at 7 and 28 days were considered as major factors which have weight factor of 3. On the other hand, plastic viscosity and yield stress determined at 60 min and 1-day

compressive strength were taken as minor factors with the weight factors of 1 to 2, as presented in Table 5.6. The star diagram and area of the diagram presented in Figures 5.6 and 5.7, respectively, indicated that the mortar made with agg/cm of 1.2 had greater overall performance compared to the other mixtures. This confirms the previous finding about rheological performance.

Table 5.6 – Weight factor set II

	1/HRWR/cm	1/Plastic viscosity at 20 min	1/Plastic viscosity at 60 min	1/ Yield stress at 20 min
Weight factor II	3	3	2	3
	1/ Yield stress at 60 min	1-day compressive strength	7-day compressive strength	28-day compressive strength
Weight factor II	2	1	3	3

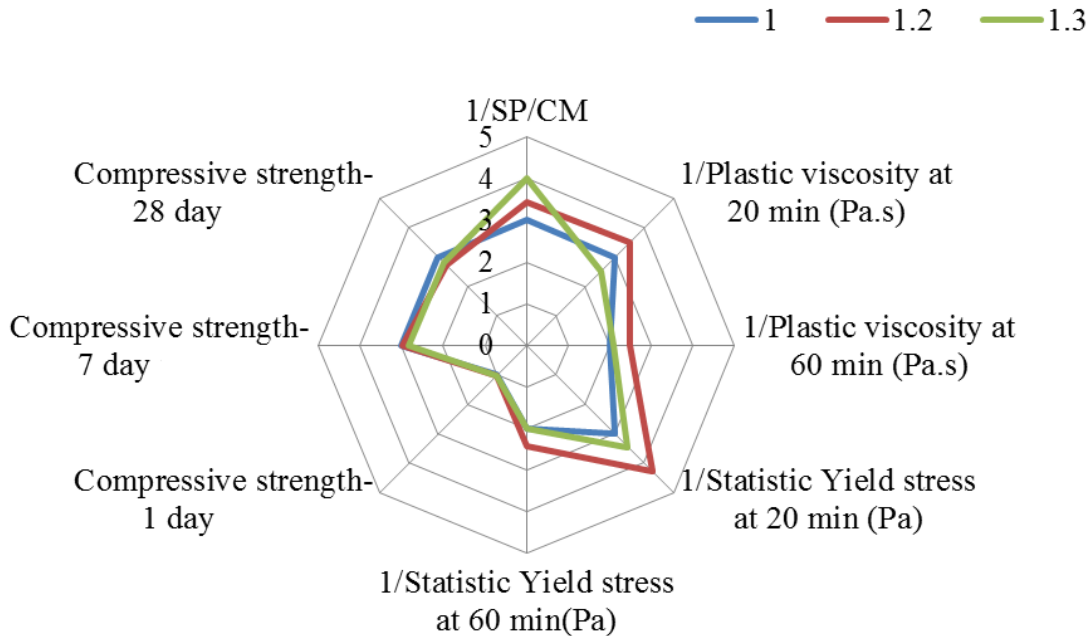


Figure 5.6 - Star diagram to compare compressive strength and rheological performance of the mortars made with different aggregate contents - weight factor set II

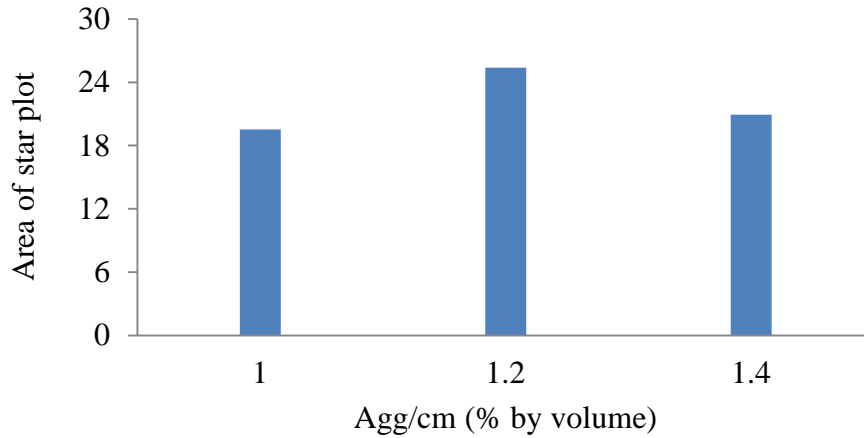


Figure 5.7 - Area generated for star diagram representing compressive strength and rheological properties of mortars - weight set II

In order to confirm the previous finding about overall performance, additional comparison was carried out using HRWR demand and compressive strength at 1, 7, and 28 days. The mini slump flow and flow time values were used in this comparison. The weight factor used for this comparison is given in Table 5.7. Unlike the case of the second series of performance comparison, the mortar made with agg/cm of 1 exhibited greater performance than the other mixtures, as shown in Figure 5.8. The area of the star diagram for the mortar with agg/cm of 1 was 7% larger than that of with 1.2 agg/cm (Figure 5.9).

Comparing all the performance comparisons resented in this section, agg/cm of 1, by volume can be considered as the optimized value since the compressive strength are a key characteristic of UHPC and there was no significant difference in the performance between the agg/cm of 1 and 1.2.

Table 5.7 - Weight factor set III

	1-day compressive strength	7-day compressive strength	28-day compressive strength	Slump	1/flow time
Weight factor III	1	3	3	3	3

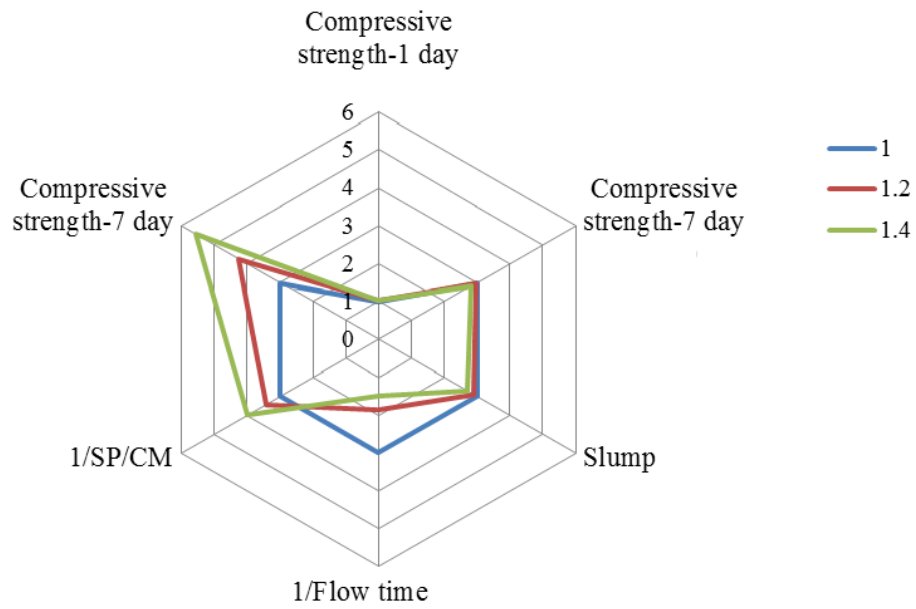


Figure 5.8 - Star diagram to compare workability and compressive strength of mortars made with different aggregate contents - weight factor set III

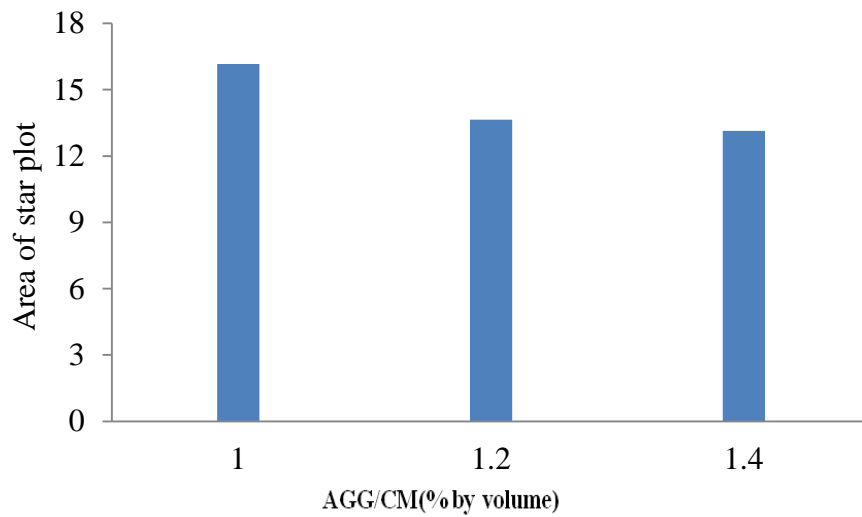


Figure 5.9 - Area for star diagram representing workability and compressive strength parameters - weight set III

# Chapter 6- Effect of Fiber Types and Contents on UHPC Performance

This section addresses performance of fiber-reinforced UHPC prepared with different types and volumes of fibers. In this study, the fiber content was selected as the main test variable and was classified into two groups (polyvinyl alcohol (PVA) and steel fibers).

## 6.1 Scope of the work

The properties of two steel fibers (#1 and #2) and one PVA used in this study presented in Table 6.1. The experimental program consisted of three parts. In the first part, the viscosity and flowability of six fiber-reinforced UHPCs using steel fiber #1 and PVA (the same matrix but different HRWR content) were determined using the mini-V funnel and mini-slump test methods. For the second part of the program, the flexural behaviour of the fiber-reinforced UHPC mixtures were determined using  $76 \times 76 \times 305$  mm beams. Compressive strength was also determined at 28 days using 50 mm cubes. In the last part, three mixtures made with steel fiber #2 were tested for the same properties as the second part. Fiber dosages used in this study are presented in Table 6.2.

Table 6.1 - Fibers properties

Type	Filament diameter	Fiber Length	Specific Gravity	Tensile strength	Flexural strength
Steel fiber #1	0.2 mm	13 mm	7.8	1900 MPa	203 GPa
Steel fiber #2	0.2 mm	13 mm	7.8	2160 MPa	-
PVA fiber	38 $\mu$ m	8 mm	1.3	1400MPa	30 GPa

Table 6.2 - Type and dosage of fibers

Fiber type	Fiber content (% by volume)	w/cm
Steel fiber #1	0.5	0.21
	1.0	0.21
	1.5	0.21
	2.0	0.21
Steel fiber #2	1.5	0.19
	2.0	0.19
	2.0	0.21
PVA fiber	0.5	0.21

## 6.2 Mixing procedure and sampling

The high-shear mortar mixer was used for the optimization of fiber types and contents, as shown in Figure 6.1. As presented in Figure 6.2, the optimized combination of fine aggregates (30% masonry and 70% river sand) was mixed in the mixer at the speed 6 (medium speed) for 1.5 min. Then cementitious materials were added and mixed for another 1.5 min at the same speed. The 90% of the mixing water with 50% of the HRWR were then, introduced, and mixing was resumed at speed 10 (high speed) to mix for 3 min. The rest of the water and HRWR were added, and the mortar was mixed for another 4 min. Finally, fibers were included gradually and mixed for 1 min.



Figure 6.1 - High-shear mortar mixer

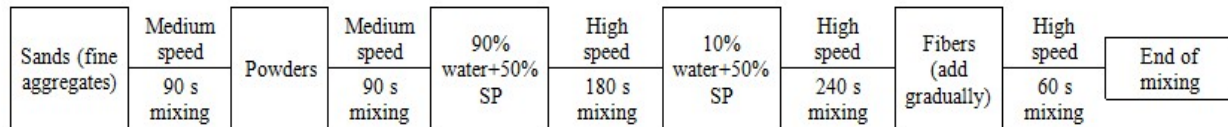


Figure 6.2 - Mixing procedure for UHPC using high-shear mortar mixer

It should be noted that during casting of each prism, special care was taken to ensure that the UHPC flowed from one end of the prism to the other for proper distribution and alignment of the steel fibers along the beam length. For this purpose, after mixing, the fresh UHPC was poured through a 1-m long chute with an inclination of approximately 30 degrees, as presented in Figure 6.3. This casting method also aided to release a part of the entrapped air.

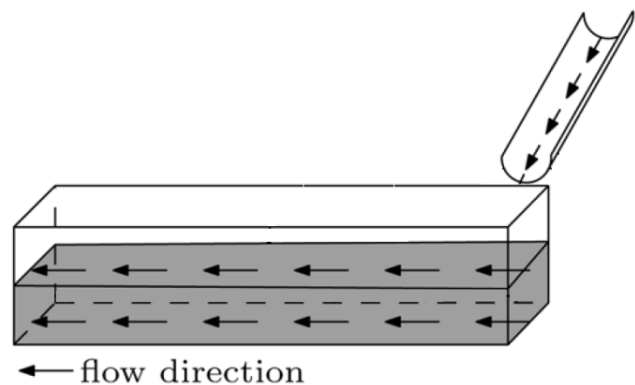


Figure 6.3 - UHPC casting procedure through inclined chute

### 6.3 Test methods

Flow properties of the fiber-reinforced UHPC were determined using mini slump and flow cone tests. In addition, rheological properties were evaluated using viscometer, as presented in Figures 6.4 and 6.5.

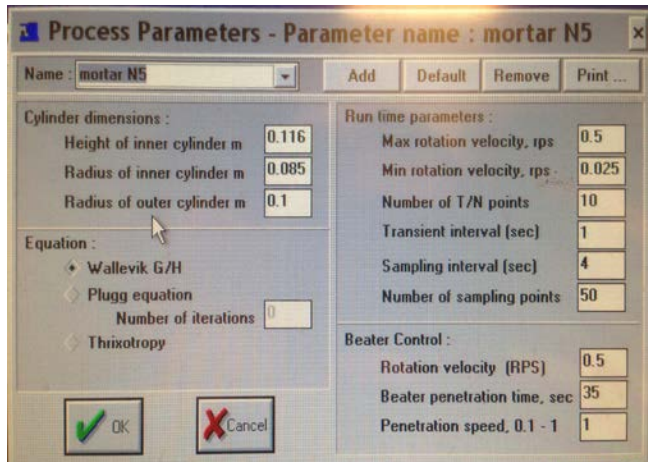


Figure 6.4 - Parameters used for the rheology test



Figure 6.5 - Viscometer

Flexural performance was evaluated on prismatic beams using third-point loading method in accordance with ASTM C1609. The beam specimens measure 305 (length)  $\times$  76 (width)  $\times$  76 mm (depth) with a bending span of 203 mm. During the test, the load and deflection at mid-span of the prism were monitored, as shown in Figure 6.6. The obtained data was used to determine the cracking strength and post-cracking toughness of the concrete. For the test setup, a yoke similar to that shown in Figure 6.6 was used to measure the mid-span deflections. LVDTs were attached to the yoke on each side of the specimen at mid-span, and the yoke was placed to the specimen at mid-depth over the support points. The LVDTs' bore on a plate was epoxied to the compression face and extended to hang over the sides of the prism. Figure 6.6 shows the deflection measurement setup for this three-point bending test.

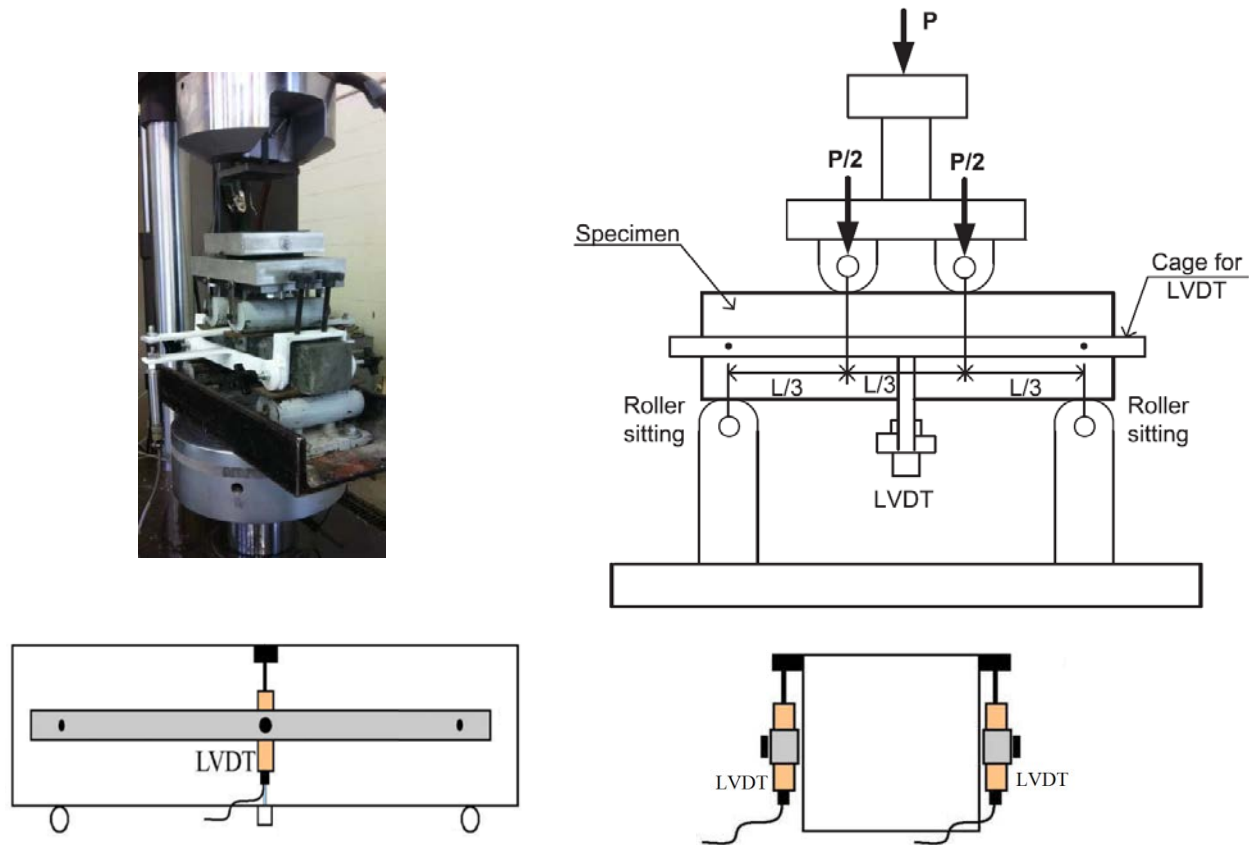


Figure 6.6 - Test setup for flexural test

#### 6.4 Fresh properties and compressive strength

Rheological properties of the investigated mixtures are summarized in Table 6.3. It should be noted that there was one control reference mixture without any fiber, four mixtures with different percentages of steel fibers, 0.5%, 1%, 1.5%, and 2%, as well as a mixture containing 0.5% PVA fiber but treated in two ways: dry and saturated in mixing water. The idea behind saturating the PVA fibers with water was to investigate whether it aids to proper dispersion of the PVA fibers. The saturation of the PVA fibers with water before mixing seemed to have no significant effect on the rheological properties according to the results.

Table 6.3 - Rheology properties test result

Code	Fiber content (% by volume)	w/cm	Yield Stress (Pa)	Viscosity (Pa.s)	f'c (MPa)
Reference	0		21.3	23.5	127
Steel fiber #1	0.5		23.2	11.4	126
Steel fiber #1	1.0		27.8	12.2	123
Steel fiber #1	1.5	0.21	28.2	9.2	145
Steel fiber #1	2.0		39.9	28.9	135
PVA	0.5		37.1	1.4	120
PVA - saturated	0.5		37.4	1.4	-

The optimized fiber volume for PVA and steel fibers was determined based on the test results of the mini slump, flow time, dynamic yield stress, and flexural strength. Given the high water adsorption of the PVA, the maximum dosage of PVA was limited to 0.5% to secure slump spread of  $300 \pm 10$  mm.

Fresh properties and compressive strength result are presented in Tables 6.4 and 6.5, respectively. In the case of w/cm of 0.21, the increase in the fiber volume from 0 to 2% led to significant increase in the HRWR demand. In particular, the fiber volume increase from 1.5% to 2.0% resulted in 0.3% increase in the HRWR demand. Such increase was ten times greater than the increase from 1% to 1.5%. In terms of 28-day compressive strength, the highest strength was obtained for the mixture made with 1.5% steel fiber. It is important to note that the fiber volume increase from 1.5% to 2.0% led to slightly decrease in the 28-day compressive strength, as presented in Table 6.5.

Table 6.4 - The fresh properties test result

Fiber type	$V_f$	HRWR dosage	Slump flow (cm)	Flow time(s)
Steel fibers #1 - w/cm = 0.21	0.0%	1.20%	30	17.1
	0.5%	1.21%	29.5	30.0
	1.0%	1.22%	29.5	28.7
	1.5%	1.25%	28	31.7
	2.0%	1.55%	28.5	25.5
Steel fibers #2 - w/cm = 0.19	1.5%	2.4%	30	37.5
	2.0%	2.4%	29.5	45.1
Steel fibers #1- w/cm = 0.21	2.0%	1.65%	29.7	19.5
PVA - w/cm = 0.21	0.50%	2%	28	13.5

Table 6.5 - Compressive strength test results

Code	w/cm	Fiber volume (%)	Test time (day)	$f'_c$ (MPa)
Reference	0.21	-	28	127
Steel fiber #1	0.21	0.5	28	126
Steel fiber #1	0.21	1.0	28	124
Steel fiber #1	0.21	1.5	28	145
Steel fiber #1	0.21	2.0	28	135
PVA	0.21	0.5	28	121
Steel fiber #2	0.19	1.5	7	104
Steel fiber #2	0.19	2.0	7	108
Steel fiber #2	0.21	2.0	7	105

## 6.5 Flexural behavior

The load-deflection curves for PVA, steel fiber #1 & #2 are presented in Figures 6.7 to 6.9. The flexural and compressive strength were determined at the age of 7 days. It was observed that the mixture with 2% steel fibers showed better deflection capacity and ultimate strength. These test results confirmed that mixtures with 2% steel fibers have the best performance.

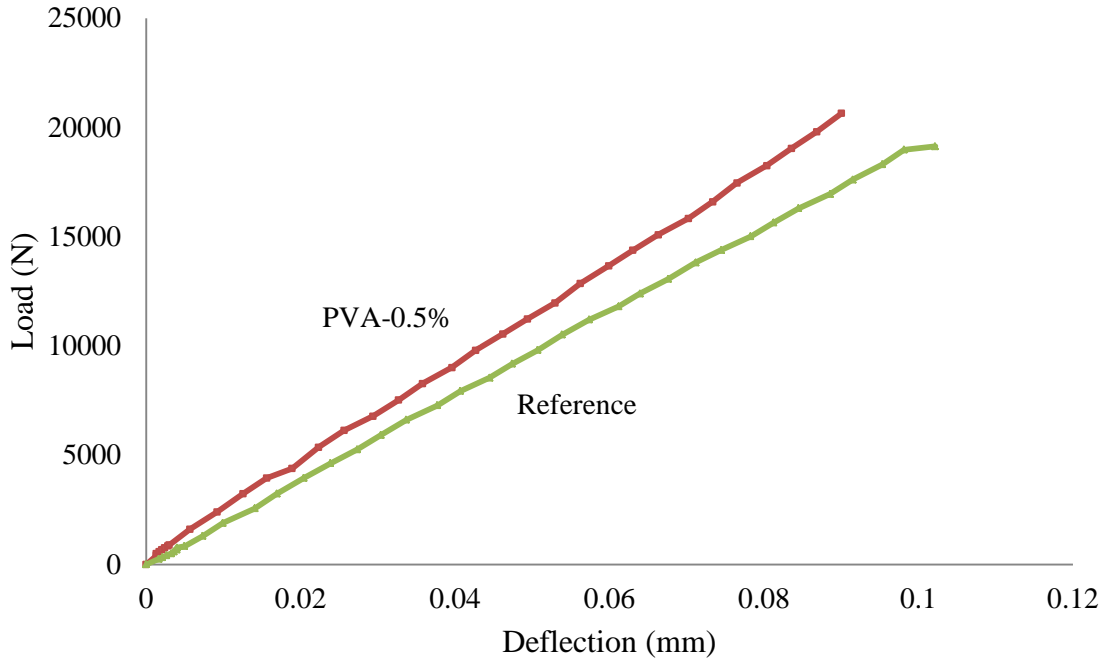


Figure 6.7 - Load-deflection curve for UHPC with PVA fibers

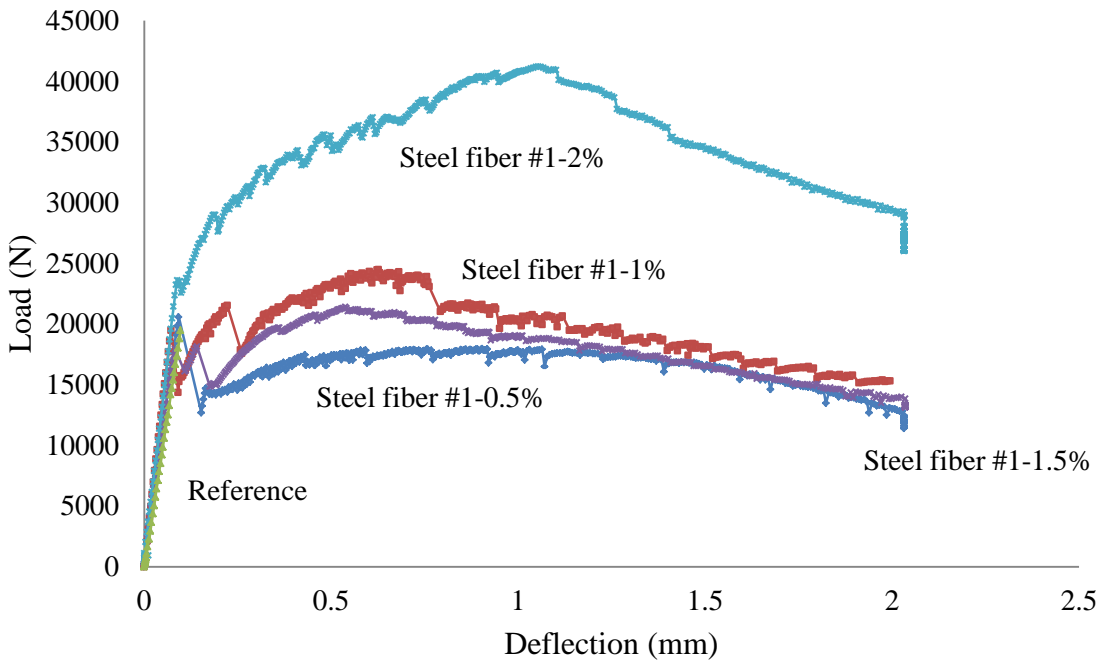


Figure 6.8 - Load-deflection curve for UHPC with steel fiber #1

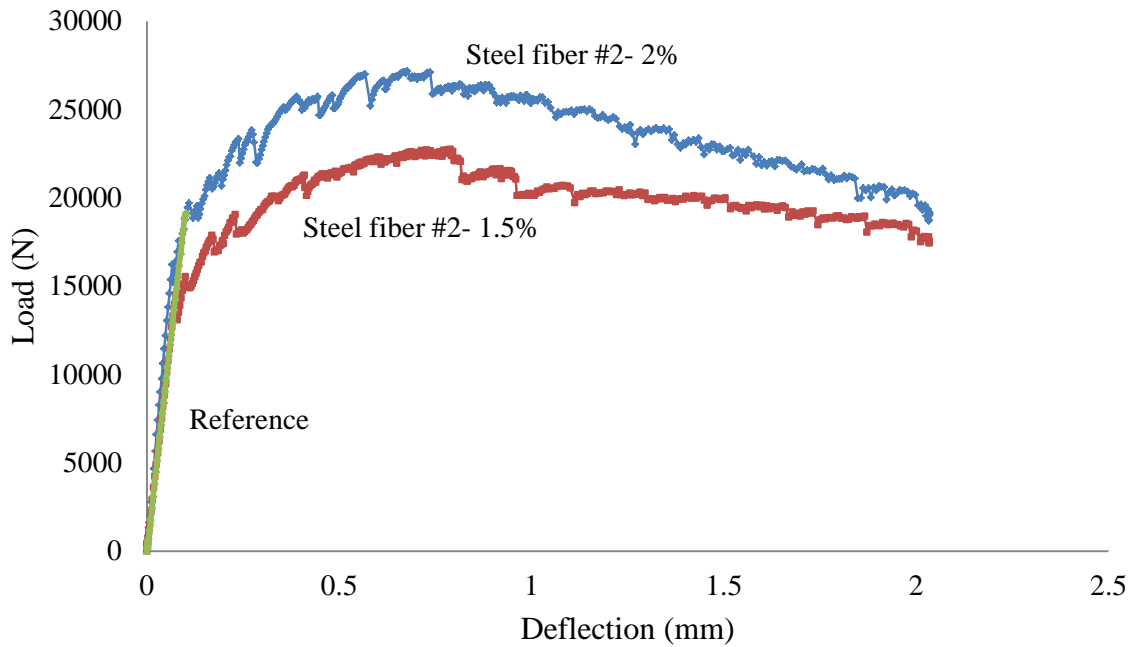


Figure 6.9 - Load-deflection curve for UHPC with steel fiber #2

More analysis of presented data is presented in Table 6.6. In addition, results in details from the load-deflection curves are compared for the first-peak load, peak load, and toughness in Figures 6.10 to 6.12, respectively. It is interesting to note that the reference and PVA mixtures exhibited similar flexural behavior. In general, the increase in the volume of steel fiber led to an increase in the peak load and toughness. Based on the performance comparison considering different types and dosage of fibers, the mixture with 2% steel fiber #1 with  $w/cm=0.21$  was selected as an optimized mixture given the highest toughness and peak load. This mixture also exhibited excellent compressive strength and flow characteristics.

Table 6.6 – Flexural behaviour analysis for different type and percentages of fibers

Code	Fiber volume (%)	Depth (mm)	Span (mm)	P1 (kN)	f1 (MPa)	$\delta_1$ (mm)	PP (kN)	fp (MPa)	$\delta_p$ (mm)	T150 (kN-mm)
Reference	-			19.7	13.6	0.10	19.7	13.6	0.10	1.01
PVA	0.5			20.8	14.3	0.09	20.8	14.3	0.09	1.01
Steel fiber #1	0.5			21.3	14.7	0.10	21.3	14.7	0.10	27.13
Steel fiber #1	1.0	76.2	304.8	20.5	14.1	0.08	24.0	16.5	0.56	39.81
Steel fiber #1	1.5			18.2	12.5	0.08	21.4	14.7	0.53	35.48
Steel fiber #1	2.0			23.8	16.4	0.09	41.2	28.4	1.05	68.72
Steel fiber #2	1.5			16.9	11.6	0.09	22.9	15.8	0.60	39.36
Steel fiber #2	2.0			18.2	12.5	0.07	27.5	18.9	0.81	47.00

\* First-peak load, P1 (kN); First-peak strength, f1 (MPa) ; First-peak deflection,  $\delta_1$  (mm); Peak load , PP (kN); peak strength,fp (MPa); Peak deflection,  $\delta_p$  (mm); L - Span length;

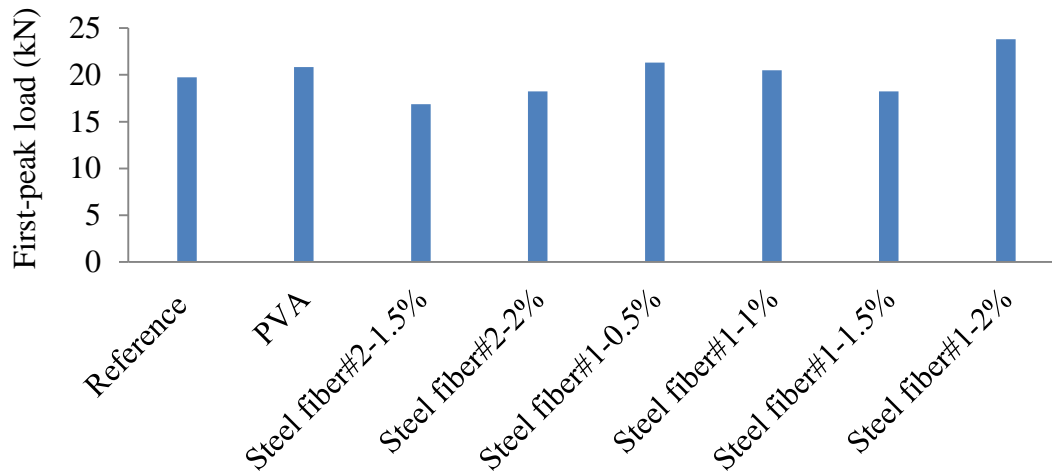


Figure 6.10 - First peak load results

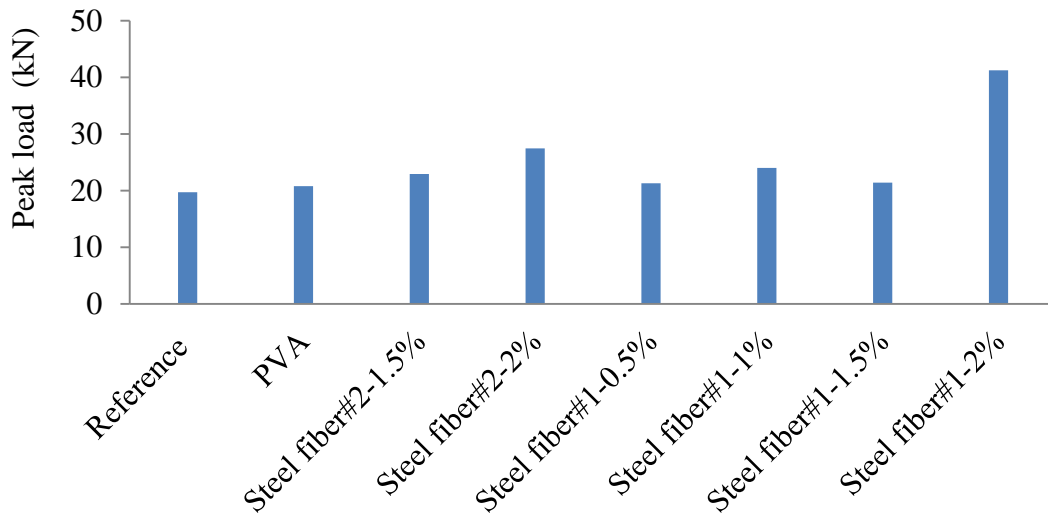


Figure 6.11 - Peak load results

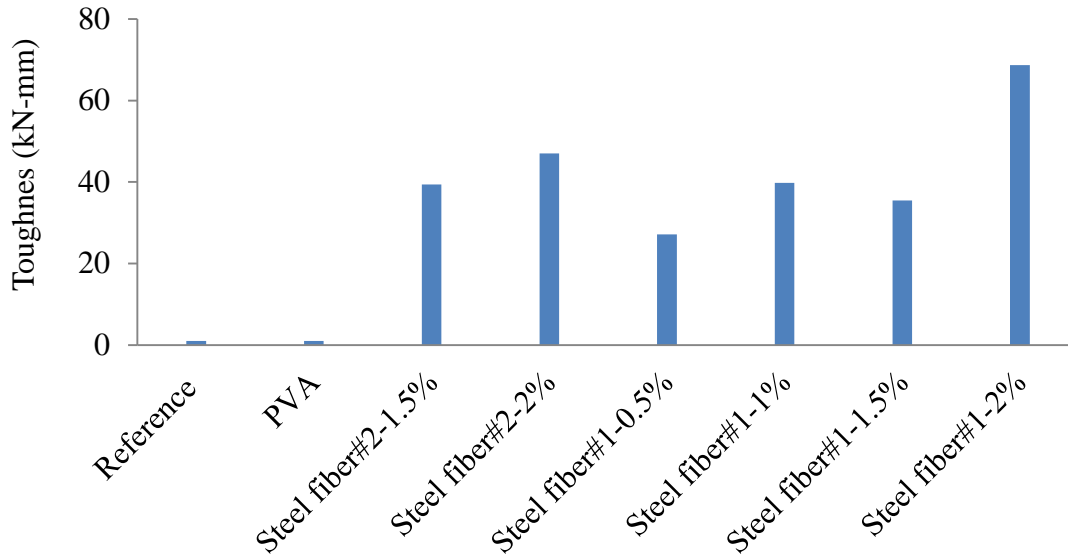


Figure 6.12 – Toughness results

## 6.6 Conclusions

The increase in the volume of steel fiber resulted in a significant increase in the peak load and toughness. The mortar containing 2% steel fiber by volume developed the best flexural performance and compressive strength. It should be noted that however, the mortar with such high volume of steel fiber is required to have additional dosage of HRWR or increase w/cm to secure the targeted flowability.

# Chapter 7- Performance of Optimized UHPC

## 7.1 Mixture proportioning and test methods

Through the optimizations presented in Chapters 4 to 6, four UHPC mixtures were selected to carry out extensive characterization. The optimized mixtures include G50SF5, G50, FAC40SF5, and FAC60, as presented in Table 7.1. One commercially available UHPC mixture was used as a reference to compare the overall performance of the optimized UHPCs. The testing programs used in this section are presented in Table 7.2.

## 7.2 Mixing procedure

Given the high batch quantity, high-intensive concrete mixer with a maximum capacity of 150 L was used, as shown in Figure 7.1. The mixing procedure is presented in Figure 7.2. It should be noted that all the samples were water-cured at the temperature of  $23 \pm 2^\circ\text{C}$  without any accelerated curing to improve the mechanical properties. The development of the UHPC of the targeted performance without any specialized curing is one of the main objectives of this study since the absence of the special curing practice reduces overall cost and can lead to broader use.

Table 7.1 - UHPC mixture proportioning for main UHPC mixes

Code	Cement (kg/m <sup>3</sup> )	SF (kg/m <sup>3</sup> )	FAC (kg/m <sup>3</sup> )	GGBS (kg/m <sup>3</sup> )	River sand (0-5 mm) (kg/m <sup>3</sup> )	Masonry sand (0-2 mm) (kg/m <sup>3</sup> )	Ground quartz (0- 0.6 mm) (kg/m <sup>3</sup> )	Fine sand (0-0.6 mm) (kg/m <sup>3</sup> )	HRWR (l/m <sup>3</sup> )	Water (kg/m <sup>3</sup> )	Steel fibers (kg/m <sup>3</sup> )
G50SF5	548	41.5	-	548	708	310	-	-	69.5	146.0	156
G50	593	-	-	546	704	298	-	-	54.2	173.7	156
FAC40SF5	663	42.1	367.4	-	717	314	-	-	51	151.1	156
FAC 60	486	-	555.6	-	722	306	-	-	23.8	179.8	156
Reference	712	231	-	-	-	-	211	1020	29.2	188.6	156

Table 7.2 - Test matrix for UHPC specimens

<b>Property</b>	<b>Test Method</b>	<b>Test Title/Description</b>
<b>Aggregate Characterization Tests</b>		
Density & Absorption	ASTM C 127	Test Method for Density, Relative Density (Specific Gravity), and Absorption of Coarse Aggregate
<b>Fresh Concrete Property Tests</b>		
Unit Weight	ASTM C 138	Test Method for Density (Unit Weight)
Air Content	ASTM C 231	Test Method for Air Content of Freshly Mixed Concrete by the Pressure Method
Mini slump	ASTM C1437	Test Method for Mini-Slump of UHPC
Fresh concrete temperature at 10 and 70 minutes	ASTM C 1064	Test Method for fresh concrete temperature
Bleeding	Investigation of ASTM Paste and Mortar Bleeding Tests Volume 3, Issue 1 (July 1981)	Test Method for Bleeding of UHPC
Setting time	ASTM C403	Test Method for Time of Setting of Concrete Mixtures by Penetration Resistance
Rheology	-	Mini-V funnel; Rheometers
<b>Mechanical Property Tests</b>		
Compressive Strength	ASTM C 109	Test Method for Compressive Strength of Cubes Specimens.
Splitting Tensile Strength	ASTM C 496	Test Method for Splitting Tensile Strength of Cylindrical Concrete Specimens.
Flexural Strength	ASTM C 1609	Test Method for Flexural Strength of Concrete.
Modulus of Elasticity	ASTM C 469	Test Method for Static Modulus of Elasticity.
Drying shrinkage (after 7 d of moist curing)	ASTM C 157	Test Method for Length Change of Hardened Hydraulic-Cement Mortar and Concrete
Autogeneous shrinkage	ASTM C1698	Standard Test Method for Autogenous Strain of Cement Paste and Mortar
<b>Durability Tests</b>		
Bulk Resistivity	ASTMC 1760	Standard Test Method for Bulk Electrical Conductivity of Hardened Concrete



Figure 7.1 - High-intensive concrete Mixer

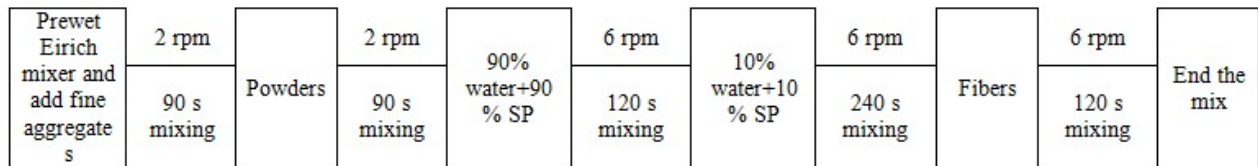


Figure 7.2 - Mixing procedures of optimizing UHPC mix designs using high shear mixer

### 7.3 Fresh properties

Fresh properties for the five UHPC mixtures are summarized in Table 7.3. All the mixtures had similar specific gravity and spread value, regardless of the mixture compositions. In addition, all the investigated mixtures exhibited excellent resistance to bleeding. It is important to note that the optimized mixtures did not have any increase in material temperature over time, which is important for the control of setting time and workability retention. The FAC60 and G50 mixtures had lowest and highest air contents, respectively. Also, the reference UHPC had lower flow time

of 12 sec compared to from 30 to 46 sec for the other optimized mixtures, thus indicating relatively low viscosity of the reference mixture.

Table 7.3 - Fresh properties

Code	Specific gravity	Air content (%)	Mini-slump (mm)	Flow time (sec)	Temp. at 10 min. (°C)	Temp. at 40 min. (°C)	Temp. at 70 min. (°C)	Bleeding
Reference	2.47	4.7	280	12	23	19	19	Non
G50SF5	2.45	5.0	270	37	24	23	22	Non
G50	2.43	5.6	270	46	25	22	21	Non
FAC40SF5	2.44	4.5	280	39	21	19	19	Non
FAC60	2.41	3.5	270	30	20	19	19	Non

Rheological properties are summarized in Table 7.4. The results for the two optimized mixtures were not determined due to a problem encounter during the rheology testing. As in the case of flow time results, the reference mixture exhibited lower plastic viscosity than the other mixtures. In general, plastic viscosity and yield stress were shown to increase with the elapsed time, as presented in Table 7.4. More details regarding these results presented in the Appendix.

Table 7.4 - Summary of rheology properties

Code	Spread value (mm)	Yield value at 20 min (Pa)	Yield value at 40 min (Pa)	Yield value at 60 min (Pa)	Flow time (sec)	Viscosity at 20 min (Pa.s)	Viscosity at 40 min (Pa.s)	Viscosity at 60 min (Pa.s)
Reference	280	36	54	72	12	17	28	35
G50SF5	270	39	48	57	37	39	51	61
FAC40SF5	280	39	55	58	39	44	88	115

#### 7.4 Mechanical properties

##### Compressive strength

Compressive strength for all reference and optimized mixtures were determined at 1 and 28 days as presented in Figure 7.3. The reference mixture had lower 1-day compressive strength than the other mixtures but developed higher 28-day strength of 135 MPa compared to between 107 to

125 MPa for the other mixtures. It is important to point out that the FAC60 mixture containing 60% fly ash developed approximately 20 MPa lower compressive strength at 28 days given the slow rate of hydration of fly ash compared to slag.

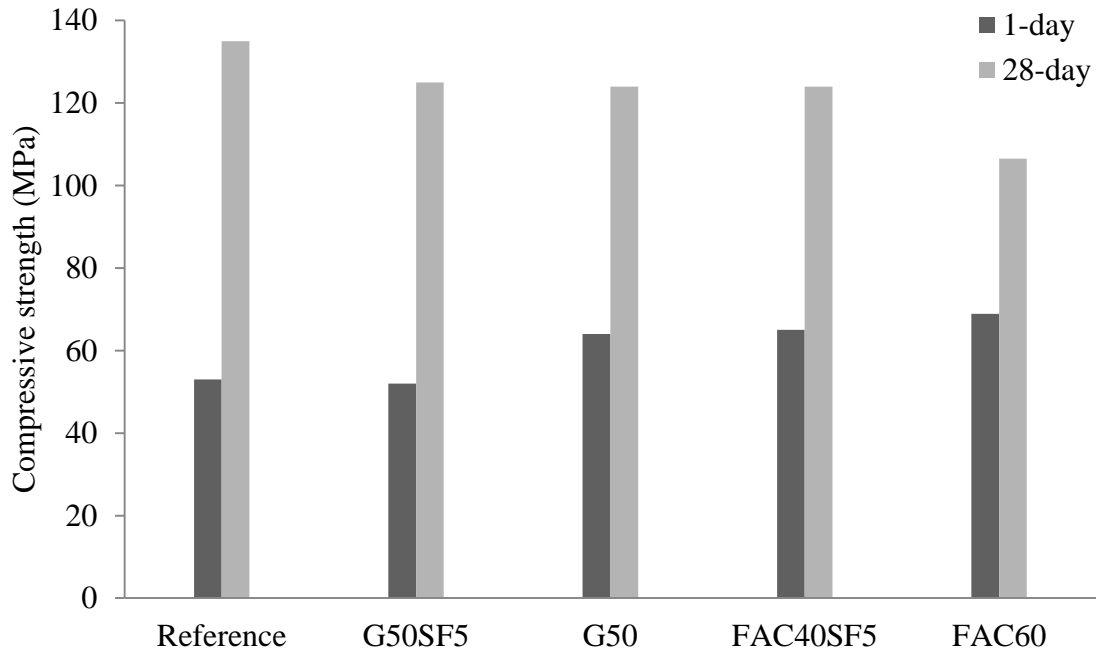


Figure 7.3 - Compressive strength results

### Splitting tensile strength

The splitting tensile strength of UHPC was determined according to ASTM C496, as presented in Figure 7.3. The splitting tensile strength results are presented in Figure 7.4. Similar to the case of compressive strength, FAC60 had the lowest peak load and splitting tensile strength. The G50SF5 mixture had the highest peak load and tensile strength among the tested mixtures. The G50 and FAC60 exhibited lower splitting tensile strength than the reference mixture.

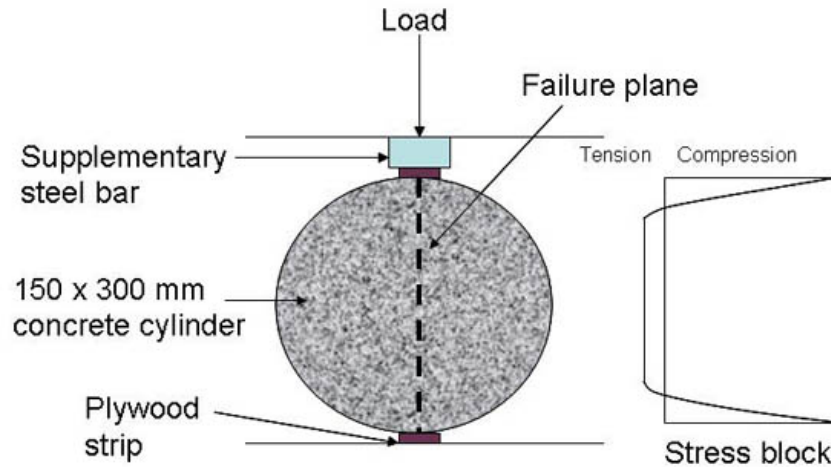


Figure 7.3 - Splitting tensile test method

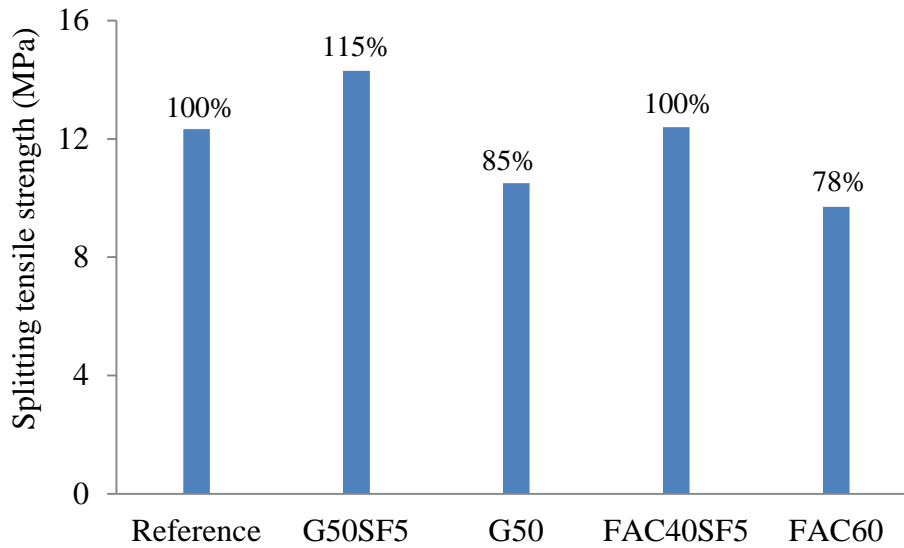


Figure 7.4 - Splitting tensile strength results

### Modulus of elasticity

The modulus of elasticity and Poisson's ratio were determined using  $76 \times 152$  mm cylindrical specimens in accordance with ASTM C469. A combined unbonded compressometer and extensometer equipped with two digital indicators measured the transverse and tangential displacements. The specimens were loaded at 1.03 MPa per second until the predetermined maximum load, based on curing regime and age. The specimens were completely unloaded at

approximately the same rate and then, the gauges were zeroed. This process repeated three times for each specimen. The initial loading was used to seat the gauges and the data was disregarded. Data from the second and third loading cycles were used to calculate the modulus of elasticity and Poisson's ratio.

Modulus of elasticity for each mixture at 28 days is presented in Figure 7.5. Similar to compressive strength and splitting tensile strength, the FAC60 mixture obtained the lowest modulus of elasticity of 45.8 MPa. Other mixtures developed similar results, although the reference mixture had slightly higher elastic modulus.

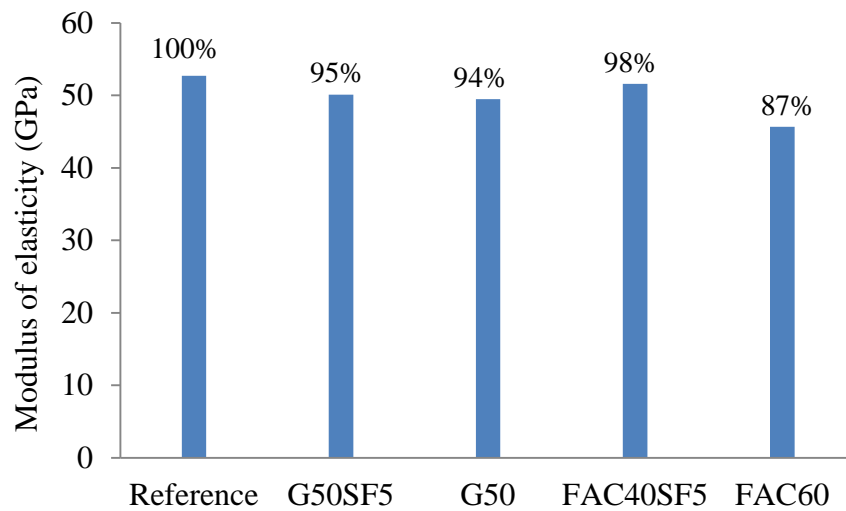


Figure 7.5 - Modulus of elasticity results

### Flexural behavior

Flexural behaviors of all optimized mixtures were investigated according to ASTM C1609. Figures 7.4 to 7.8 illustrate the load-deformation curves for FAC60, G50, G50SF5 and FAC40SF5, respectively. For each mixture, three specimens were tested.

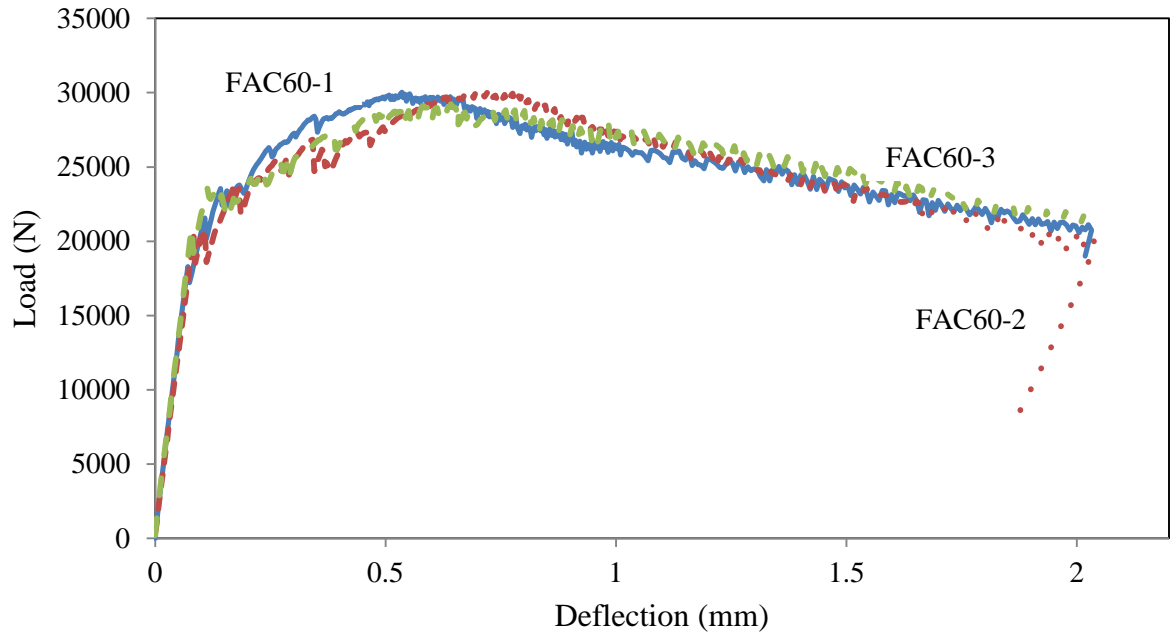


Figure 7.6 - Load-deflection curve for FAC60

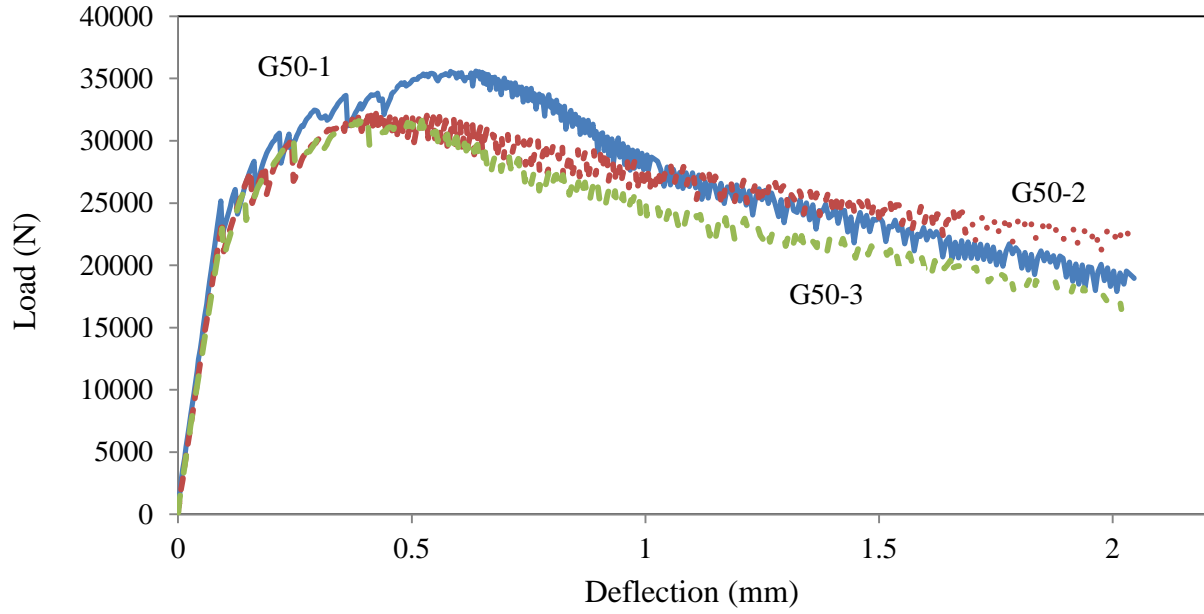


Figure 7.7 - Load-deflection curve for G50

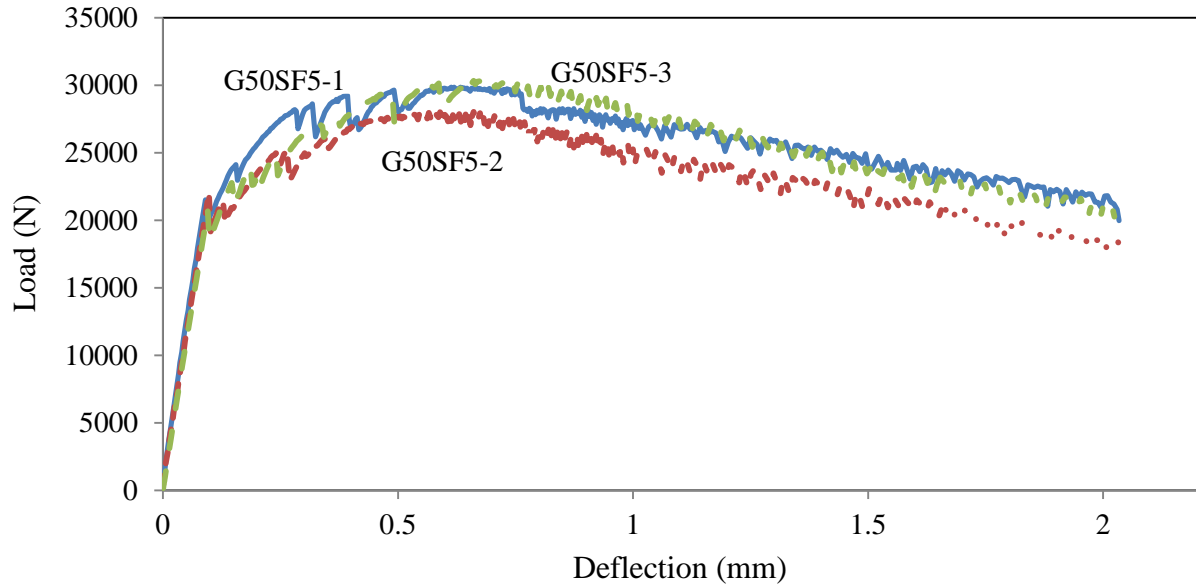


Figure 7.8 - Load-deflection curve for G50SF5

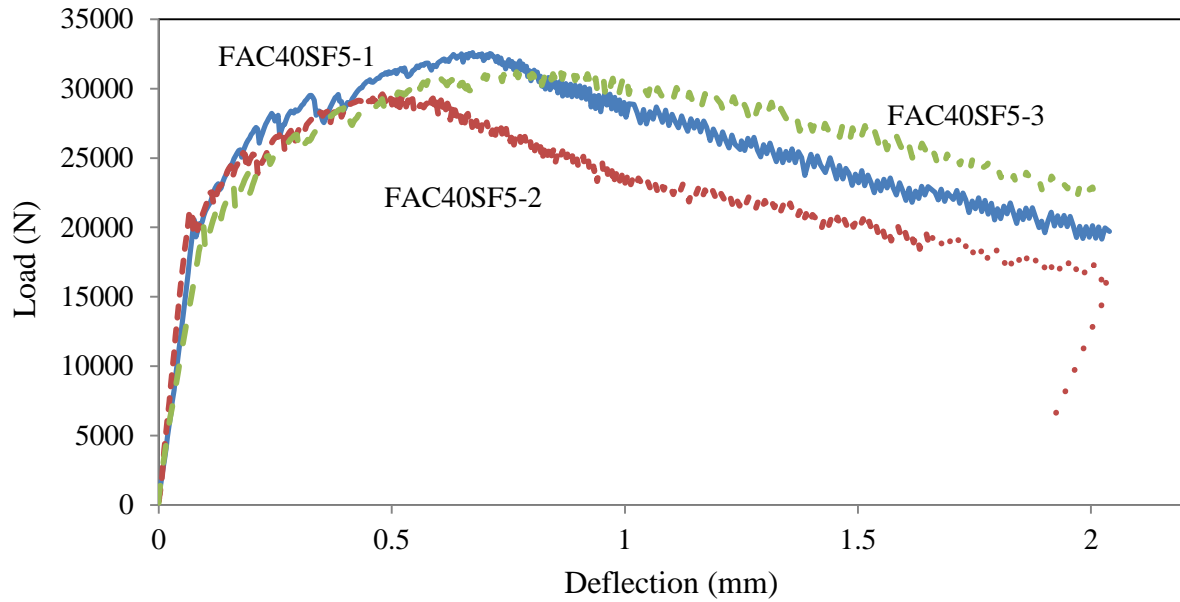


Figure 7.9 - Load-deflection curve for FAC40SF5

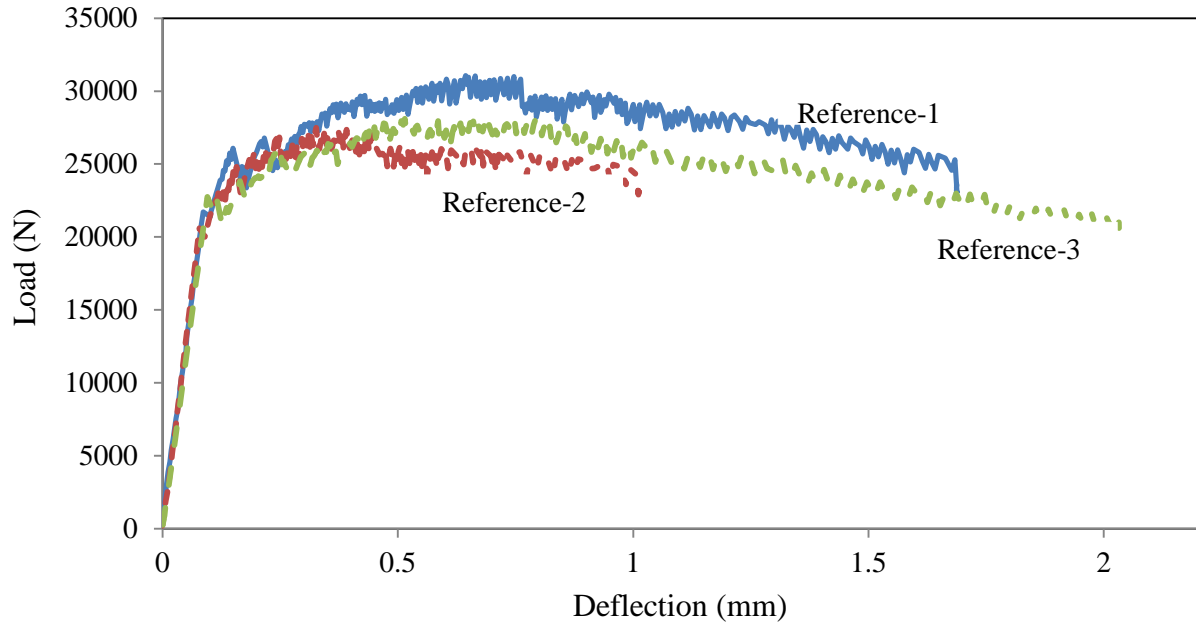


Figure 7.10 - Load-deflection curve for reference mixture

The analysis of load-deformation curves are detailed in Table 7.5. In general, no significant difference was found for the peak load and toughness index of the optimized mixtures, regardless of the mixture composition. First peak load, peak load and toughness for all mixtures were almost identical, as presented in Table 7.8. It is interesting that the toughness index of T150 for the reference mix was lower than the other optimized mixtures, although the difference was not significant.

Table 7.5 – Flexural behaviour analysis for different UHPC mix design

Code	Depth (mm)	Span (mm)	P1 (kN)	f1 (MPa)	$\delta_1$ (mm)	PP (kN)	f <sub>p</sub> (MPa)	$\delta_p$ (mm)	T150 (kN-mm)
Reference	76.2	304.8	22.2	15.3	0.09	29.2	20.1	0.63	45.8
FAC60	76.2	304.8	19.8	13.6	0.08	29.5	20.3	0.64	49.4
FAC40SF5	76.2	304.8	21.2	14.6	0.07	31.0	21.3	0.68	50.1
G50	76.2	304.8	24.0	16.5	0.09	33.1	22.8	0.49	51.5
G50SF5	76.2	304.8	21.3	14.7	0.10	29.3	20.2	0.64	48.8

## 7.5 Drying and autogenous shrinkage

Drying shrinkage of the investigated mixtures are presented in Figure 7.11. As in the case of flexural responses, there was no significant difference in the drying shrinkage among the tested mixtures, except for the FAC40SF5 mixture that had a sudden increase in the shrinkage for the initial 5 days of drying. Beyond the first 5 days, all the mixtures exhibited similar increase in the drying shrinkage with respect to time.

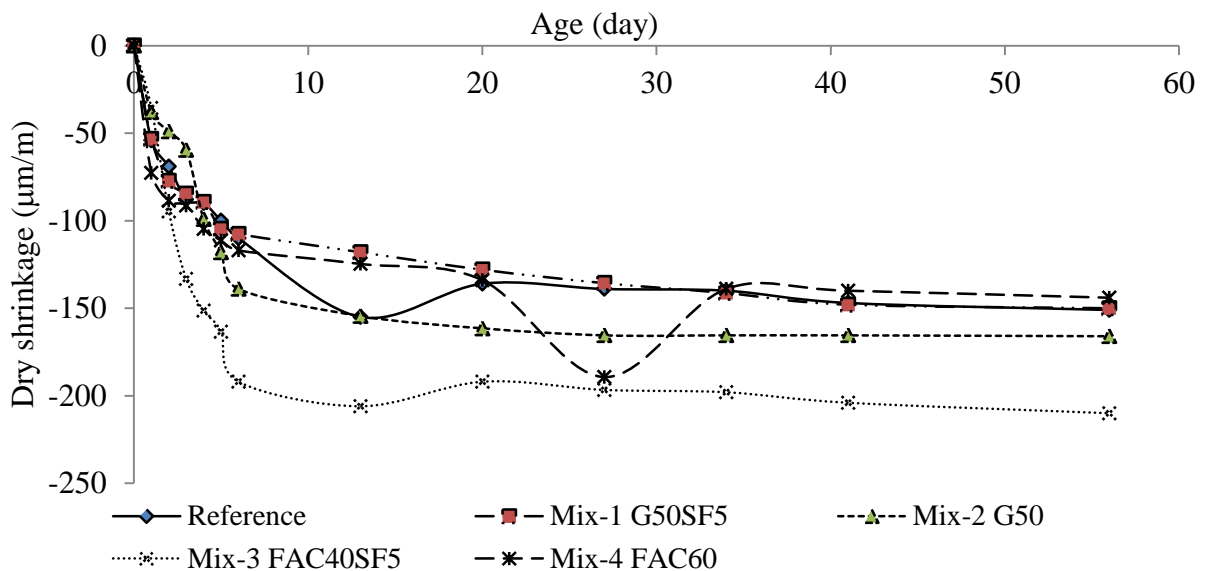


Figure 7.11 - Dry shrinkage results

Figure 7.12 presents the autogenous shrinkage of the four optimized mixtures and the reference. The reference mixture had higher autogenous shrinkage compared to the four optimized mixtures. The G50 mortar containing 50% slag exhibited significantly lower autogenous shrinkage of 100  $\mu\text{m/m}$  compared to 220 to 260  $\mu\text{m/m}$  for the other optimized mixtures. The G50SF5, FAC40SF5, and FAC60 mixtures had similar autogenous shrinkage, as presented in Figure 7.10.

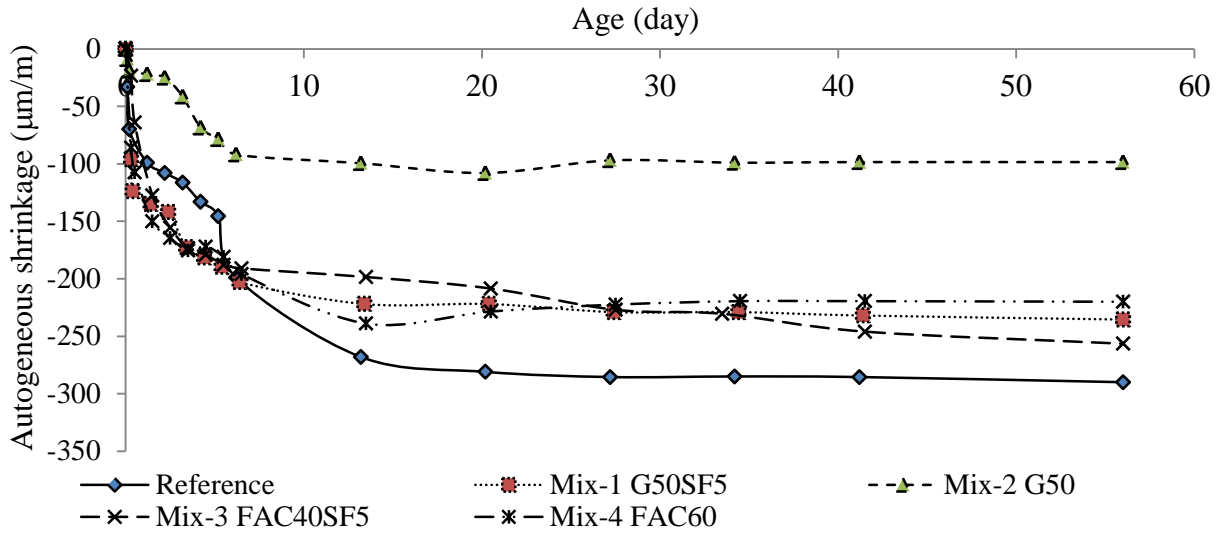


Figure 7.12 - Autogenous shrinkage results

## 7.6 Electrical resistivity

Electrical resistivity was determined using  $100 \times 200$  mm cylindrical specimens at 28 days in accordance with ASTM C1760. The test involves the determination of the bulk electrical conductivity of saturated specimens. The electrical resistivity provides a rapid indication of the concrete's resistance to the penetration of chloride ions by diffusion. The process is affected by several parameters, mainly the porosity and pore structure of the materials. The pores of concrete can contain water with diluted salts in it, therefore making the concrete electrically conductive. This method measures the electrical current through a saturated specimen with a potential difference of 60 V current maintained across the ends of the specimen.

Table 7.6 summarizes the surface resistivity and bulk resistivity results. The reference mixture had the highest electrical resistivity values which are approximately two times of those of the other mixtures.

Table 7.6 - Electrical resistivity for five mixtures

Code	Bulk resistivity average (KΩcm)	Surface resistivity average (KΩcm)
REF	25	45
G50SF5	11	20
G50	13	22
FAC40SF5	11	19
FAC60	15	28

## 7.7 Conclusions

The optimized UHPC mixtures developed similar to or slightly lower compressive strength than the reference UHPC. It is interesting to note that the optimized mixtures were shown to have equal to or greater splitting tensile strength than the reference despite slightly lower compressive strength of the former concrete. This can be due to the use of optimized aggregates of high packing density, which contribute to an increase in aggregate interlocking compared to the smooth and round silica sand. The optimized UHPC mixtures had significantly lower drying shrinkage of 150 μm/m. The G50SF5, G50 and FAC60 mixtures had lower drying shrinkage than the reference UHPC.

# Chapter 8 – Effect of Temperature on UHPC Performance

## 8.1 Introduction

In this chapter, the robustness of the UHPC mixture at different temperatures was evaluated to determine the effect of temperature fluctuations on HRWR demand, fresh properties, and mechanical properties. The effect of curing temperatures on the performance of UHPC was also determined.

For the low temperature condition, in addition to putting ice into the mixer for 3 minutes before mixing to cool down the mixer temperature, a part of the mixing water was replaced with ice in order to reach the targeted temperature of  $10 \pm 2^\circ\text{C}$ . In addition, all the constituent materials were stored in a chamber at approximately  $0^\circ\text{C}$  for 24 hours before mixing. For high temperature conditions of  $30 \pm 2^\circ\text{C}$ , neither the materials nor the mixer were cooled down. After demolding, all the specimens were water-cured in the temperature controlled chamber set at the targeted temperatures until the age of testing.

## 8.2 Fresh concrete properties

HRWR dosage was adjusted to secure the slump flow of  $280 \pm 20$  mm, regardless of the temperature condition to compare and evaluate the effect of the temperature on the performance. The HRWR dosages of the investigated mixtures were presented in Figure 8.1, and the HRWR dosage of the high and low temperature relative to that of  $23^\circ\text{C}$  was also given.

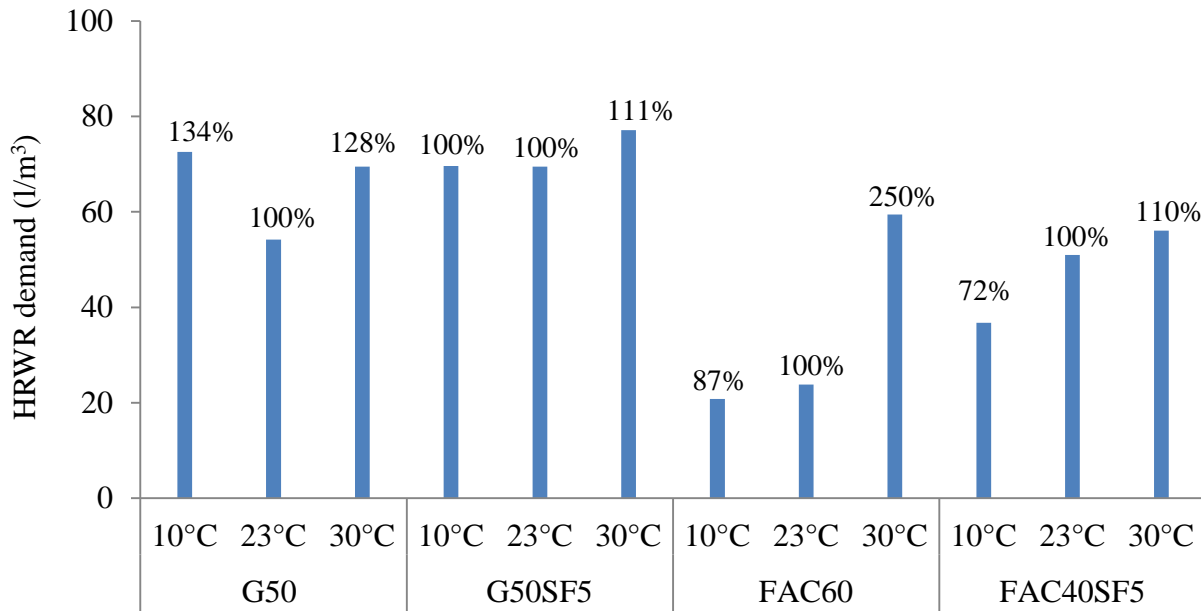


Figure 8.1 - HRWR demand for UHPC mixtures at different temperatures

In general, the increase in the temperature led to an increase in the HRWR demand. For example, mixtures with high temperature of 30°C necessitated 10% to 150% higher HRWR demand compared to those with 23°C. It is interesting to note that the effect of the temperature on the HRWR demand varies with the SCM in use. The mixtures containing Class C fly ash were shown to be more sensitive to the temperature in terms of the HRWR demand compared to those made with GGBS. It can be concluded that the mixtures incorporating GGBS is more stable than those of containing fly ash for temperature fluctuations. In addition, mixtures containing 5% of silica fume exhibited more stable HRWR demand compared to those without silica fume.

Fresh properties of UHPC mixtures of different temperatures are summarized in Table 8.1. Results indicated that air contents at low temperature are higher than those at high temperature. The mini slump in all the mixtures were in the range of 250 to 280 mm. Results from the mini v-funnel test showed that flow time of all high temperature mixtures were faster than those of the

low temperature mixtures. It should be noted that there was no bleeding in any of the evaluated mixtures, regardless of the temperature.

Table 8.1 - Fresh properties of four optimized UHPC mixtures at different temperatures

Code	Temperature conditions (°C)	Air content (%)	Spread value (mm)	Flow time (sec)	Temperature (°C)	Bleeding
G50	10	5.5	285	31	9	Non
	23	5.6	270	46	24	Non
	30	3.8	280	20	29	Non
G50SF5	10	6.2	250	63	13	Non
	23	5.0	270	37	24	Non
	30	4.2	275	14	28	Non
FAC60	10	5.0	260	46	9	Non
	23	3.5	270	30	20	Non
	30	3.8	280	12	29	Non
FAC40SF5	10	5.5	250	34	9	Non
	23	4.5	280	39	21	Non
	30	4.3	260	16	30	Non

### 8.3 Compressive strength

Figures 8.2 and 8.3 compare the compressive strengths at 1 and 28 days for the four UHPC mixtures at 10, 23, and 30°C. Results for 1-day compressive strength indicated that with increasing the temperature, the compressive strength increased generally. The highest difference was for G50 with 61% increase at 30°C compared to 10°C and FAC40SF5 obtained the lowest fluctuations with less than 13% difference among different temperatures. Similar results were found for 28-day compressive strength. It should be note that mixtures containing Class C fly ash exhibited similar compressive strengths, regardless of the temperature. On the other hand, those made with GGBS exhibited more difference in the compressive strength with respect to the temperature condition.

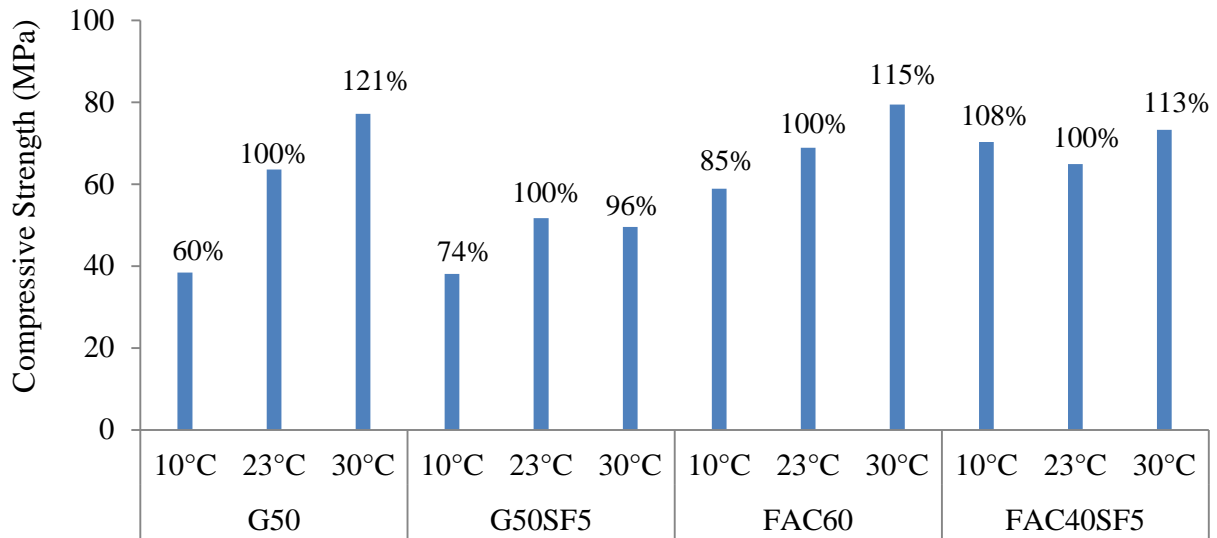


Figure 8.2 - Comparison of 1-day compressive strengths of UHPC mixtures made at different temperatures

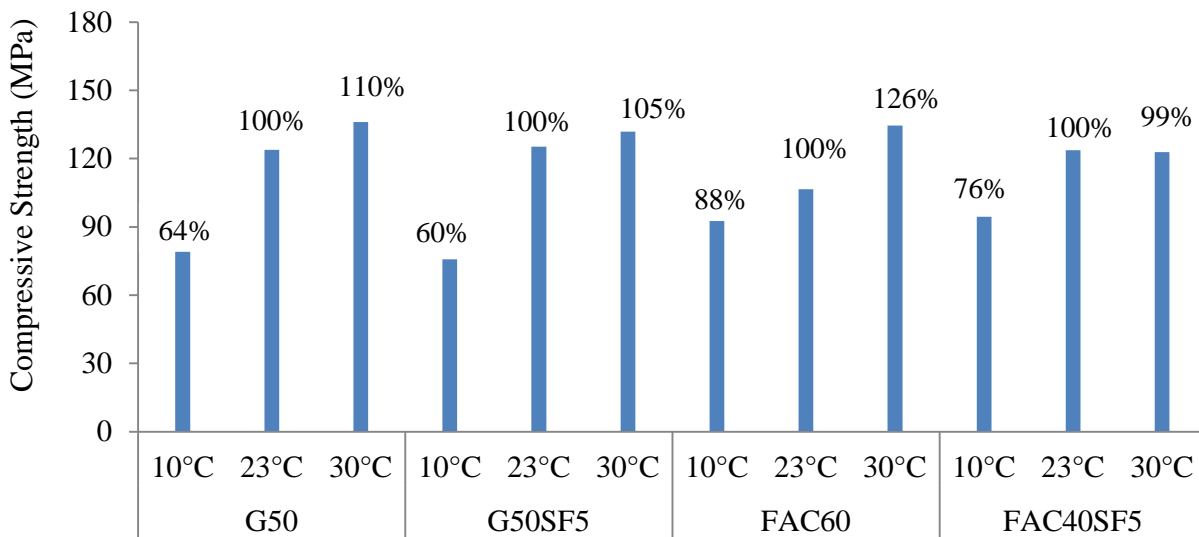


Figure 8.3 - Comparison of 28-day compressive strengths of UHPC mixtures made at different temperatures

#### 8.4 Splitting tensile strength

Splitting tensile strength results are compared in Figure 8.4 for the UHPC mixtures at different temperatures. As in the case of compressive strength, mixtures at higher temperature had higher splitting tensile strength than those of low temperature mixtures. The strength difference among the three temperature conditions was greater for the mixtures containing GGBS. Similar to the

compressive results, all mixtures achieved the highest and lowest strengths in high and low temperatures, respectively. Also, G50SF5 with 80% and FAC40SF5 had the highest and lowest differences between low and high temperatures. It can be concluded that the mixtures with fly ash had more stability to the temperature fluctuations than those of with GGBS.

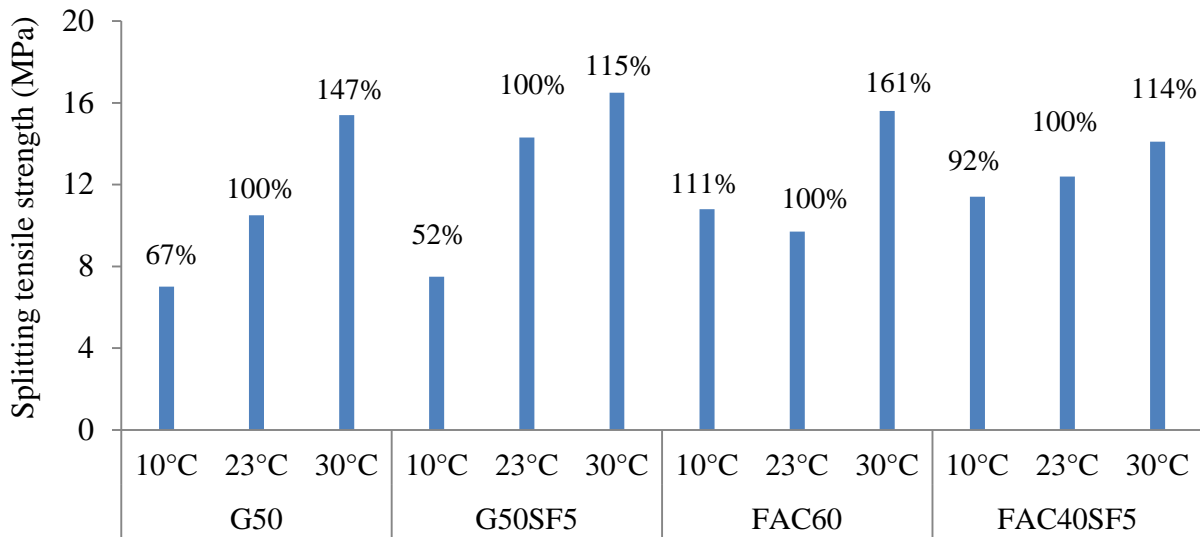


Figure 8.4 – Splitting tensile strength results for 28 days tests

### 8.5 Flexural behavior

The results of flexural strength tests are presented in Figures 8.5 to 8.8. As in the case of compressive and splitting tensile strength, mixtures with high temperature of 30°C had higher flexural strength than those at 10°C. As presented in Figure 8.4, the FAC60 mixture with high temperature had higher load-deflection curve compared to that of at low temperature. Similar results were found for the other mixtures. More detail results of the flexural responses are presented in Table 8.2 and Figures 8.9 to 8.11.

It can be seen that the first peak load increases with increasing temperature. Similar to compressive and tensile strength results, the GGBS mixtures exhibited higher fluctuation in the

peak load with respect to the temperature compared to those containing fly ash. Similar to the first peak load, the increases in temperature led to an increase in peak load and toughness. It is interesting to note that the FAC40SF5 mixture achieved similar first peak loads, regardless of the temperature.

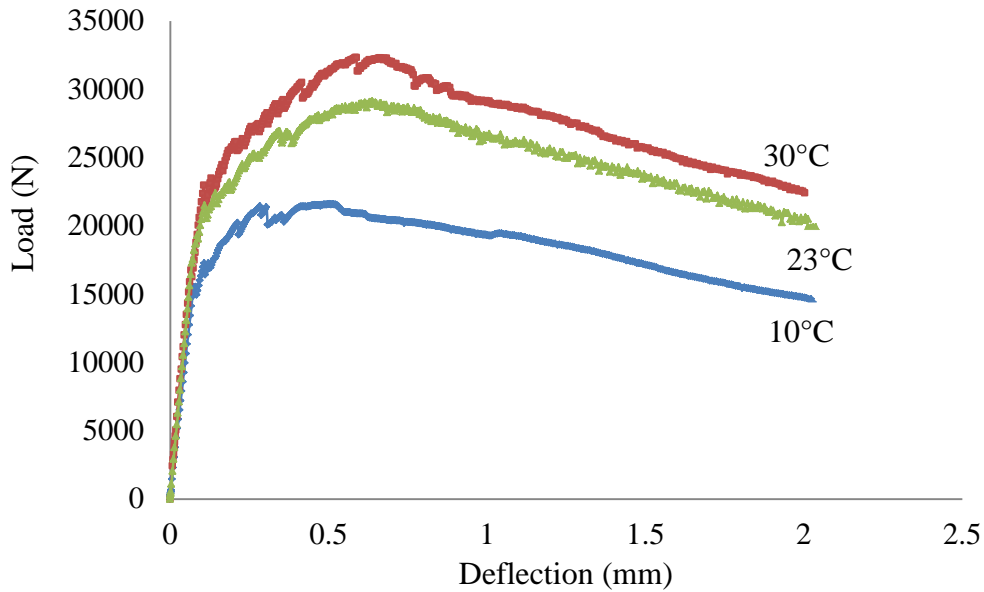


Figure 8.5 - Load-deflection curve for FAC60 mixture prepared at high and low temperatures

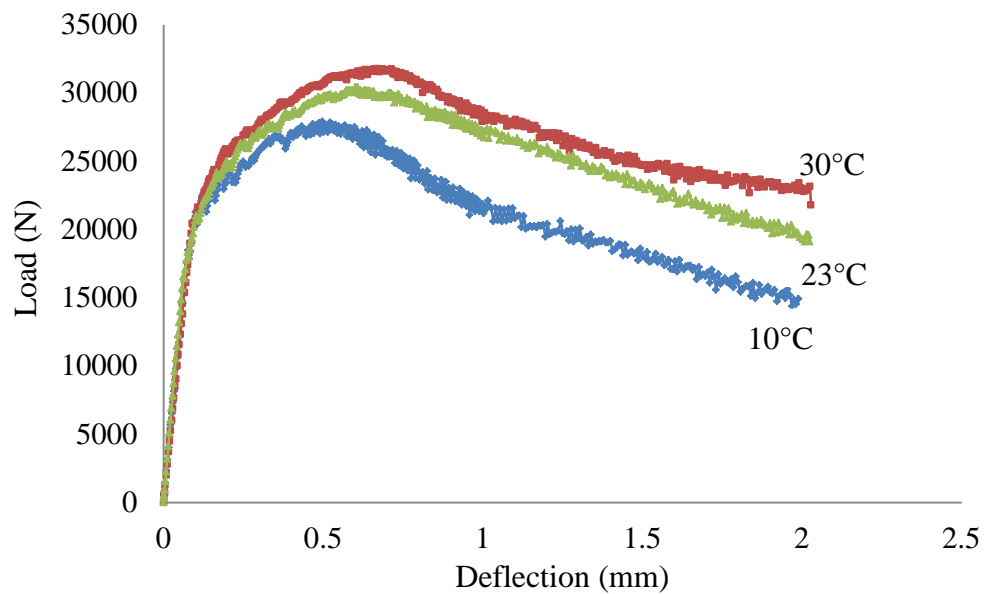


Figure 8.6 - Load-deflection curve for FAC40SF5 mixture prepared at high and low temperatures

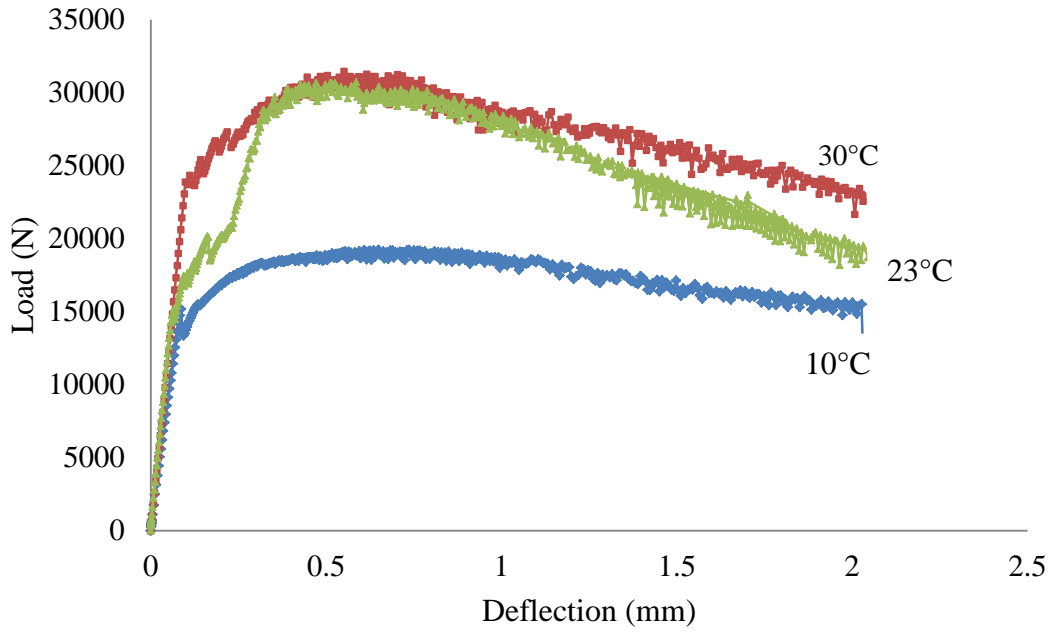


Figure 8.7 - Load-deflection curve for G50 prepared at high and low temperatures

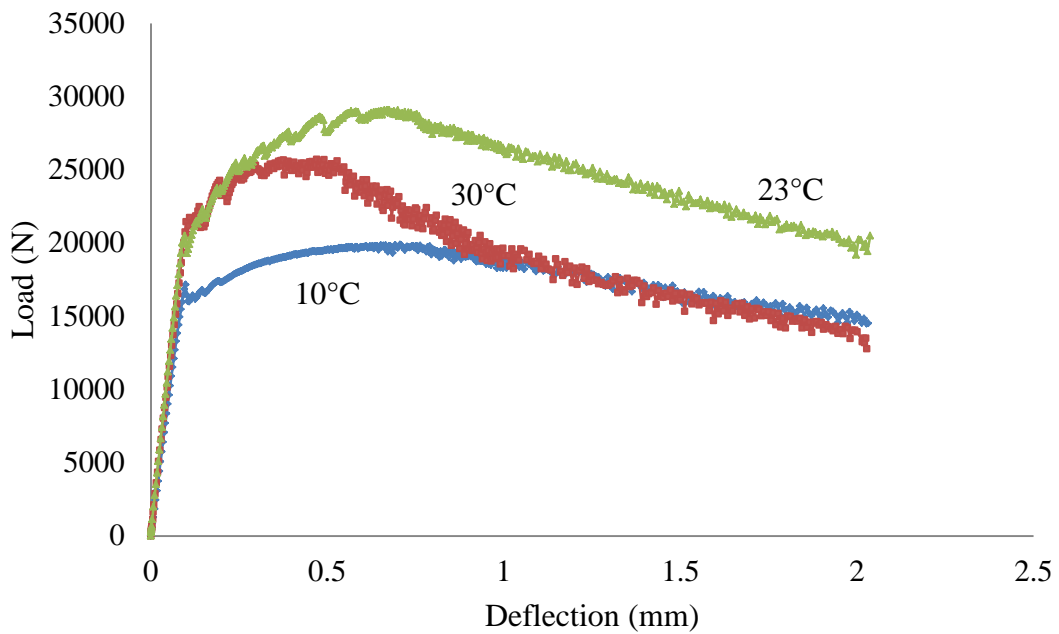


Figure 8.8 - Load-deflection curve for G50SF5 prepared at high and low temperatures

Table 8.2 - Results of flexural behavior for different temperatures

Code	Temperature condition (°C)	Depth (mm)	Span (mm)	P1 (kN)	f1 (MPa)	$\delta_1$ (mm)	PP (kN)	fp (MPa)	$\delta_p$ (mm)	T150 (kN-mm)
G50	10	76.2	304.8	15.4	10.6	0.09	19.7	13.5	0.83	34.6
	23			24.0	16.5	0.09	33.1	22.8	0.49	51.5
	30			25.1	17.3	0.10	31.8	21.9	0.57	53.8
G50SF5	10	76.2	304.8	17.2	11.9	0.10	20.1	13.8	0.70	34.9
	23			21.3	14.7	0.10	29.3	20.2	0.64	48.8
	30			24.6	16.9	0.10	26.6	18.3	0.43	38.6
FAC60	10	76.2	304.8	16.3	11.2	0.08	21.9	15.1	0.45	36.4
	23			19.8	13.6	0.08	29.5	20.3	0.64	49.4
	30			21.6	14.9	0.09	32.5	22.3	0.59	53.8
FAC40SF5	10	76.2	304.8	21.2	14.6	0.09	28.2	19.4	0.54	42.2
	23			21.2	14.6	0.07	31.0	21.3	0.68	50.1
	30			21.1	14.5	0.09	32.6	22.4	0.62	52.9

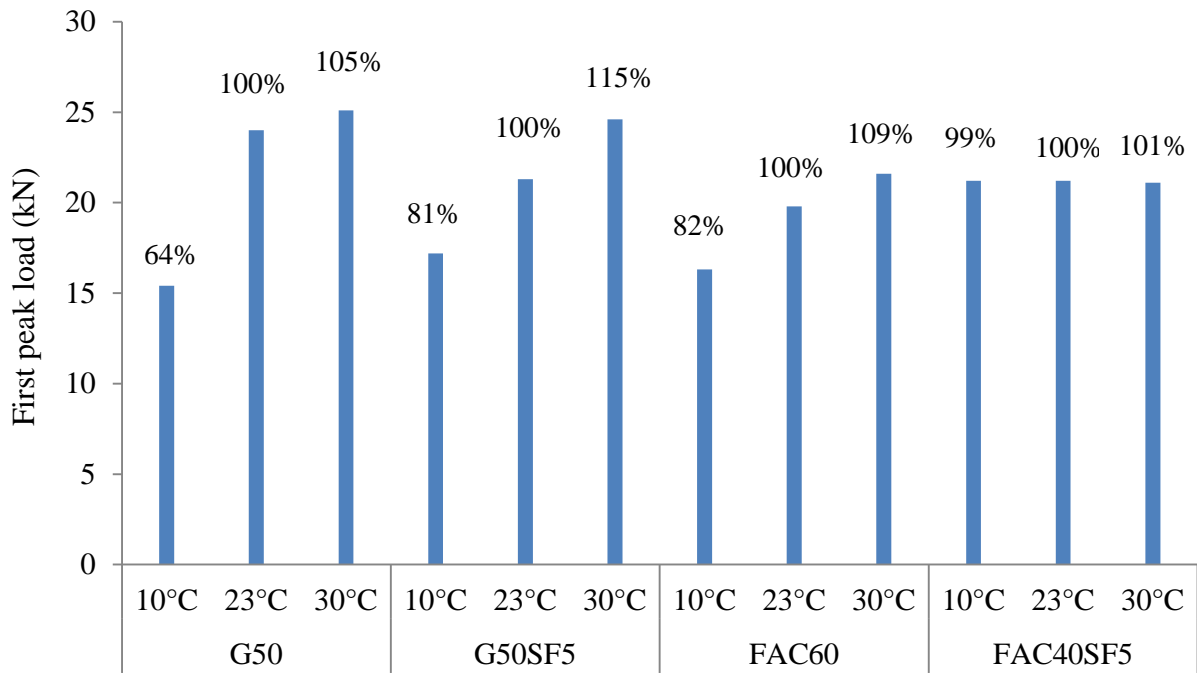


Figure 8.9 - First peak load results for different temperatures

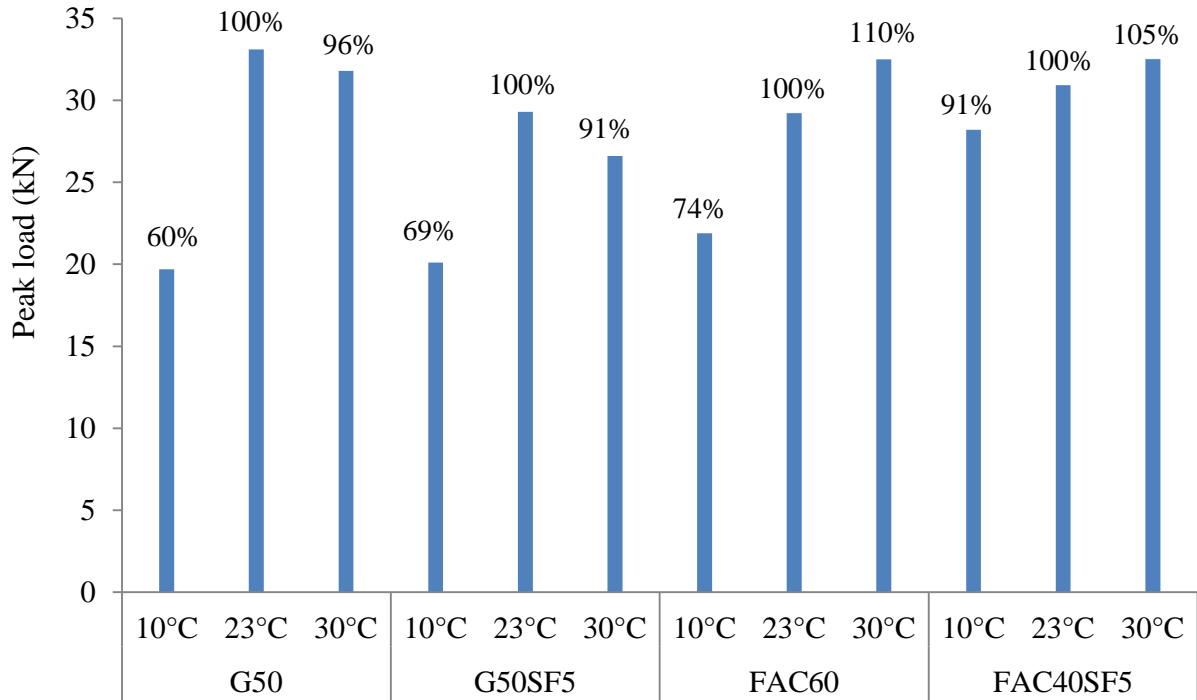


Figure 8.10 - Peak load results for different temperatures

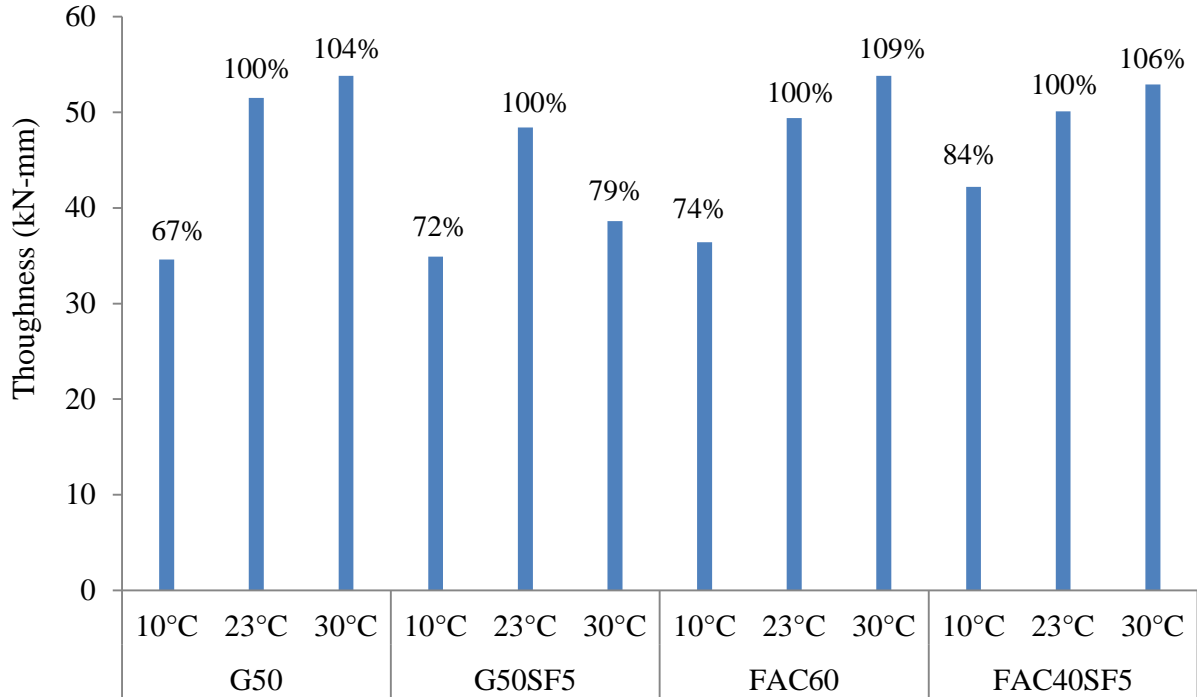


Figure 8.11 - Toughness results for different temperatures

## 8.6 Conclusions

In general, the UHPC mixture at high temperature can have greater mechanical properties than similar mixture at low temperature. It is important to note that mixtures containing Class C fly ash were more stable to the temperature fluctuations than those containing GGBS. In addition, the mixture with fly ash had less HRWR demand compared to GGBS mixtures in order to reach similar spread value in corresponding temperatures. This difference in low temperature was greater than high temperature.

# Chapter 9 – Bond Behavior of UHPC

## 9.1 Introduction

Bond strength of the optimized UHPC mixtures to the substrate concrete was evaluated using point load and flexural tests. The point load test was carried out on the cylinders that consisted of the half of UHPC and the other half of the substrate concrete sections. In addition, the flexural test (ASTM C1609) was used to evaluate the effect of overlay thickness on the flexural performance of the repaired beams. The optimized G50 mixture was used for the UHPC overlay material for the bond behavior evaluation.

## 9.2 Bonding test methods

The bonding test presented in Figure 9.1 was used to determine the bond strength in concrete placed in different layers used in repair over an existing substrate. The test consists of using a point load test at the joint between the two materials, as presented in Figure 9.1. A splitting tensile stress normal to the bond surface is produced by applying a point load at the joint. This test was carried out according to ASTM C1245 [48]. The schematic of the point load test is presented in Figure 9.1.

For the determination of the bond strength, several  $100 \times 200$  mm cylinders were used. First, conventional concrete was cast up to the half of each cylinder. The concrete was demolded at 1 day and then, are water-cured for 14 days. At the end of the curing, the top surface of the substrate concrete was sandblasted to remove all dirt and unbonded particles, as presented in Figure 9.2. After the sandblasting, the specimens were then, washed using high pressure water jet to ensure a clean surface and maintain a moist surface condition for casting the UHPC overlay,

which is required for better bond between the two layers. The other half of the cylinder was filled with the G50 mixture. After the completion of the overlay, the composite samples were water-cured for additional 28 days.

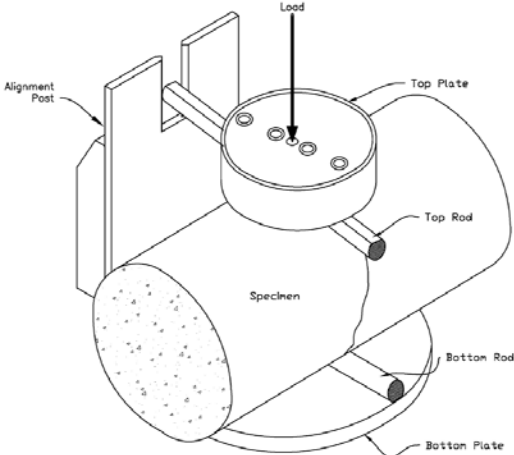


Figure 9.1 - Schematic of Loading Method [48]



Figure 9.2 - Photos of sandblasting, high-pressure water jet cleaning, and sample preparation

After the completion of the curing, the cylinders with the two layers were subjected to a point load using the test assembly setup fabricated for the point loading, as presented in Figure 9.3. During the testing, the cylinders were completely fixed without any movement in both horizontal and vertical directions. The load was applied in the vertical direction exactly on the interface layer, and the cylinder was placed firmly on one point of the bottom support to ensure pure tension without any bending moment, as shown in Figure 9.3.

Bond strength results for the G50 mixture are presented in Table 9.1. Mean bond strength of the five samples was approximately 24 MPa. The initial crack started at the interface between the two concrete, however, the crack went through the weak substrate concrete side, as presented in Figure 9.4. This indicates that the bond strength between the UHPC and substrate concrete is greater than the bond strength of the substrate concrete. Therefore, the bond strength at the overlay interface is adequate to be used as the bonded overlay of the pavements and bridge decks.



Figure 9.3 - Details about set-up and test method for debonding test

Table 9.1 - Bond strength	
Sample	(MPa)
G50-1	20
G50-2	26
G50-3	24
G50-4	30
G50-5	21



Figure 9.4 - Photos of broken specimens

### 9.3 Flexural bonding

Flexural test was used to evaluate the bond strength of the UPHC overlays with different thicknesses. Prismatic specimens measuring  $76 \times 76 \times 406$  mm were first cast with conventional concrete as a substrate. The substrate concrete beams were water-cured for 14 days and then, were properly sandblasted on the top surface of the beams. The top surfaces were completely washed with a high pressure water jet to have a clean and moist surface for better bonding, as presented in Figure 9.5. The G50 UHPC mixture was then cast to have overlay thicknesses of 6.5, 12.5, 19, 25.5 mm without any mechanical consolidation, as presented in Figure 9.6. For the flexural testing, the overlay section was positioned on the bottom of the beam so that the UHPC overlays were in tension, as shown in Figure 9.7.



Figure 9.5 - Details of preparing substrate specimens before UHPC overlay



Figure 9.6 - Photos of substrate concrete and casting of UHPC overlay



Figure 9.7 - Photo of flexural test setup used for the UHPC overlay specimens

Figures 9.8 to 9.11 present the load-deflection behaviors of the beams with 6.5, 12.5, 19 and 25.5-mm of UHPC overlays, respectively. In general, the use of the UHPC overlay led to significant increase in flexural strength and toughness of the beams over the monolithic beam case with conventional concrete, regardless of the overlay thickness. For example, the specimen with 6.5-mm UHPC overlay exhibited 45% increase in the flexural peak load compared to the monolithic reference beam (Figure 9.12). The increase in the overlay thickness resulted in an increase in the flexural strength. It is important to note that, however, the increase in the flexural strength slowed down beyond the 19-mm thickness. The 19-mm overlay beam had greater increase in the flexural strength of 152% compared to 115% for that with 25.5-mm overlay.

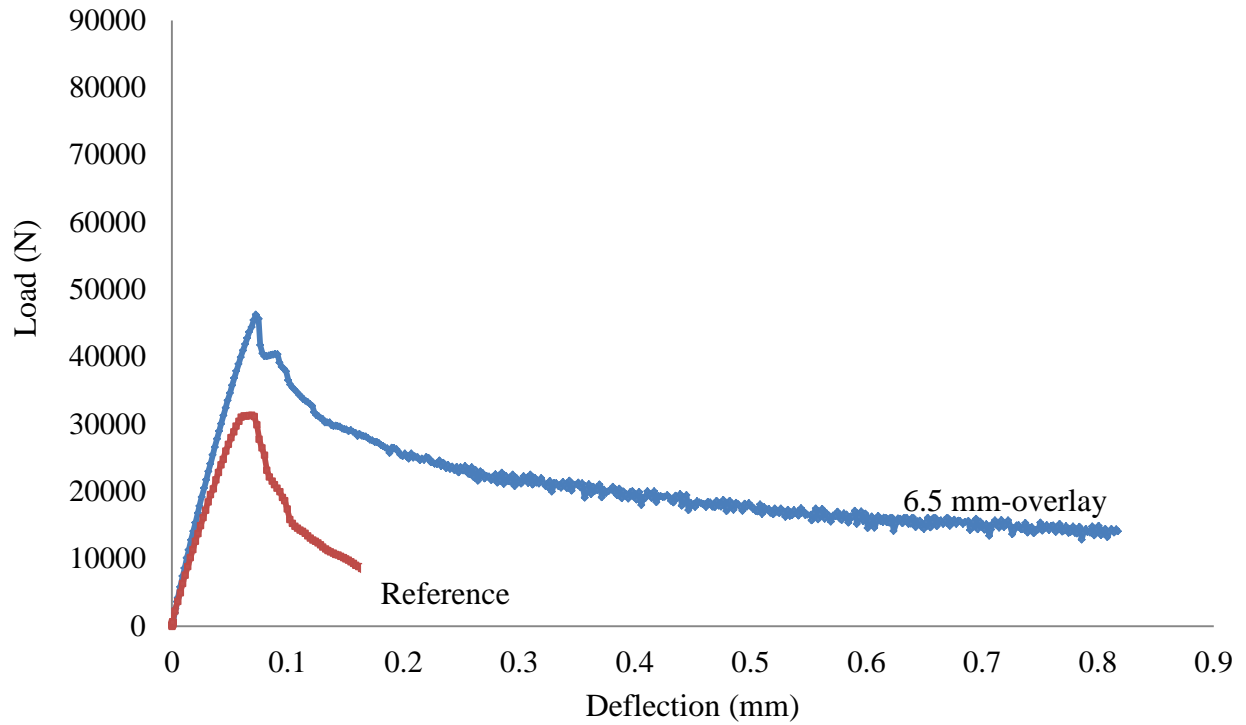


Figure 9.8 - Load-deflection curve for UHPC overlay with 6.5-mm thickness

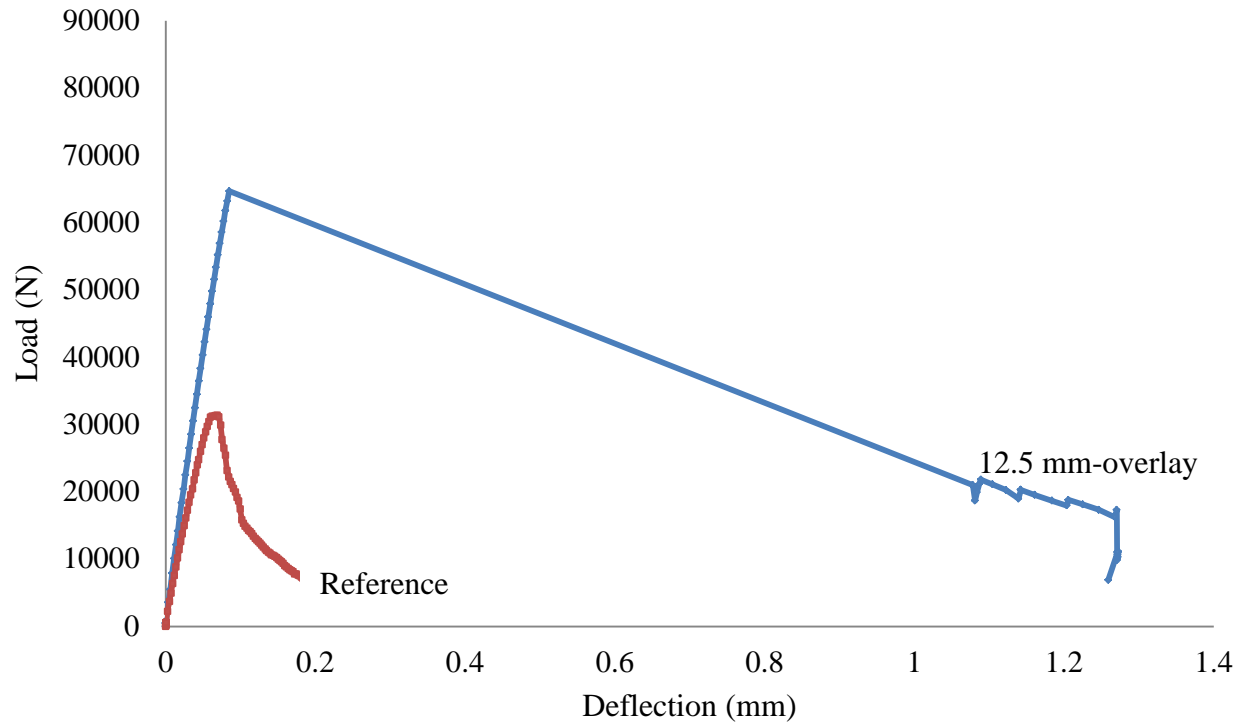


Figure 9.9 - Load-deflection curve for UHPC overlay with 12.5-mm thickness

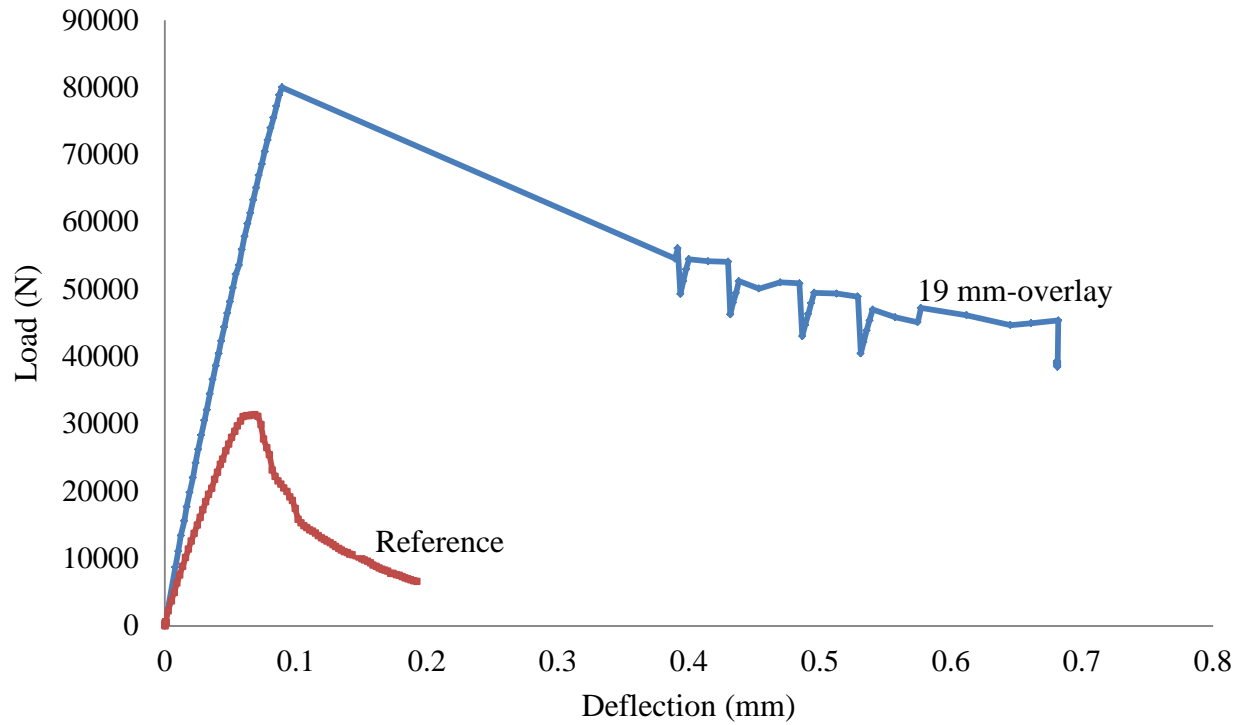


Figure 9.10 - Load-deflection curve for UHPC overlay with 19-mm thickness

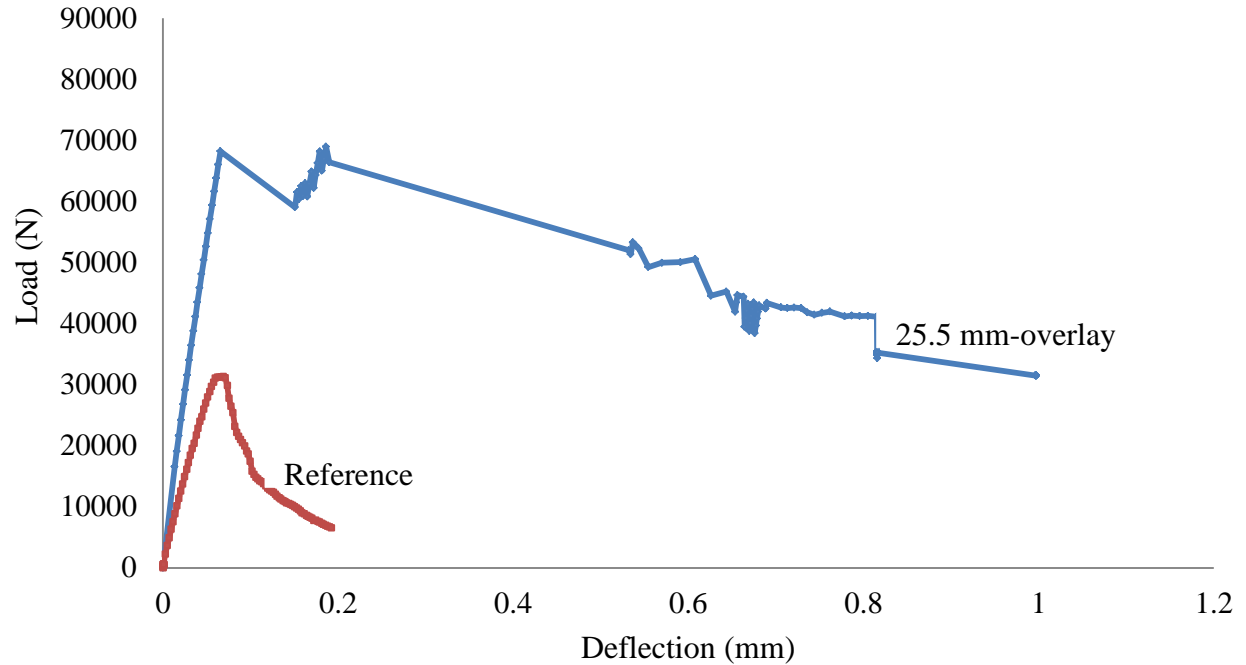


Figure 9.11 - Load-deflection curve for UHPC overlay with 25.5-mm thickness

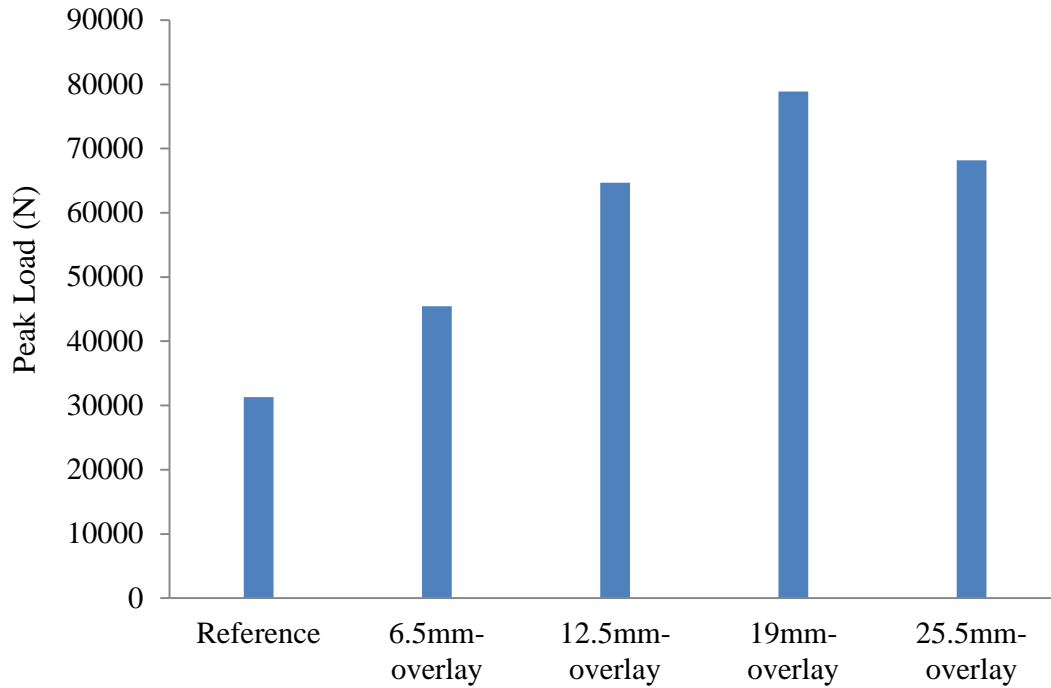


Figure 9.12 - Results for peak load of different thicknesses

#### 9.4 Conclusions

Bond strength of the optimized G50 UHPC to the substrate concrete was evaluated. The bond strength between the substrate concrete and the UHPC overlay was shown to be greater than that of the substrate concrete, thus indicating the feasibility of using the UHPC overlay as a bonded overlay. In addition, the use of the UHPC overlay led to significant increase in flexural strength and toughness of the beams over the monolithic beam case with conventional concrete, regardless of the overlay thickness. The thickness of the UHPC overlay could be limited equal to or lower than 19 mm. Further study is required to evaluate cost-performance aspect for the different overlay thickness.

## Chapter 10 – Conclusions

Ultra-high performance concrete is a new class of cement-based materials that exhibit extremely high durability and mechanical properties. This novel material is characterized as a concrete which has an extremely low w/cm and optimum packing density to eliminate capillary pores. The objective of this study is to develop sustainable UHPC materials for pavement applications with optimized combinations of aggregates, SCMs, and fibers to prolong service life of rigid and flexible pavement. Based on the results in this study, the following conclusions can be made.

- The workability and rheological properties of cement paste and UHPC can vary with the mixer type and mixing time in use. Care should be taken to select the mixer and optimize mixing procedure for the UHPC materials.
- The use of SCMs as a cement replacement can improve the workability and rheological properties of UHPC.
- The type and combination of SCMs can affect the workability, rheology, and robustness of the cement-based materials. The FAC60 paste containing 60% Class C fly ash and the G50SF5 with 50% slag and 5% silica fume had lower minimum water content to initiate flow and higher relative water demand compared to the other pastes, thus indicating higher packing density and greater robustness to the fluctuation of water.
- For a given w/cm, the G50 containing 50% slag replacement and the G50SF5 mixtures with 50% slag and 5% silica fume replacement exhibited lower plastic viscosity compared to the other SCM compositions. This indicates that the w/cm of the G50 and G50SF5 mixture can be further reduced to increase mechanical properties and durability.
- Start plot was used to compare overall performance of cement pastes with various SCM

combinations. The G50 (50% GGBS), FAC40 (40% Class C FA), FAC40SF5 (40% Class FA, 5% SF), G50SF5 (50% GGBS, 5% SF), and FAC40SF5G10 (40% Class C FA, 5% SF, and 10% GGBS) exhibited superior performance to the other mixtures and were used for the SCM compositions for the UHPC optimizations.

- Packing density of aggregates was evaluated using gyratory impactation tester to optimize the aggregate combination for the UHPC materials. The combination of 30% river sand of 0 to 5 mm and 70% of masonry sand of 0 to 2 mm was shown to have the highest packing density and was used for the UHPC mixture compositions.
- Rheological properties of the UHPC materials were evaluated using to optimize total aggregate content. The mortar proportioned with total aggregate-to-cementitious materials of 1, by volume, exhibited superior flow properties and greater compressive strength compared to those with other aggregate contents.
- The incorporation of 2% high-strength steel fibers, by volume led to a post cracking flexural strength up to 28 MPa which is about two times that of UHPC reinforced with 0.5% fibers, and also had a deflection at peak load of 1.05 mm which is more than 10 times of the UHPC without fibers.
- The optimized UHPC mixtures can develop comparable performance to the commercially available UHPC. It is important to point out that the reference UHPC mixture contains large amount of silica sand and higher volume of silica fume compared to the optimized UHPCs. In addition, all the UHPC materials can develop adequate mechanical properties without any accelerated curing or treatment.
- Mechanical properties of the optimized UHPC mixtures were compared to those of the

reference of the commercial UHPC. The optimized UHPC mixtures developed similar to or slightly lower compressive strength than the reference UHPC. It is interesting to note that the optimized mixtures were shown to have equal to or greater splitting tensile strength than the reference, despite slightly lower compressive strength of the former concrete. This can be due to the use of optimized aggregates of high packing density, which contribute to an increase in aggregate interlocking compared to the smooth and round silica sand.

- The optimized UHPC mixtures had significantly low drying shrinkage which is lower than 150  $\mu\text{m/m}$ . The G50SF5, G50 and FAC60 mixtures had lower drying shrinkage than the reference Ductal mixture. In addition, the G50 mixture had only 100  $\mu\text{m/m}$  after 50 days of age.
- In general, the UHPC mixture at high temperature can have greater mechanical properties than similar mixture at low temperature. It is important to note that mixtures containing Class C fly ash were more stable to the temperature fluctuations than those containing GGBS.
- The bond strength between the substrate concrete and the UHPC overlay was shown to be greater than that of the substrate concrete, thus indicating the feasibility of using the UHPC overlay as a bonded overlay.
- The use of the UHPC overlay led to significant increase in flexural strength and toughness of the beams over the monolithic beam cast with conventional concrete, regardless of the overlay thickness. The thickness of the UHPC overlay could be limited equal to or lower than 19 mm. Further study is required to evaluate cost-performance aspect for the different overlay thickness.

## References

- [1] De Larrard, F., The High-Performance Cementitious Material (HPCM), a Cousin of UHPFRC for Long-Life Pavement. BFUP, 2009.
- [2] Shann, S.V., Application Of Ultra High Performance Concrete (UHPC) as a Thin-Bonded Overlay for Concrete Bridge Decks, in Department of Civil and Environmental Engineering. Michigan Technological University, 2012.
- [3] Krauss P, Lawler J, Steiner K. Guidelines for Selection of Bridge Deck Overlays, Sealers, and Treatments. Northbrook, IL: Wiss, Janney, Elstner Associates, Inc. 2009.
- [4] Knight ML, Wilson GS, Seger WJ, Mahadevan S. Overlay Types Used as Preventive Maintenance on Tennessee Bridge Decks. Maintenance and Management of Pavement and Structures. 2004, 1866 :79-84.
- [5] Griffin JJ, Issam E. Harik, Choo CC. Performance Evaluation of Bridges with Structural Bridge Deck Overlays (SBDO). Lexington, KY: University of Kentucky: Kentucky Transportation Centery. No. KTC-06-05 / FRT81-82-97-1F, 2006.
- [6] FHWA. Bridge Inspector's Reference Manual (BIRM). Washington, DC: Federal Highway Administration, 2006.
- [7] Krstulovic-Opara N, Haghayeghi AR, Haidar M, Krauss PD. Use of Conventional and High-Performance Steel-Fiber Reinforced Concrete for Bridge Deck Overlays. ACI Materials Journal 1995, 92(6),:669-67.
- [8] Dong Hyun Kim, Materials Selection for Concrete Overlays. Master thesis at The University of Texas at Austin, 2011.
- [9] Saucier, F., et al., A Combined Shear-Compression Device to Measure Concrete to Concrete Bonding. Experimental Techniques, 1991. 15(5): p. 49-55.
- [10] Geissert, D.G., Li, Shigen., Frantz, Gregory.c., Stephens, Jack.E., Splitting Prism Test Method to Evaluate Concrete-to-Concrete Bond Strength. ACI materials Journal, 1999. 96(3).
- [11] Li, S., Geissert, David G., Frantz, Gregory C., Stephens, Jack E., Durability and Bond of High Performance Concrete and repaired portland Cement Concrete. University of Connecticut, no. JHR 97-257, 1997.

- [12] Sarkar, J., Characterization of the Bond Strength between Ultra High Performance Concrete Bridge Deck Overlays and Concrete Substrates, in Civil Engineering. Michigan Technological University, 2010.
- [13] Kriegh, J.D., Arizona Slant Shear Test: A Method to Determine Epoxy Bond Strength. ACI Journal, 1976. 73(7): p. 372-373.
- [14] Wall, J.S. and N.G. Shrive, Factors Affecting Bond Between New and Old Concrete. ACI Materials Journal, 1988: p. 117-125.
- [15] Habel K, Charron JP, Denarié E, Brühwiler E. Autogenous deformations and viscoelasticity of UHPFRC in structures. Part I: experimental results. Magazine of Concrete Research. 2006, 58(3):135-145.
- [16] Naaman AE, Wille K. The Path to Ultra-High Performance Fiber Reinforced Concrete (UHP-FRC): Five Decades of Progress. Proceedings of Hipermat- 3rd International Symposium on UHPC and Nanotechnology for Construction Materials; 2012; Kassel, Germany: Kassel University Press. 2012, p. 3-15.
- [17] Resplendino J. State of the Art of Design and Construction of UHPFRC Structures in France. Proceedings of Hipermat- 3rd International Symposium on UHPC and Nanotechnology for Construction Materials; Kassel, German: Kassel University Press. 2012, p. 27-41.
- [18] Aitcin, P.-C., Y. Delagrave, and R. Beck. , A 100-m High Prefabricated Concrete Pole: Why Not?, In Transmission and Distribution Construction, Operation and Live-Line Maintenance Proceedings. 2000 IEEE ESMO-2000 IEEE 9th International Conference on. 2000. p. 365-374.
- [19] Gao, R., Zhi Min Liu, Li Qian Zhang, and Piet Stroeven, Static Properties of Plain Reactive Powder Concrete Beams. Key Engineering Materials, 2005. 302: p. 521-527.
- [20] Walraven, J.C. From Design of Structures to Design of Materials. Innovations and Developments in Concrete Materials and Construction. in Proceedings of the International Conference Held at the University of Dundee, Scotland, UK on 9-11 Sept. London. 2002.
- [21] Design and Performance Verification of Ultra-High Performance Concrete Piles for Deep Foundations. The Iowa Highway Research Board (IHRB Project TR-558) and the Iowa Department of Transportation (CTRE Project 06-264), 2008.
- [22] Ma, J., and H. Schneider, Properties of Ultra-High-Performance Concrete. Leipzig Annual Civil Engineering Report (LACER), 2012.

- [23] Richard, P., and M. Cheyrezy, Composition of Reactive Powder Concretes. *Cement and Concrete Research*, 1995. 25(7): p. 1501-1511.
- [24] Stovall T., d.L.F., Buil M., Linear Packing Density Model of Grain Mixtures. *Powder Technology*, 1986. 48(1): p. 1-12.
- [25] Dr. Theresa M. Ahlborn, M.E.J.P., Mr. Donald Li Misson, Ultra-High Performance Concrete for Michigan Bridges Material Performance – Phase I. Center For Structural Durability, Michigan Tech Transportation Institute, 2008.
- [26] Dugat, J., Roux, N., and G. Bernier, Mechanical Properties of Reactive Powder Concretes. *Materials and Structures*, 1996. 29: p. 233-240.
- [27] Castellote, M., Llorente, I., Andrade, C., and C. Alonso., Accelerated Leaching of Ultra High Performance Concretes by Applications of Electrical Fields to Simulate Their Natural Degradation. *Materials and Structures*, 2003. 36: p. 81-90.
- [28] Droll, K., Influence of Additions on Ultra High Performance Concretes – Grain Size Optimisation, in *Proceedings of the International Symposium on Ultra-High Performance Concrete*, Kassel, Germany. 2004, p. 285-301.
- [29] de Larrard, F., and T. Sedran, Optimization of Ultra-High-Performance Concrete by the Use of a Packing Model. *Cement and Concrete Research*, 1994. 24(6): p. 997-1009.
- [30] Lee, M.-G., Chiu, C.-T., and Y.-C. Wang., The Study of Bond Strength and Bond Durability of Reactive Powder Concrete. *Journal of ASTM International*, 2005. 2(7): p. 104-113.
- [31] Blais, P.Y., and M. Couture., Precast, Prestressed Pedestrian Bridge – World’s First Reactive Powder Concrete Structure. *PCI Journal*, 1999. 44(5): p. 60-71.
- [32] Huh, S.-B., and Y.-J. Byun., Sun-Yu Pedestrian Arch Bridge, Seoul, Korea. *Journal of the International Association for Bridge and Structural Engineering (IABSE)*, 2005. 15(1): p. 32-34.
- [33] Xing, F., Huang, L.-D., Cao, Z.-L., and L.-P. Deng., Study on Preparation Technique for Low-Cost Green Reactive Powder Concrete. *Key Engineering Materials*, 2006. 302-303: p. 405-410.
- [34] Voo, J.Y., Foster, S.J., Gilbert, R.I., and N. Gowripalan., Design of Disturbed Regions in Reactive Powder Concrete Bridge Girders. *High Performance Materials in Bridges*, in *American Society of Civil Engineers*. 2001. p. 117-127.

- [35] Suleiman, M., Sri Sritharan., and T.L. Vande Voort, Design and Performance Verification of UHPC Piles for Deep Foundations. Center for Transportation Research and Education Iowa State University, 2008.
- [36] Cheyrezy, M., and M. Behloul., Creep and Shrinkage of Ultra-High Performance Concrete, in Creep, Shrinkage and Durability Mechanisms of Concrete and other Quasi-Brittle Materials – Proceedings of the Sixth International Conference CONCREEP-6@MIT., MA, USA, 2001. p. 527-538.
- [37] Graybeal BA. Material Property Characterization of Ultra-high Performance Concrete. McLean, VA: Federal Highway Administration (FHWA). No. FHWA-HRT-06-103, 2006.
- [38] Misson DL. 2008. Influence of Curing Regime on the Durability of an Ultra-High Performance Concrete Material, Thesis. Houghton, MI: Michigan Technological University, 2008.
- [39] Bonneau, O., Poulin, C., Dugat, J., Richard, P., and P.C. Aïtcin., Reactive Powder Concretes: From Theory to Practice. Concrete International, 1996. 18(4): p. 47-49.
- [40] Blais, P.Y., and M. Couture., Precast, Prestressed Pedestrian Bridge – World’s First Reactive Powder Concrete Structure. PCI Journal,, 1999. 44(5): p. 60-71.
- [41] Suleiman, M., Sri Sritharan., and T.L. Vande Voort, Design and Performance Verification of UHPC piles for deep foundations. 2008, Center for Transportation Research and Education Iowa State University, 2008.
- [42] Bruhwiler, E.a.E.D., Rehabilitation of Concrete Structures Using Ultra-High Performance Fibre Reinforced Concrete, in Second International Symposium on Ultra High Performance Concrete. Kassel,Germany, 2008.
- [43] Denarie, E., E. Bruhwiler, and A. Znidaric, Full Scale Application of UHPFRC for Rehabilitation of Bridges-from the Lab to the Field, in 5th FWP/ SAMARISSustainable and Advanced Material for Road Infrastructures. 2005.
- [44] Yuguang, Y., J.D. Uijl, and J. Walraven, Study on Bending Behavior of an UHPC Overlay on a Steel Orthotropic Deck, in Second International Symposium on Ultra High performance Concrete. Kassel,Germany. 2008, p. 639-646.
- [45] Lee, M.-G., Y.-C. Wang, and C.-T. Chiu, A Preliminary Study of Reactive Powder Concrete as a New Repair Material. Construction and Building Materials, 2005. 21: p. 182-189.

- [46] N. B.S.Julio, E., F. A.B. Branco, and V. D.Silva, Concrete-to-Concrete Bond Strength Influence of the Roughness of the Substrate Surface. *Construction and Building Materials*, 2004. 18: p. 675-681.
- [47] Bassam A. Tayeh, B.H. Abu Bakar, M.A. Megat Johari, Yen Lei Voo, Mechanical And Permeability Properties of the Interface between Normal Concrete Substrate and Ultra High Performance Fiber Concrete Overlay, *Construction and Building Materials*, 2012, 36, 538–548.
- [48] ASTM C1245, Standard Test Method for Determining Relative Bond Strength Between Hardened Roller Compacted Concrete Lifts (Point Load Test), 2012.

## Appendix - Rheology Result for UHPC

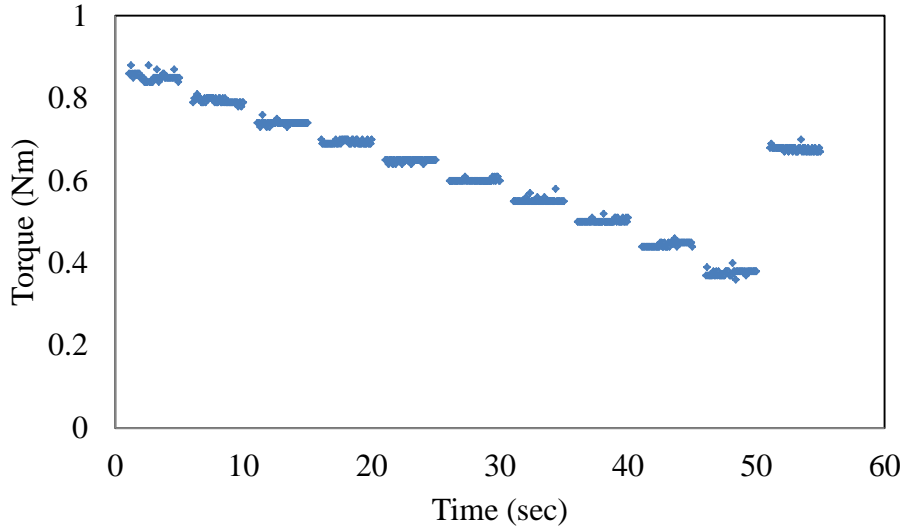


Figure A.1 - Reference UHPC: Shear stress versus time at 20 minute

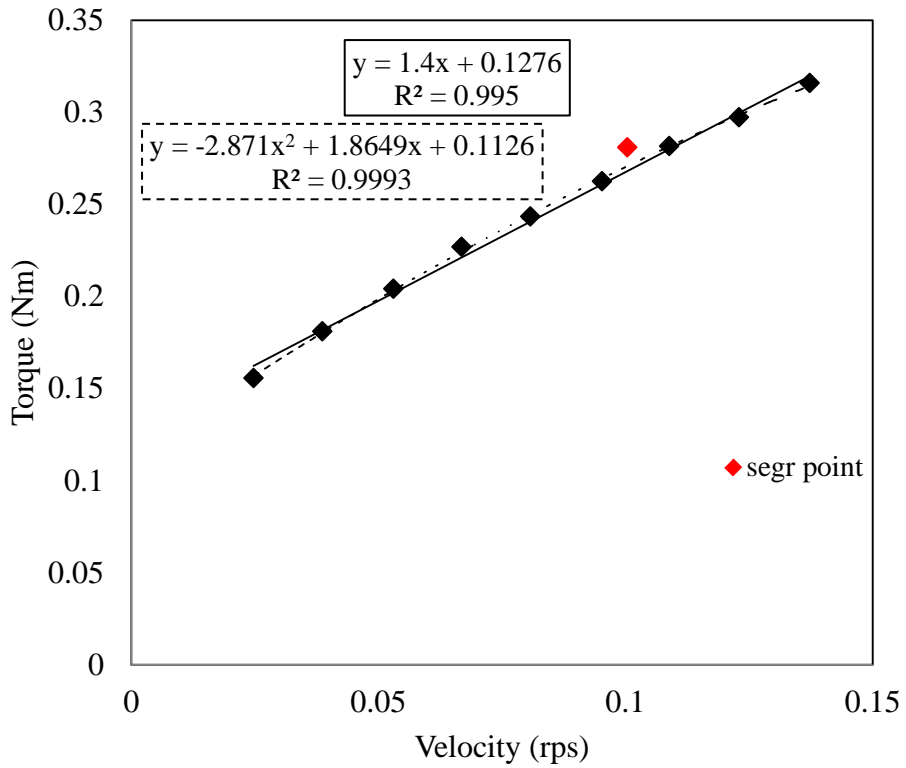


Figure A.2 - Reference UHPC: Torque versus rotational speed at 20 minutes

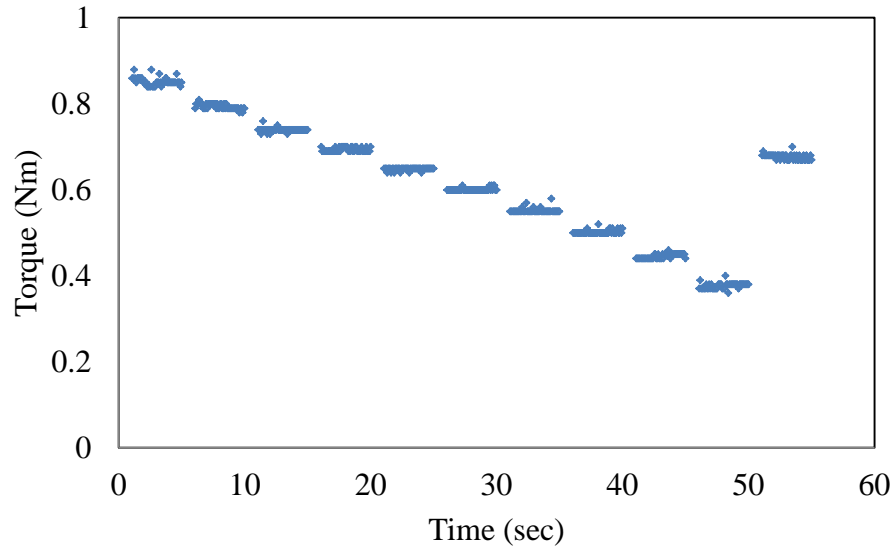


Figure A.3 - Reference UHPC: Shear stress versus time at 40 minute

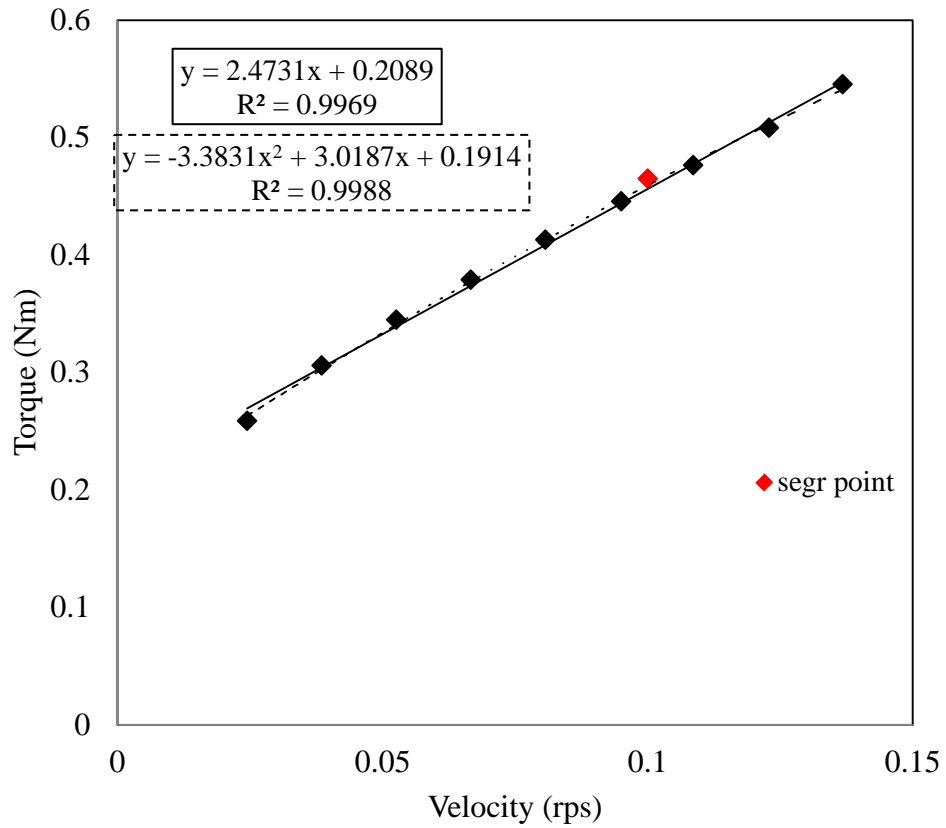


Figure A.4 - Reference UHPC: Torque versus rotational speed at 40 minutes

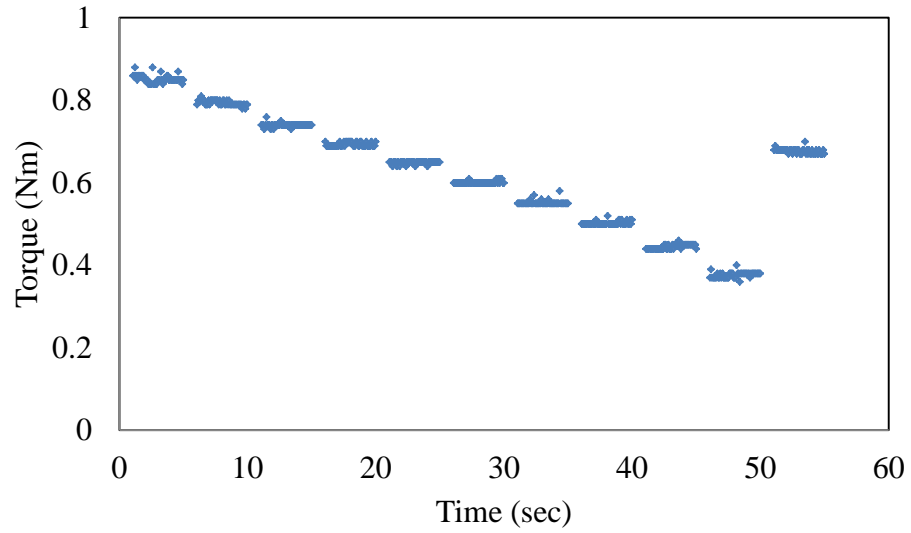


Figure A.5 - Reference UHPC: Shear stress versus time at 40 minute

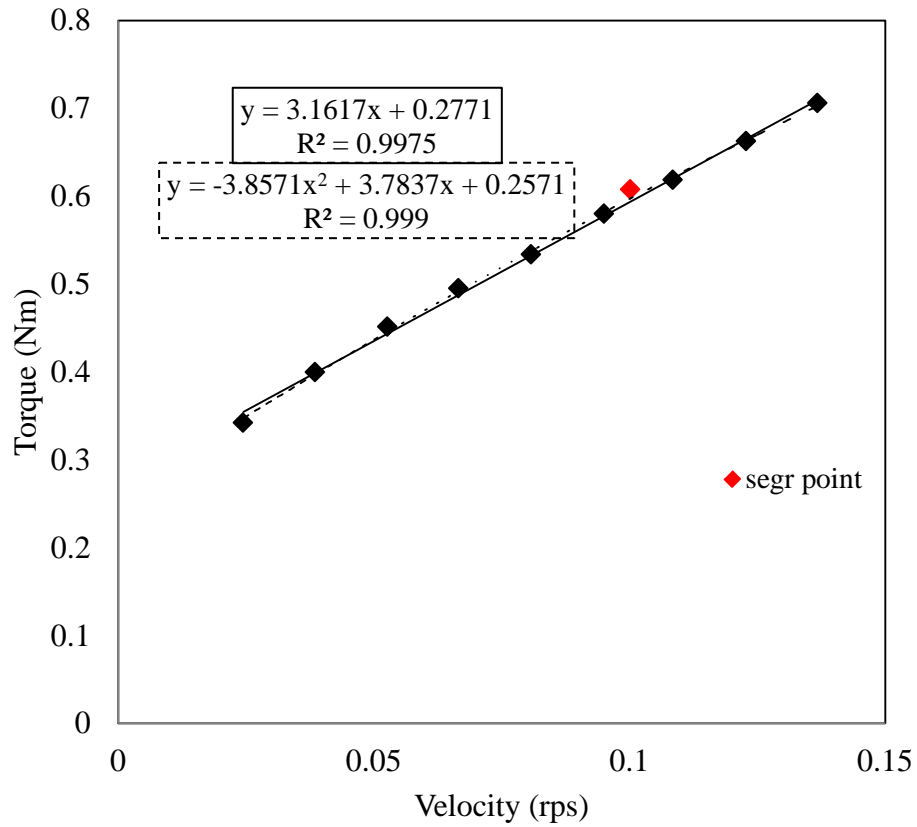


Figure A.6 - Reference UHPC: Torque versus rotational speed at 60 minutes

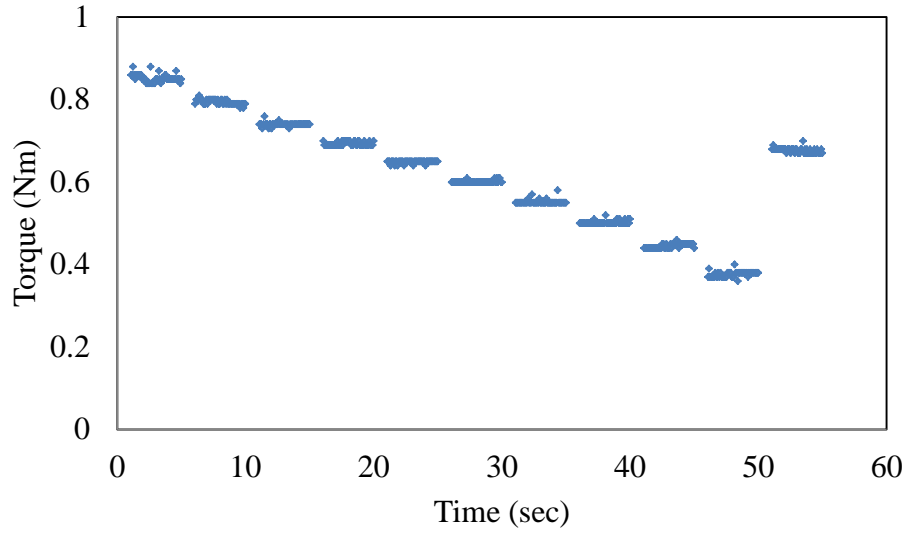


Figure A.7 - G50SF5: Shear stress versus time at 20 minute

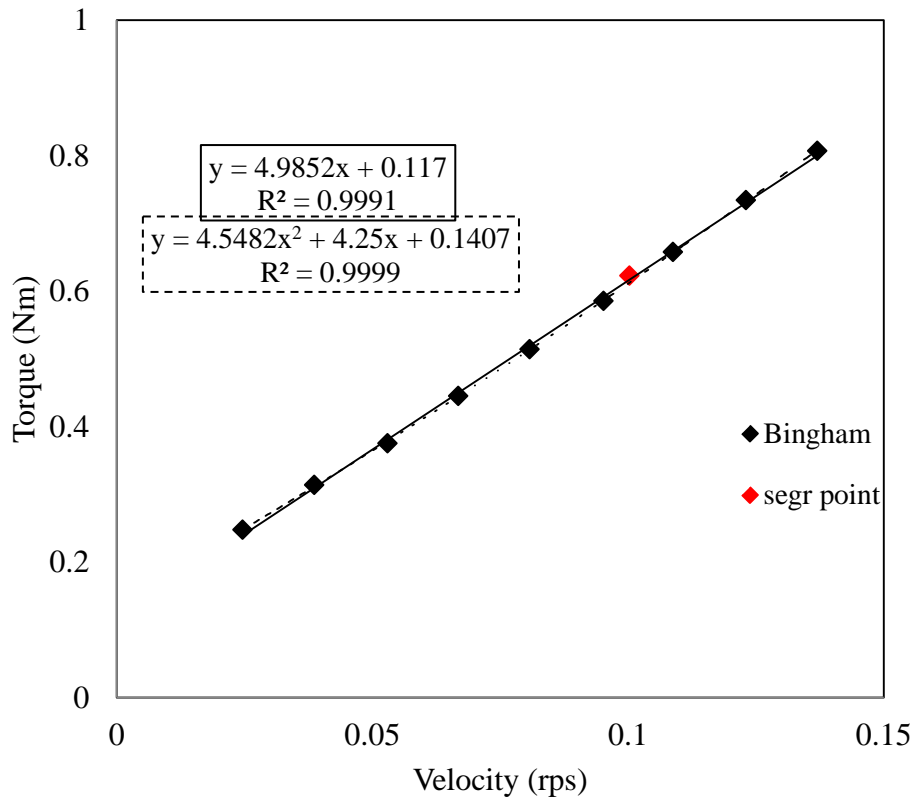


Figure A.8 - G50SF5: Torque versus rotational speed at 20 minutes

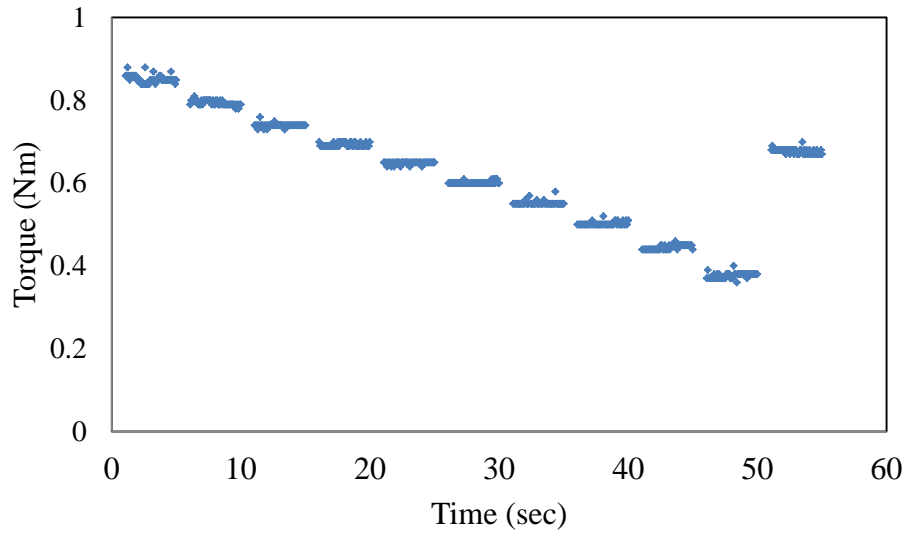


Figure A.9 - G50SF5: Shear stress versus time at 40 minute

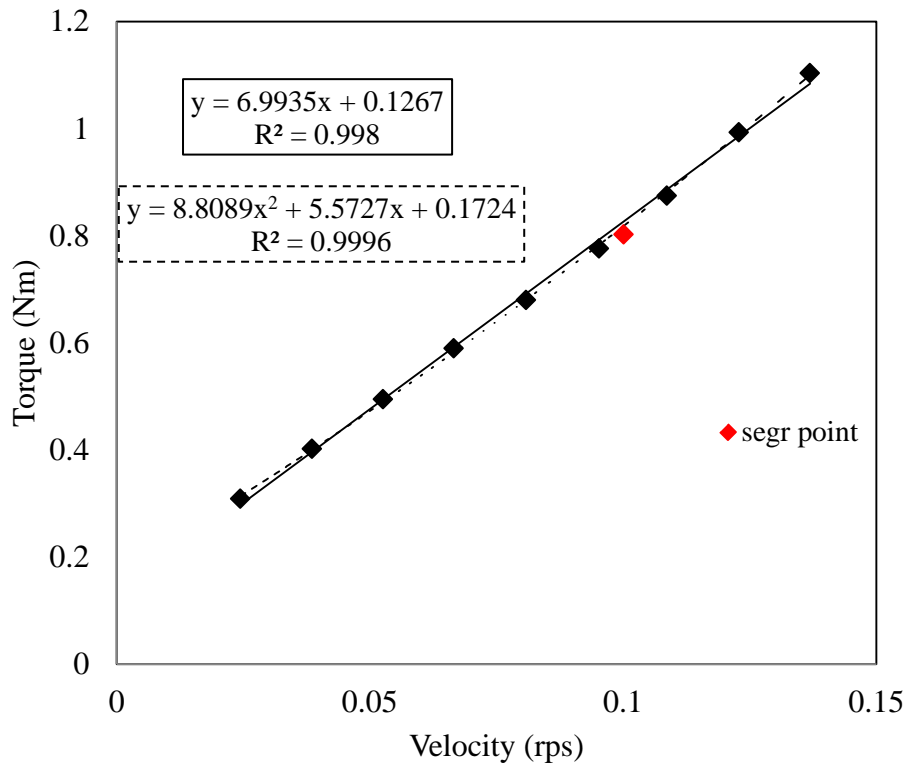


Figure A.10 - G50SF5: Torque versus rotational speed at 40 minutes

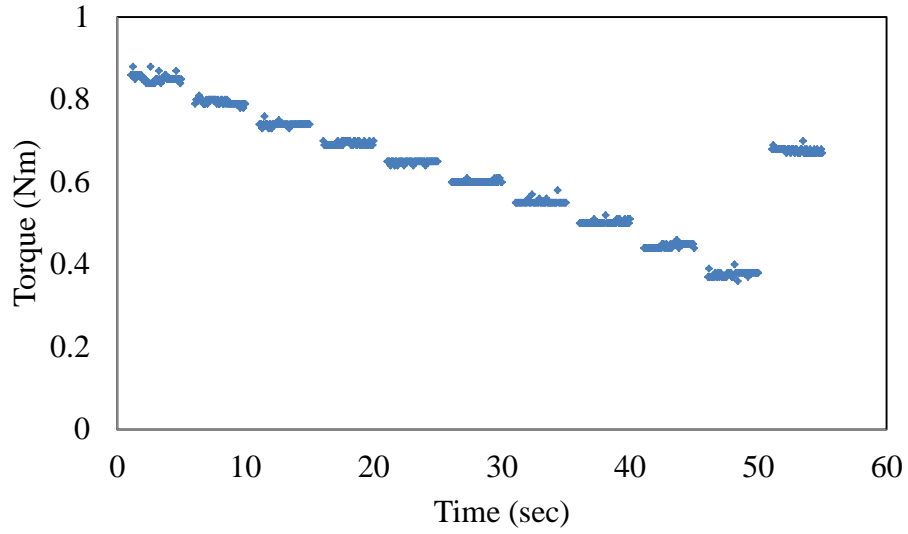


Figure A.11 - G50SF5: Shear stress versus time at 60 minute

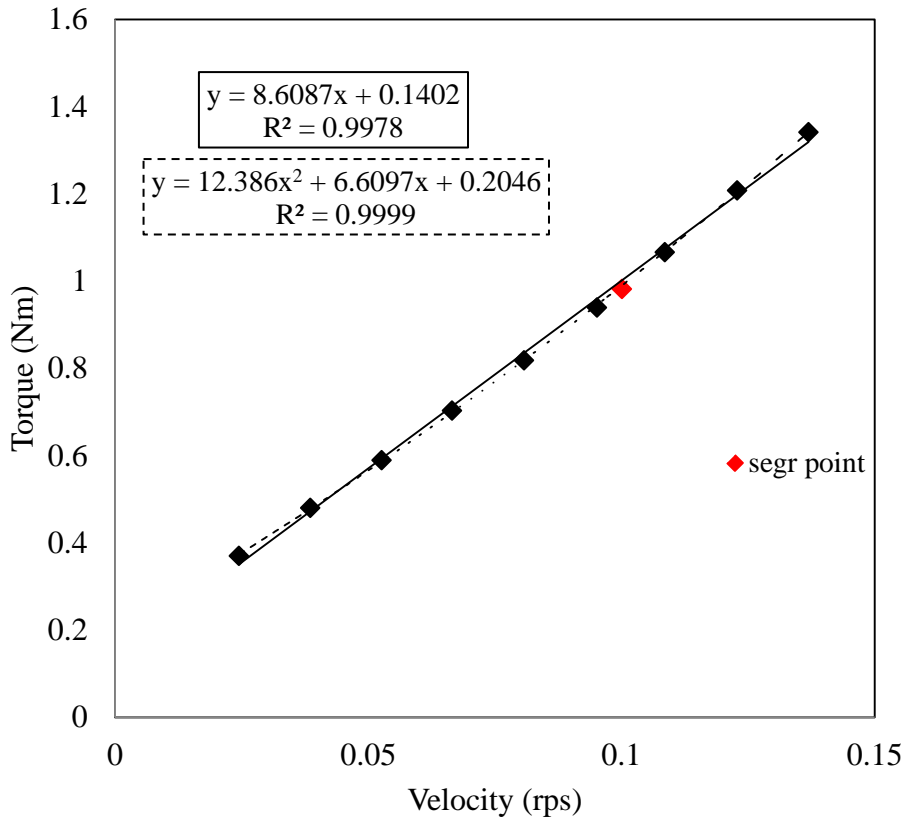


Figure A.12 - G50SF5: Torque versus rotational speed at 60 minutes

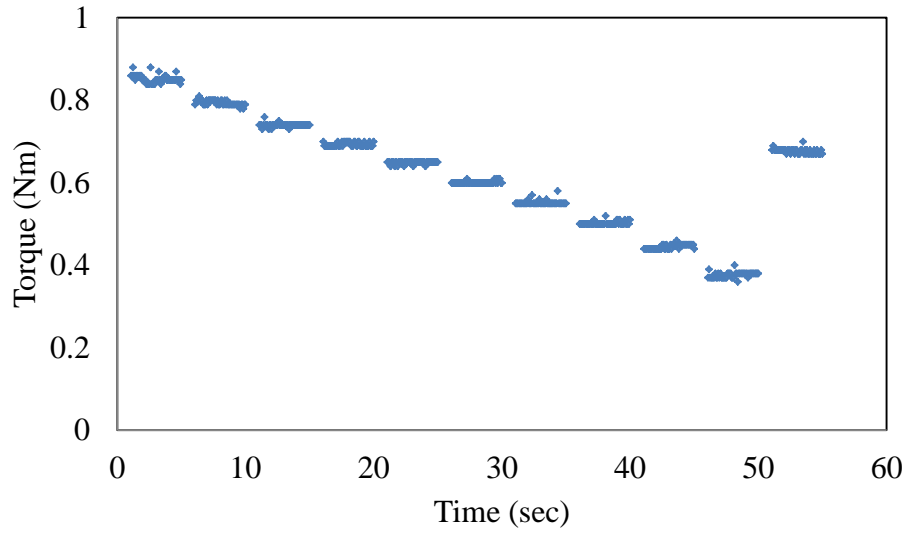


Figure A.13 - FAC40SF5: Shear stress versus time at 20 minute

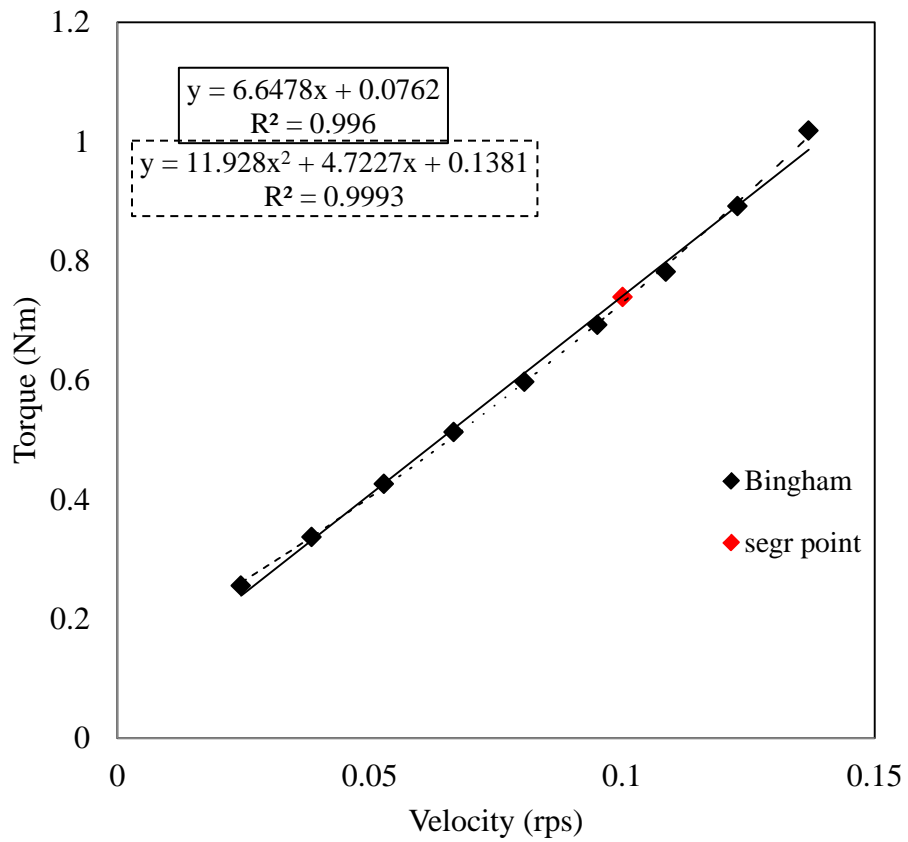


Figure A.14 - FAC40SF5: Torque versus rotational speed at 20 minutes

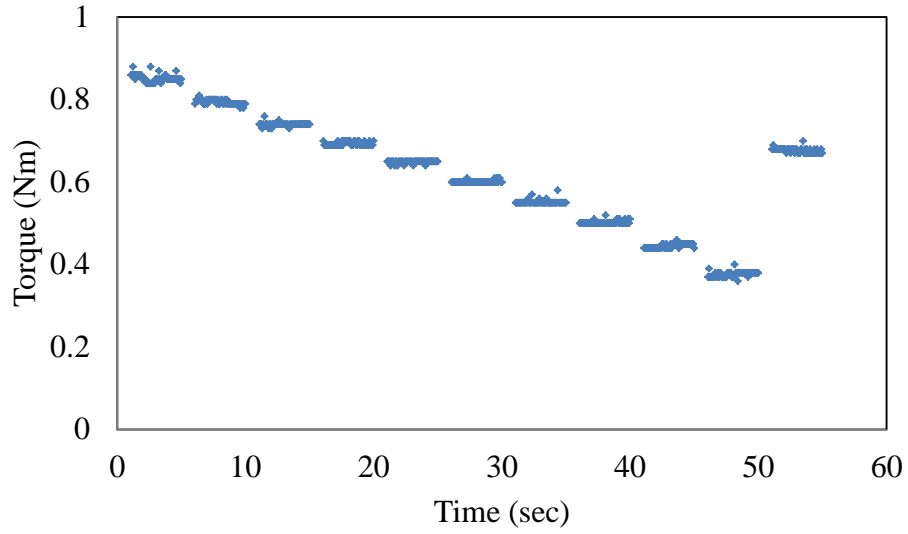


Figure A.15 - FAC40SF5: Shear stress versus time at 40 minute

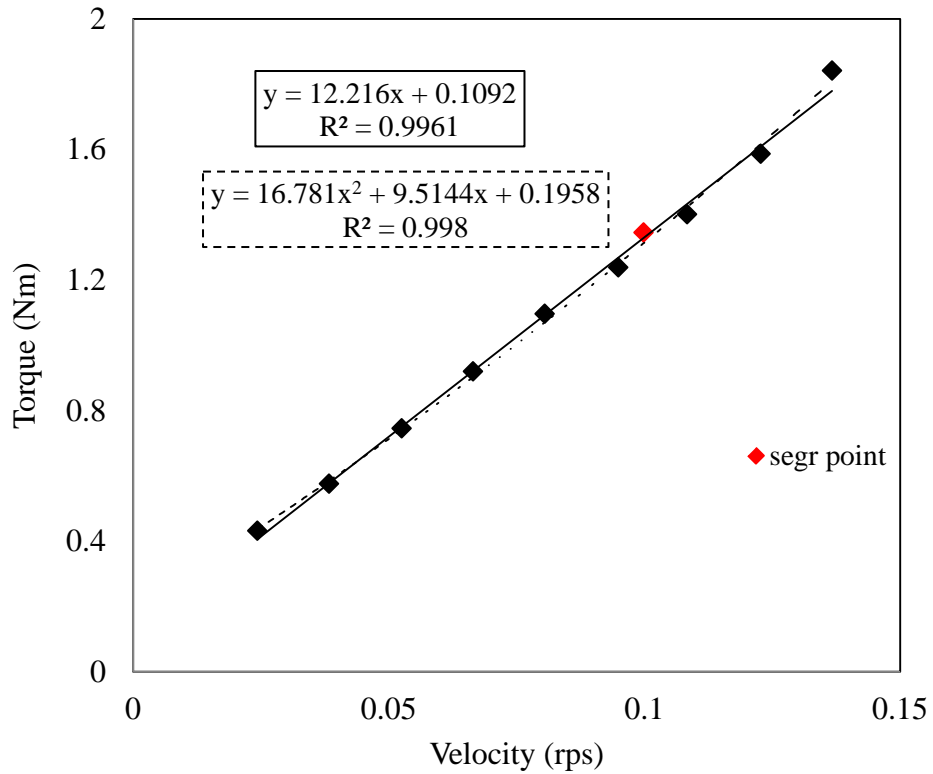


Figure A.16 - FAC40SF5: Torque versus rotational speed at 40 minutes

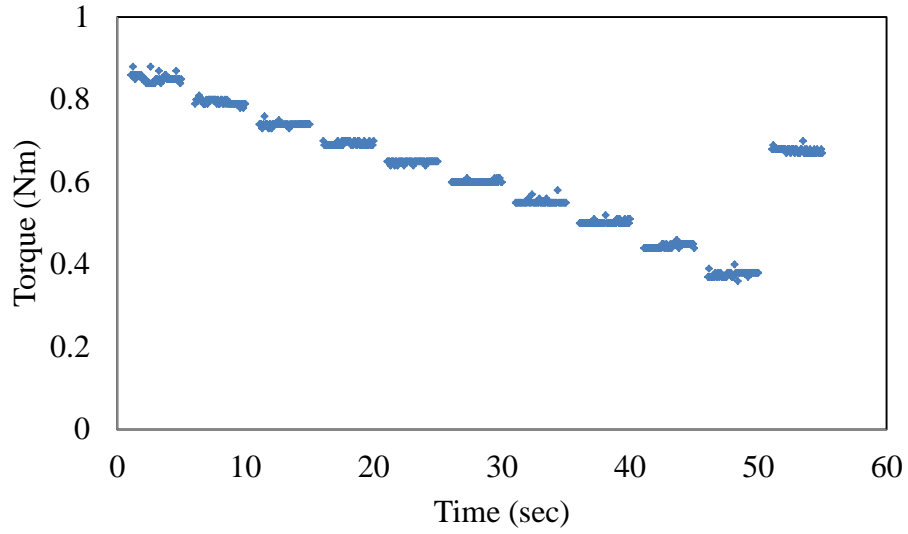


Figure A.17 - FAC40SF5: Shear stress versus time at 60 minute

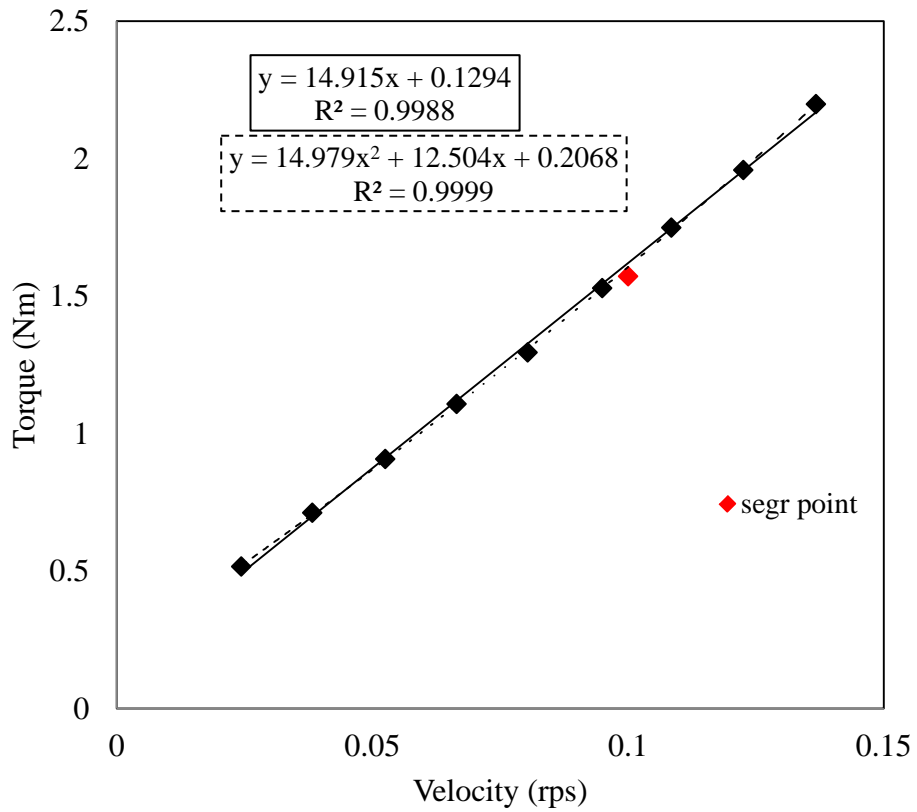


Figure A.18 - FAC40SF5: Torque versus rotational speed at 60 minute